

84p.

full

JPL-SPS-37-26 Vol III

001
N64-19594* 23

CODE-1

(NASA CR-53833)

OTS: \$8.10 ph

Space Programs Summary No. 37-26, Volume III,

FOR THE PERIOD 1 January 1963 - 29 February 1964, (2 space)
~~for the period January 1, 1963 to February 29, 1964~~

al copy

The Deep Space Instrumentation Facility

31 Mar. 1964 84p ref

(NASA Contract NAS7-100)

OTS PRICE

XEROX

\$

8.10 ph

MICROFILM

\$

2.72 ref.

jpl

JET PROPULSION LABORATORY
CALIFORNIA INSTITUTE OF TECHNOLOGY
PASADENA, CALIFORNIA

1 389964

March 31, 1964

EXACT COPY

Space Programs Summary No. 37-26, Volume III

for the period January 1, 1963 to February 29, 1964

The Deep Space Instrumentation Facility

JET PROPULSION LABORATORY
CALIFORNIA INSTITUTE OF TECHNOLOGY
PASADENA, CALIFORNIA

March 31, 1964

Preface

The *Space Programs Summary* is a six volume, bimonthly publication designed to report on JPL space exploration programs, and related supporting research and advanced development projects. The subtitles of all volumes of the *Space Programs Summary* are:

- Vol. I. The Lunar Program (Confidential)
- Vol. II. The Planetary—Interplanetary Program (Confidential)
- Vol. III. The Deep Space Instrumentation Facility (Unclassified)
- Vol. IV. Supporting Research and Advanced Development (Unclassified)
- Vol. V. Supporting Research and Advanced Development (Confidential)
- Vol. VI. Space Exploration Programs and Space Sciences (Unclassified)

The *Space Programs Summary*, Volume VI consists of: an unclassified digest of appropriate material from Volumes I, II, and III; original presentation of the JPL Space Flight Operations Facility development progress; and a reprint of the space science instrumentation studies of Volumes I and II.



W. H. Pickering, Director
Jet Propulsion Laboratory

Space Programs Summary No. 37-26, Volume III

Copyright © 1964, Jet Propulsion Laboratory, California Institute of Technology
Prepared under Contract No. NAS 7-100, National Aeronautics & Space Administration

Contents

I. Résumé	1
A. Tracking Station Operations	1
B. Engineering Developments	1
C. Research and Development	2
D. Advanced Antenna System	4
II. Tracking Station Operations	5
A. <i>Ranger 6</i>	5
Reference	10
III. Engineering Developments	11
A. Systems Engineering	11
B. Tracking Data Monitoring Program	16
C. Pointing Errors Due to Quadripod Leg Distortions of New Truss Type Quadripod at Echo Station	21
D. <i>Mariner C</i> 100-kw Transmitter	22
References	22
IV. Research and Development	23
A. Ground Antennas	23
B. Planetary Radar Project	30
C. Ranging and Tracking System Development	38
D. RF Signal Generation and Control	57
E. S-Band Implementation for DSIF	61
F. Mesa Antenna Range	62
References	64
V. Advanced Antenna System	66
A. Synopsis	66
B. Supporting Studies	72
References	80

I. Résumé

The DSIF is a precision tracking and data acquisition network which is designed to track, command, and receive data from deep space probes. It utilizes large antennas, low-noise, phase-lock receiving systems, and high-power transmitters at stations positioned approximately 120 deg around the Earth. Its policy is to continuously conduct research and development of new components and systems and to engineer them into the DSIF so as to continually maintain a state-of-the-art capability. Identification of stations is given in the following tabulation:

Goldstone Pioneer	DSIF 11
Goldstone Echo	DSIF 12
Goldstone Venus	DSIF 13
Goldstone Mars (under construction)	DSIF 14
Woomera	DSIF 41
Canberra (under construction)	DSIF 42
Johannesburg	DSIF 51
Mobile Tracking	DSIF 59
Madrid (under construction)	DSIF 61
Spacecraft Monitoring	DSIF 71

A. Tracking Station Operations

1. *Ranger 6*

a. Goldstone. The Pioneer Station acted as a backup to the Echo Station, and both stations successfully tracked

and received telemetry data from *Ranger 6* during all of the Goldstone visibility periods. The 10-kw S-band transmitter, Cassegrainian cone, hyperbolic reflector, acquisition aid antenna, and acquisition aid collimation tower have been installed at the Pioneer Station. An interim S-band building is under construction.

b. DSIF tracking performance. The tracking data generated by all the DSIF Stations on the *Ranger 6* launch was excellent. The polynomials used in the computer to correct for systematic angular pointing errors need to be corrected to represent RF errors rather than errors obtained optically.

B. Engineering Developments

1. *Systems Engineering*

a. Project engineering. Specifications, analyses of reports, and plans for tests have been made for all the projects; Technical Memorandum 33-26 is being revised; a preliminary design of the Spacecraft Monitoring Station at Cape Kennedy is in process; and work is being done on various system integration and engineering projects.

b. Suitcase telemetry study. Suitcase telemetry stations have been proposed as an extremely portable, inexpensive means of obtaining telemetry from space probes between launch and DSIF acquisition in those portions of their trajectories which are not covered by existing stations. Using analyses of certain portions of *Mariner 2* nominal trajectories, it has been calculated that the maximum tracking error of an Az-El mounted antenna which is moved in a single plane (tilted azimuth) is less than 5 deg. This means that a 10-deg beamwidth antenna would probably be usable.

2. Tracking Data Monitoring Program

a. Program improvements. The computer program which has been developed to monitor in near real-time the tracking data from a DSIF Station has been found from experience to require a few modifications and corrections. Some input parameters have been made constant; additional output routines have been added to allow different types of typewriter output, and the output doppler has been modified to cps rather than continuous. A doppler prediction program for the SDS 920 has been written.

b. A trajectory-independent method of estimating the noise spectral density of tracking data. A method of monitoring tracking data by means of monitoring the spectral density function of the noise on the data in near real-time has been developed. The method, which is a generalization of analyses of variance to correlated data, has been found to give estimates of the spectrum that are very nearly like more conventional trend-removing schemes.

3. Pointing Errors Due to Quadripod Leg Distortions of New Truss Type Quadripod at Echo Station

The STAIR Computer Program was used to compute the estimated hour angle and declination angle errors due to live loads at the end of the new truss type quadripods which are used on the 85-ft antennas. Maximum hour angle errors of 0.0263 and 0.0195 deg, and maximum declination angle errors of 0.0133 and 0.0098 deg were calculated with loads of 1150 and 450 lb, respectively. This is a 25% increase in accuracy over the old telescoping pipe quadripod based on a load of 650 lb.

4. Mariner C 100-kw Transmitter

A contract for assembling the 100-kw amplifier subsystem, which will be used with *Mariner C*, has been awarded to Energy Systems of Palo Alto, California. Final tests will be made at the Goldstone Venus site.

C. Research and Development

1. Ground Antennas

a. Precision drive system for 30-ft antenna. The drive system of the 30-ft antenna has been modified to use a system similar to that used on the 85-ft Az-El antenna but with improvements. This system utilizes both high- and low-speed hydraulic motors, each controlled by an electronic second-order servo system with hydraulic pressure and motor rate feedback. A new mechanical counter has been developed which will operate at 6 deg/sec but with some increase in ambiguity.

b. Antenna instrumentation. A second scanner has been added to monitor the wire span temperatures of the extensometers in order to provide temperature correction information. Of six tests outlined in the last *Space Programs Summary*, four were successfully carried out on tests of the 85-ft Az-El antenna after the new surface had been installed.

c. Radio astronomical techniques. The technique of using radio stars for calibrating large antennas was used on January 8 and 9, 1964 to measure the gain of the Echo Station antenna at L-band. This was determined to be 45.6 ± 1.5 db. It is hoped to decrease the uncertainty by improving the calibration of the test loads.

d. Radio calibration techniques. Using cryogenic loads and the audio frequency substitution method, measurements have been made on the insertion losses of various portions of the microwave system in the Cassegrainian cone on the 85-ft antenna at the Venus site. These compare favorably with previous measurements and estimates. It was learned that periodic checks and repair of the cryogenic loads are desirable.

e. 85-ft Az-El antenna, reflector resurfacing. The new surface on the Venus 85-ft Az-El antenna meets all of the specifications except that for erection tolerance. The $1-\sigma$ value for this error is about three times that specified, and is apparently due to hysteresis in the reflector backup structure. This problem is under study. The new surface material is 0.072-in.-thick aluminum with 0.125-in.-diameter holes providing a porosity of 25%.

2. Planetary Radar Project

a. 100-kw S-band transmitter. During the period between completion of Venus and Jupiter tracking opera-

tions and the resumption of planetary radar tracking, several improvements and tests have been made on the 2388-Mc, 100-kw transmitter. The "crowbar" protective circuit electronics have been redesigned and improved; transient "crowbar" operations have been recorded; the dc water load has been relocated and partially automated; the 220-v, 400-cps motor generator set and amplidyne units have been relocated; new temperature insensitive attenuators have been installed in the RF power measuring equipment; and measurements have been made of the klystron harmonic power.

b. Nine-channel autocorrelator. The nine-channel autocorrelator automatically extracts from the pseudonoise-coded, biphase-modulated, transmitted, and reflected signal the signal components from nine adjacent range zones. An additional function has been added which makes it possible to subtract the autocorrelation function of pure noise from the autocorrelation function of signal plus noise. The autocorrelator has been tested in the laboratory and has now been installed at the Venus site.

3. Ranging and Tracking System Development

a. Microwave system design performance. The 30-ft antenna at the Venus site will be used at S-band to make lunar and satellite radar measurements with a monostatic system. Detailed calculations of the system losses and gains have been made; these calculations indicate a radiated power of 70.81 dbm, an antenna gain of 42 db, a receiver noise temperature of 516°K for the main channel and 2542°K for the angle error channels, and a receiver threshold of -155.4 dbm.

b. Monostatic satellite and lunar radar synchronous sideband detector. The subsystem designed for odd-order keying sideband lock detection is ineffective on "even" even-order sidebands and requires a predetection bandwidth wider than is optimum for the main-receiver channel. Using a synthesized ramp in time signal four times the keying rate, a 12-db margin of immunity to carrier detection was achieved. Hardware complexity might be reduced by combining reference spectra prior to modulation; this method is being investigated.

c. Monostatic satellite and lunar radar receiver module development. In order to protect the receiver in a monostatic radar operating at a keying rate of several hundred cycles per second, a two-stage, solid-state limiter with a low-level loss of only 0.15 db has been procured. Final

approval awaits a resolution of an intermittent condition. A commercial mixer preamplifier has been selected which is smaller than the present JPL standard unit.

d. 10-kw S-band transmitter. The design of the 10-kw S-band transmitter is being improved in four different areas. A beam modulator at rates up to 1000 cps is required; but because of high costs and complexity as proposed by commercial concerns, it may have to be designed by JPL. The diode rectifier which provides cathode heating has been redesigned to withstand peak inverse voltages of 17 kv. The variable attenuators used in the RF forward and back power meter have been replaced with units which are relatively insensitive to temperature changes; in addition, they will be kept in a temperature controlled oven. The beam power supply has been tested with respect to conformity with specification, and its dynamic internal impedance has been measured.

e. Ranging coders. With an assumed maximum target range of 8000 km, the ranging code period is 53300/sec. For this period the optimal number of component codes is 5 and the optimal length is 9. However, because of the clock component and the relative ease by which certain sequences are generated, the component code lengths were selected to be 2, 7, 11, 15 and 23. Four coders will be procured: two for the range gate subsystem and two for target ranging.

f. Register display for Mod III stored program controller. Although it was not thought necessary to include internal register displays of the Mod III stored program controller, it has been found by experience that they are very useful. Consequently, a complete subsystem register display has been designed using primarily standard logic circuits. It has a 14-register capability with a provision for adding 10 additional.

4. Signal Generation and Control

a. Parametric frequency dividers. A parametric $\div 75$ frequency divider has been designed which reduces 35.625 Mc to 475 kc at a bandwidth of 2 Mc. Phase noise measurements indicate that the divider contributes less than 0.002 deg peak-to-peak.

b. PN generator frequency synthesizer. An experimental PN generator frequency synthesizer has been measured to have less than 0.1 deg peak-to-peak phase noise in $2B_L = 5$ cps. The PN generator had a full period

of 762 μ sec and a digit period of 6 μ sec. Some planned improvements are:

- (1) Use of better crystals to lower the system noise.
- (2) Reduction of the bandwidth in the 10-Mc IF amplifier.
- (3) Modification of the PN generator to obtain variable line spacing and finer frequency resolution.

5. S-Band Implementation for DSIF

a. TWM for DSIF. The traveling wave maser was installed in the Cassegrainian cone at the Pioneer Station; test measurements indicated all specifications were met except the gain stability which is still being investigated. A noise temperature of $9 \pm 1^\circ\text{K}$ was measured with a gain of 33 db. The prototype closed cycle refrigeration at the Venus site was recently serviced after operating for a total of 7000 hr.

b. Acquisition aid for DSIF. The basic design of the acquisition aid antenna has been completed and three units have been ordered.

6. Mesa Antenna Range

The remote transmitter site, "The East Mesa", of the new $\frac{3}{4}$ -mi antenna range is now complete. This site has a tower with provisions for mounting and positioning two 10-ft-diameter paraboloidal antennas. On the Mesa side of the range, a tower with an azimuth rotator for mounting spacecraft models has been installed. A control room and monitoring antennas have yet to be added.

D. Advanced Antenna System

1. Synopsis

The Advanced Antenna System consists of a 210-ft-diameter parabolic reflector antenna mounted so as to be positioned in azimuth and elevation. It includes a concrete cylindrical pedestal, a concrete and steel instrument tower, a structural steel alidade and alidade building, an azimuth hydrostatic thrust gearing, an azimuth radial shear bearing, an elevation and azimuth drive assembly, a hydraulic drive system, an electronic servo system, an elevation bearing assembly, a 210-ft reflector, an intermediate reference structure, a feed cone, a quadripod, and a subreflector.

2. Supporting Studies

a. Scale model feed for AAS. RF tests which have been done at X-band frequencies using the 30-ft antenna at the Venus site are now being extended to K_u -band frequencies. The Mesa antenna range will use K_u frequencies for tests of AAS model feeds.

b. Master Equatorial preliminary design analysis. A preliminary calculation of some of the possible errors in the Master Equatorial mounting yoke indicate a total error of about 6 sec of arc in both hour angle and declination. This includes consideration of gravity, bearing run-out, thermal gradient, and orthogonality.

c. Wind study program. Final checkout of the wind data recording instrumentation system has been completed; the system has been used since December 20, 1963. It was found necessary to ground the van, guys, and towers and to build a drag sphere calibration box for calibrating a sphere in a zero wind environment.

II. Tracking Station Operations

A. *Ranger 6*

1. *Goldstone*

From mid-December through February, Goldstone activities were primarily concerned with the *Ranger 6* mission, from prelaunch preparations to post-mission tracking data analysis. *Ranger 6* was launched at 15:49:09 GMT on January 30, 1964 and achieved lunar impact at 09:24:33 on February 2. During the mission, the Pioneer and Echo Stations experienced three successful tracking periods.

Preparations. Prior to the launch of *Ranger 6*, the Pioneer and Echo Stations participated in a series of tests involving the entire DSIF. Since both stations were to track the spacecraft simultaneously, all coordination problems between the two stations were resolved at this time. The tests performed were as follows:

- (1) DSIF compatibility test No. 5, December 18, 1963.
- (2) Command test, December 19, 1963.
- (3) DSIF-SFOF net integration test No. 1, January 7, 1964.

- (4) DSIF-SFOF net integration test No. 2, January 16, 1964.
- (5) DSIF-SFOF operational readiness test No. 1, January 21, 1964.
- (6) DSIF-SFOF operational readiness test No. 2, January 24, 1964.

All station personnel who would be involved in the *Ranger* mission participated in the above tests. Both normal and abnormal conditions were programmed into the tests to provide a thorough check of equipment operation, and to test personnel reactions during equipment failures and communications outages. Emergency procedures were utilized frequently and were correlated with normal procedures. Equipment and operational irregularities were resolved as they were discovered.

The equipment complement at Echo was completed with the installation on January 27 and 28 of a backup duplicate L-band transmitter exciter synthesizer. All subsystems then received a final thorough inspection, adjustment, and test. Questionable items were replaced or repaired and were performance tested for final integration.

Launch. Echo and Pioneer prepared for the launch with an early morning countdown on January 30. In the event of a nonlunar transfer and resulting Earth orbit, the two stations were prepared to track the spacecraft and record any transmitted telemetry. However, the lunar transfer occurred as scheduled, and both stations went to standby to wait the first view period approximately 10 hr later.

First view period. A second station countdown was performed the afternoon of January 30. The acquisition of the spacecraft occurred at 05:31:21 GMT, with all systems functioning normally as Goldstone's first view period began. The Echo first view period was considered the critical period, as the midcourse maneuver would be performed at that time. The station was advised by Net Control to expect a possible loss of lock with the spacecraft during this maneuver.

The midcourse maneuver command sequence began at 07:20 GMT. The antenna switchover command was sent at 08:20 GMT and completed at 08:23:25 GMT with no loss of signal. The midcourse command was sent at 08:30 GMT, and the final maneuver command was sent at 09:40 GMT. At 09:46:22 GMT, the maneuver was successfully completed. A momentary loss of signal occurred once during the maneuver. The received signal strength was -110.5 dbm and steady.

Second view period. The station countdown was performed the afternoon of January 31. Acquisition occurred at 05:37:40 GMT; all systems were functioning normally, and an uneventful view period was experienced. A defective teletype reperforator was repaired and returned to operation, and a data address experienced minor difficulty which was corrected by replacing a program card. These outages, which occurred during the early part of the view period, were quickly corrected and no further trouble was experienced.

Third view period. The station countdown was performed the afternoon of February 1. The receiver parametric amplifier failed prior to the countdown, and a new parametric amplifier klystron was installed and tuned. After being repaired, the measured gain was 19.7 db and the receiver was operating normally.

Acquisition for the third view period occurred at 05:36 GMT. All systems were functioning normally. The IF bandwidth for the video system was 2.9 Mc. The receiver signal level held steady at -118.5 dbm, with only tenths of a dbm change from acquisition to impact. Prior to sending the final commands, the video equipment bandwidth was again checked; there was no change.

The preparatory commands were sent to the spacecraft in 2-min intervals at 08:10 and 08:12 GMT. The first TV operational command was sent at 09:08 GMT and acknowledged by the spacecraft. When no video indication appeared, a second command was sent 7 min later at 09:15:29 GMT, and also acknowledged. The third and final command was sent at 09:20 GMT. Spacecraft telemetry indicated the command was received. There was no indication of video on either channel, and at 09:24:33 GMT the flight of *Ranger 6* ended with lunar impact.

Both Echo and Pioneer had tracked the three view periods with a minimum of equipment trouble. All systems performed within specifications and, except for the momentary loss of lock during the midcourse maneuver, the spacecraft was under constant surveillance while it remained above the Goldstone horizon.

a. General activities.

Echo Station. The microwave circuits between Goldstone and Pasadena, and between the Echo Station and Venus site (Ref. 1), are completed and operating.

A liquid nitrogen storage tank with the equivalent capacity of 120,000 ft³ of nitrogen gas has been installed near the maser trailer. The new tank provides for storage of a greater supply of liquid nitrogen; the liquid was formerly delivered in 50-liter containers.

Pioneer Station. The S-band installation (Ref. 1) is progressing on schedule. Installation of the transmitter and the maser have been completed. The transmitter has been operated at its rated 10-kw output using a water load. A signal generator was used in lieu of an S-band exciter to supply excitation for the transmitter during this test. The Cassegrainian cone and the hyperbola (Fig. 1) have been installed on the antenna. The maser cryogenic and the transmitter coolant lines have been installed on the antenna mounted equipment and have been operationally tested.

Pioneer S-band construction includes a folding collimation tower which will be used in conjunction with the acquisition-aid antenna mounted on the 85-ft antenna. The collimation tower foundation columns and pad, and the stowage position pad, have been poured. Preliminary excavation is in progress for the foundation footings of an interim prefabricated building (G-9) which will house the Pioneer S-band ground support equipment.

Venus site. The amplidyne (Fig. 2) and the 400-cps motor generator (Fig. 3) were moved to the hydromechanical building.

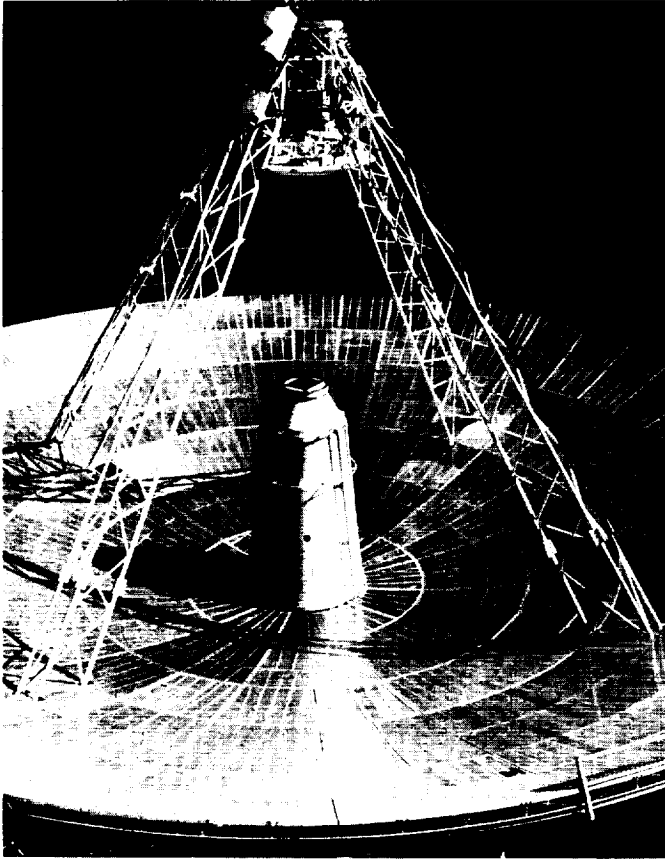


Fig. 1. S-band Cassegrainian cone and hyperbola



Fig. 2. Amplidyne at Venus site

Canberra instrumentation support. Aiding the implementation of the Canberra installation, personnel are being trained and equipment is being checked at Goldstone. A mockup duplicate of the planned instrumentation equipment for the Canberra-Madrid projects is in the

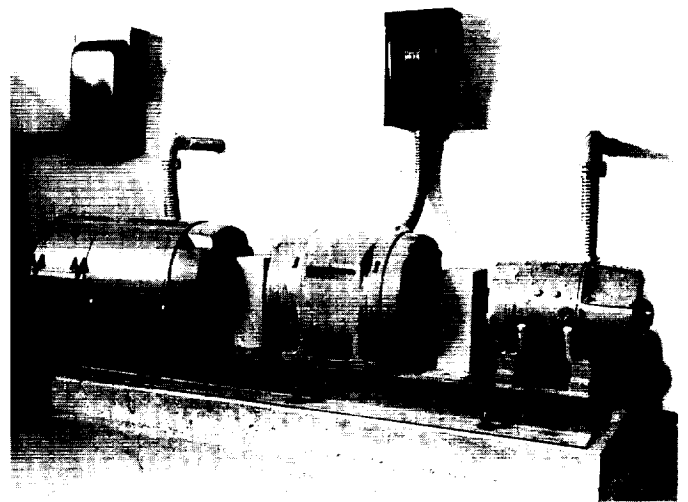


Fig. 3. 400-cps motor generator at Venus site

process of being installed at the Pioneer Station. Currently, two instrumentation engineers from Canberra are at the station assisting in the installation, and are becoming familiar with the equipment and procedures. As equipment arrives for operational checkout, it is tested and adjusted prior to overseas shipment.

2. DSIF Tracking Performance for Ranger 6 Mission

a. Mission history. The *Ranger 6* spacecraft was launched from Cape Kennedy, Florida, at 15:49:09.092 Greenwich Mean Time (GMT: hr, min, sec) on January 30, 1964. At the time of first *Agena* cutoff, the *Agena B-Ranger 6* spacecraft was in a circular parking orbit which was terminated by second *Agena* ignition. Second *Agena* cutoff marked the time of injection into the lunar transfer orbit.

Agena-spacecraft separation occurred, and *Ranger 6* continued on a lunar impact trajectory. Event blips B-2-4 and B-2-1 Number 4, observed by Woomera at 16:50:06 and 16:52:01.8, respectively, indicated solar panel extension and initiation of the Sun acquisition sequence. Earth acquisition was confirmed by observance of event blip B-2-1 Number 5 at 19:20:02 by Woomera.

The first ground commands were sent to the spacecraft by Johannesburg on January 30. Two "clear commands" (RTC-0) were sent at 21:08:00 and 21:10:00. These were followed by the spacecraft antenna changeover command (RTC-3) sent at 21:12:00. This last command switched the spacecraft transmitter from the omni-antenna to the

¹All other times referred to will be GMT unless otherwise specified.

high-gain antenna. A rise in received signal strength and the observance of a B-20 event blip at 21:12:40 confirmed the antenna switchover.

Preliminary spacecraft orbit computations indicated that a trajectory correction was required to achieve lunar impact in the preselected target area. The corrective maneuver commands were sent to the spacecraft by the Echo Station (DSIF 12) starting at 07:20:00 on January 31. These commands, with their associated times, are listed in Table 1. All guidance commands were correctly received on board the spacecraft, changeover was made from the high-gain antenna to the omni-antenna, and the midcourse maneuver execute command was initiated at 08:30:00.

Midcourse maneuver motor ignition occurred at 08:57:08 and terminated at 08:58:17. The two-way doppler shift during the maneuver and the time duration of the shift indicated that the midcourse maneuver had been executed as planned. After the maneuver the spacecraft, responding to on board commands, reacquired first the Sun then the Earth. Echo then sent the command to switch the spacecraft transmitter from the omni-antenna to the high-gain antenna (RTC-3).

Ranger 6 was again in a cruise mode proceeding on a lunar impact trajectory. Based on subsequent orbital computations using post-midcourse tracking data, it was decided that a terminal maneuver would not be required. At 09:08:00 on February 2, Echo sent the backup command (RTC-7) for activating the TV subsystem warmup. Two additional RTC-7 commands were sent to the spacecraft in what proved to be a futile attempt to obtain some video or engineering telemetry data. *Ranger 6* impacted the lighted side of the lunar surface at the Sea of Tranquility at 09:24:33.145² on February 2. Total flight time was 65^h35^m24^s.053.

b. Tracking performance. The DSIF stations tracked the *Ranger 6* spacecraft from shortly after injection into the lunar transfer orbit at 16:16:48.40 on January 30, 1964 until lunar impact at 09:24:33.145² on February 2, 1964. Actual tracking periods for each station are given in Table 2.

In general, the quality of the tracking data received from the DSIF Stations was excellent. A summary of the tracking data used in the orbit determination program (ODP), together with the noise statistics, is presented in Table 3.

²Impact time recorded at station; this does not include light time correction.

Table 1. Ground commands sent to *Ranger 6* by DSIF Stations

Command	Initiated (date/GMT)	Verified ^a (GMT)	Sent by DSIF Station	Associated T/M event blips recorded at station
RTC-0	30/21:08:00	21:08:39	51	N.A.
RTC-0	30/21:10:00	21:10:40	51	N.A.
RTC-3	30/21:12:00	21:12:39	51	Channel B-20 at 21:12:40
RTC-0	31/07:20:00	07:20:39	12	N.A.
RTC-0	31/07:22:00	07:22:39	12	N.A.
SC-1	31/07:24:00	07:24:39	12	Channel B-20 at 07:24:40
SC-2	31/07:26:00	07:26:39	12	Channel B-20 at 07:26:40
SC-3	31/07:28:00	07:28:39	12	Channel B-20 at 07:28:40
RTC-3	31/08:20:00	08:20:39	12	Channel B-20 at 08:20:40
RTC-4	31/08:30:00	08:30:39	12	Channel B-20 at 08:30:40
RTC-0	31/09:40:00	09:40:39	12	N.A.
RTC-0	31/09:42:00	09:42:39	12	N.A.
RTC-3	31/09:44:00	09:44:39	12	Channel B-20 at 09:44:40
RTC-0	2/08:11:00	08:11:39	12	N.A.
RTC-0	2/08:13:00	08:13:39	12	N.A.
RTC-7	2/09:08:00	09:08:39	12	Channel B-20 at 09:08:42
RTC-7	2/09:15:29	09:16:08	12	Channel B-20 at 09:16:11
RTC-7	2/09:19:21	09:20:00	12	Channel B-20 at 09:20:03

^aVerified by ground station read—write—verify (RWV) system.

Preliminary analysis of the angular data indicates that the correction polynomials used to describe the systematic angular pointing error are not adequate. This is evidenced by an approximate bias of 0.04 deg remaining after the corrections had been applied to the inflight data. The reason for this discrepancy is that the correction polynomials are based on a series of optical star tracks which will describe the optical error. But since the optical axis and the RF axis do not necessarily coincide, the remaining angular error may be attributed to RF error. A new method of determining correction polynomials based on celestial radio source tracks is required.

Angular residuals, (ODP-computed values minus observed values) are, with exception of the Johannesburg hour angle, comparable with those observed on previous missions. In the Johannesburg hour angle residuals, there appears to be a general degradation which was first

Table 2. Nominal^a view periods versus actual tracking periods at DSIF Stations

Date	DSIF Station	Nominal rise (GMT)	Nominal set (GMT)	Nominal view period	Acquisition by station	Loss of signal by station	Actual view period
January 30, 1964	51	16:19:19	16:36:24	00 ^b 17 ^m 05 ^s	16:19:44	16:42:00	00 ^b 22 ^m 16 ^s
	41	16:36:22	23:27:23	06 ^b 51 ^m 01 ^s	16:33:53	23:53:02	07 ^b 19 ^m 09 ^s
	51	18:43:20	07:07:13 ^b	12 ^b 23 ^m 53 ^s	18:43:25	07:30:51	12 ^b 47 ^m 26 ^s
January 31, 1964	11	05:56:56	16:43:42	10 ^b 46 ^m 46 ^s	05:58:38	17:07:00	11 ^b 08 ^m 22 ^s
	12	05:56:56	16:43:42	10 ^b 46 ^m 46 ^s	05:31:21	17:06:50	11 ^b 35 ^m 29 ^s
	41	12:48:46	00:05:16 ^b	11 ^b 16 ^m 30 ^s	12:25:00	00:33:00	12 ^b 08 ^m 00 ^s
	51	20:13:14	07:26:08 ^b	11 ^b 12 ^m 54 ^s	20:12:20	07:51:04	11 ^b 38 ^m 44 ^s
February 1, 1964	11	06:02:53	17:06:41	11 ^b 03 ^m 48 ^s	06:08:45	17:25:50	11 ^b 18 ^m 41 ^s
	12	06:02:53	17:06:41	11 ^b 03 ^m 48 ^s	05:37:40	17:25:50	11 ^b 17 ^m 05 ^s
	41	13:08:21	00:10:41 ^b	11 ^b 02 ^m 20 ^s	12:46:10	00:37:30	11 ^b 51 ^m 20 ^s
	51	20:26:14	07:30:00	11 ^b 03 ^m 46 ^s	20:27:23	07:53:37	11 ^b 26 ^m 14 ^s
February 2, 1964	11	06:01:56	09:24:33	03 ^b 22 ^m 37 ^s	06:10:55	09:23:33.1 ^c	03 ^b 13 ^m 38 ^s
	12	06:01:56	09:24:33	03 ^b 22 ^m 37 ^s	05:36:00	09:24:33.145 ^c	03 ^b 13 ^m 38 ^s
^a Based on 5-deg elevation angle. ^b Set occurs on next day after rise. ^c Time of lunar impact observed at stations.							

Table 3. Summary of DSIF tracking data used in Ranger 6 spacecraft orbit computations

Phase	DSIF Station	Data type	Beginning date/time	Ending date/time	Number of points	Standard deviation	Root mean squared (rms)
Premidcourse ^a maneuver	12	CC3 ^b	31/06:35:22	31/06:46:32	31	0.0229 cps	0.0542 cps
	41	CC3 ^b	30/16:59:32	30/20:34:32	136	0.0259 cps	0.0283 cps
	41	HA	30/16:47:02	30/23:01:02	340	0.0139 cps	0.0373 deg
	41	Dec	30/16:47:02	30/23:01:02	342	0.0072 cps	0.0210 deg
Premidcourse maneuver	51	HA	30/16:21:37	30/16:30:47	108	0.0227 deg	0.0521 deg
	51	Dec	30/16:21:37	30/16:30:47	108	0.0228 deg	0.0231 deg
	51	CC3 ^b	30/16:26:49	31/06:20:32	485	0.0361 cps	0.0374 cps
	51	HA	30/19:15:02	31/06:33:02	577	0.0143 deg	0.0244 deg
	51	Dec	30/19:15:02	31/06:33:02	576	0.0105 deg	0.0109 deg
Postmidcourse ^c maneuver	11	CC3 ^d	31/09:07:32	31/16:00:32	396	0.0237 cps	0.0237 cps
	11	CC3 ^b	1/07:42:32	1/17:28:32	571	0.0146 cps	0.0154 cps
	12	CC3 ^b	31/09:06:32	31/16:00:32	384	0.0146 cps	0.0152 cps
	12	CC3 ^b	1/06:12:32	1/17:24:32	665	0.0142 cps	0.0142 cps
	41	CC3 ^b	31/16:08:32	31/21:03:32	230	0.0310 cps	0.0317 cps
	41	CC3 ^b	1/17:36:32	1/20:38:32	161	0.0587 cps	0.0611 cps
	51	CC3 ^b	31/21:06:32	1/05:55:32	397	0.0310 cps	0.0310 cps
	51	CC3 ^b	1/23:55:32	2/01:54:32	100	0.0467 cps	0.0468 cps
^a Refers to last premidcourse maneuver orbit. ^c Refers to fourth postmidcourse orbit CC. ^b Two-way doppler data, one station. ^d Pseudo two-way doppler, two stations.							

noted in the recent *Atlas-Centaur* (AC-2) mission. This is still being investigated.

Preliminary evaluation of the two-way doppler data indicated very good agreement between the residuals, ODP-computed values minus observed values, observed on this mission and previous missions. A good example of the reduction in doppler noise obtained by using the frequency synthesizer rather than the voltage controlled oscillator (VCO) may be seen by comparing the noise statistics of Echo data on January 31 and February 1.

TDA activities. During missions, the Tracking Data Analysis group (TDA) is a member of the Flight Path Analysis and Command group. Its primary real-time purpose is to monitor and evaluate DSIF tracking performance, and to assist the ODP group in interpreting and utilizing the tracking data.

The following specific functions were performed by TDA during the *Ranger 6* mission.

- (1) Inputs were prepared for the Tracking Data Editing Program (TDEP) utilizing information from

tracking data, station reports, and information obtained over the voice line to the stations.

- (2) At the request of TDA, seven sets of tracking predictions were generated, verified, and sent to the DSIF Stations. TDA is also responsible for deciding whether the AMR predictions are accurate, and whether they should be used instead of the pre-flight nominal predictions. The Woomera and Johannesburg look angles provided by AMR were plotted on preprepared station stereographic maps containing trajectories for standard launch azimuths. Based on the results, it was decided to use the nominal predictions for a launch azimuth of 95 deg.
- (3) TDA personnel assisted in the real-time orbital computations by providing correct ground station frequencies, specifying rejection criteria, and isolating areas of suspected bad data. To detect the bad data areas, a real-time Tracking Data Monitoring Program was operated at JPL. Also, real-time analysis of Echo data was performed by TDA personnel at Goldstone.

Reference

1. "Equipment Installation," *Space Programs Summary No. 37-25*, Vol. III, pp. 7-8, Jet Propulsion Laboratory, Pasadena, California, January 31, 1964.

III. Engineering Developments

A. Systems Engineering

1. Project Engineering

a. Surveyor. The Hughes Aircraft Company test report on the compatibility of the command and data console (CDC) and the DSIF feasibility model receiver (Ref. 1) has been released. The report contains a full description of the compatibility tests together with recommendations for modifications and changes to both the CDC and the DSIF feasibility model receiver. As a consequence of changes to the DSIF receiver design, the interface with the CDC has been revised. Compatibility between the DSIF receiver and the CDC has now been achieved, and the interface document has been amended accordingly. The revised Project Document No. 6 was scheduled for release in February 1964.

DB Allocation and Telecommunications Margin Summary reflecting the most recent changes in the DSIF and spacecraft systems for the *Surveyor* DSIF telecommunications subsystem has been received from Hughes Aircraft Company and is undergoing review.

b. Pioneer. A JPL-prepared description of the DSIF interface requirements with the Ames *Pioneer* solar probe program has been prepared and is being reviewed at JPL.

This document will be combined with a Space Flight Operations Facility (SFOF) interface document and will constitute, along with Ames inputs, a *Pioneer*-Deep Space Net interface document.

Tentative frequency allocations of DSIF Channels 6 and 7 have been released to the *Pioneer* Project. Dual receivers on the spacecraft, which can be frequency addressed separately, require the allocation of two transmit and two receive frequencies. Allocation of a third frequency is under consideration for one-way, noncoherent reception from the spacecraft. Trajectory studies indicate that there is a period when the *Pioneer* spacecraft will cross the Earth-Sun line with consequent loss of communications capability. A study of solar noise contributions throughout this period was prepared for the Ames *Pioneer* project office. Studies of the DSIF automatic gain control (AGC) response characteristics of the ground receiver have been forwarded to Ames Research Center as an input to its spacecraft orientation maneuver design.

The present *Pioneer* Project development schedule indicates that telecommunications feasibility tests should be conducted at Goldstone between November 15 and December 15, 1964. This schedule is presently under review, as there is a possible conflict with the *Mariner C* launch window.

c. *Ranger Block III.* A rough draft of the revised version of the functional specification for the *Ranger Block III* L-band radio and ground tracking systems commitment was prepared. The revision provides updated information on the DSIF L-band configuration and commitments.

This project provided the DSIF manager with systems advisory support during *Ranger 6* operations. A series of common view, equal range, signal level measurements was made during the course of *Ranger 6* activities to determine the relative accuracies of signal level recordings between the various stations. This data is now being analyzed, and the results will be reported in SPS 37-27, Vol. III.

d. *Mariner C.* Plans are under preparation for a compatibility test of the *Mariner C* Proof Test Model (PTM) and the DSIF. Tentative plans call for bringing the PTM spacecraft to Goldstone for complete communications compatibility tests, and for SFOF-DSIF-spacecraft operational tests. These tests will probably be conducted in early June of 1964.

Present schedules provide for DSIF *Mariner C* readiness at all stations by August 1, 1964. The *Pioneer* Station at Goldstone will be operational by May 15 with the full S-band system. Johannesburg will be operational by July 15 with the L- to S-band conversion system and Woomera by July 20, also with the L- to S-band conversion system.

2. Systems Analysis

a. *Technical Memorandum 33-26.* The DSIF technical manual, TM 33-26, is being completely revised and updated to fully describe the new S-band system. Vol. 1 of the new manual will provide a comprehensive description of the Deep Space Instrumentation Facility for high-level, nontechnical personnel. Vols. II and III will contain theory of operations at the system and subsystem levels. A contract has been awarded to Volt Technical Corporation of Van Nuys, Calif., for the writing, illustration, and production of the publication.

b. *L-Band RF system calibration.* A program is underway to provide more accurate information on DSIF performance in the areas of antenna gain, signal level, and system noise temperature calibration. This program is being conducted in three phases:

- (1) Phase 1, which is just being completed, consists of the accumulation of past information on the calibration of the DSIF net in an attempt to determine

what the actual performance and tolerances are at present. Preliminary gain calibration tests of the antenna and receiving system at the Echo Station were conducted, and results are presently undergoing analysis.

- (2) Phase 2 of this program involves the recalibration, according to standardized procedures, of the RF systems throughout the net with an attempt to improve performance and reduce tolerances that are now presently reported.
- (3) Phase 3 involves the conduct of periodic standardized testing of critical RF parameters at each station and will result in the publication of a standard DSIF performance chart maintained up-to-date on a monthly basis.

c. *Spacecraft Monitoring Station.* A preliminary systems design has been undertaken for DSIF 71, the Spacecraft Monitoring Station at the Atlantic Missile Range (AMR). This station will essentially provide last-minute DSIF spacecraft compatibility tests to assure that the spacecraft performance is nominal and properly mates with the DSIF equipment designed to support it. The primary purposes of this station are to:

- (1) Provide system verification of spacecraft telecommunications RF parameters.
- (2) Provide verification of the command system and telemetering system operability and thresholds.
- (3) Verify the ranging system performance.
- (4) Provide postinjection DSIF Stations with spacecraft frequency information.
- (5) Provide a DSIF-spacecraft interface for prelaunch SFOF-centered spacecraft operational tests.

To meet the above requirements, it will be necessary to provide a facility which is essentially equivalent to a DSIF Station, except that the facility will employ only a 10-ft antenna and will not be required to obtain tracking information. All other subsystems will be identical to those used in a standard DSIF Station. The facility must accommodate all special equipment necessary for support of the various spacecraft programs at the AMR.

d. *Suitcase telemetry study.* A feasibility study and prototype development program was conducted for a portable telemetry station which can be quickly transported to remote sites and manned by a two-man crew.

The systems concept is that several of these stations are to be employed to cover the trajectory sequence from near injection to first DSIF acquisition, thus providing critical telemetry coverage in regions not covered by other stations. Considerations of trajectory coverage, communications thresholds, acquisition requirements, location requirements, and operational feasibility were studied under this program. An operational test of the system will be performed covering the *Mariner C* mission in October–December 1964.

The main purpose of the study was to determine what antenna beamwidth would be necessary to ensure acquisition of a spacecraft in a circular parking orbit at an altitude of approximately 100 nm, using an antenna which tracks in azimuth at a fixed, but optimum, elevation angle. In addition, some insight was needed into the magnitude of the angular tracking error which would be expected, and information was needed concerning coverage and other station parameters for the proposed station locations.

The study was divided into two parts: (1) a trajectory analysis and (2) an antenna axis investigation. The trajectories used were those for the parking orbit of *Mariner 2* with launch azimuths of 93 through 108 deg and for nominal booster burn. Because of limited computer time, only five of the 12 proposed stations were chosen for analysis. These stations were:

- (1) Ship, latitude 13°N , longitude 42°W .
- (2) Praia, Cape Verde Islands.
- (3) Fernando de Noronha, Brazil.
- (4) Cabinda, Africa.
- (5) Fort Dauphin, Malagasy Republic.

Parking orbit data were not available for nominal launch azimuths of 90, 111, and 114 deg, nor for $3\text{-}\sigma$ dispersions caused by short or long booster burn.

Trajectory analysis. A trajectory program written for the IBM 1620/SDS 920 computer was used to perform the trajectory analysis (Ref. 2). Briefly, the program integrates the equations of motion (of a spacecraft) using a variable step size Runge–Kutta integration scheme. Integration is started at injection epoch with the Earth-referenced, space-fixed, cartesian components of the position and velocity vectors. Results obtained were:

- (1) Station view periods versus launch azimuth.
- (2) Maximum elevation angle versus launch azimuth for each station (Figs. 1 through 5).

- (3) View periods versus maximum elevation angle for station horizon masks of 0, 2, 7 deg, and for a probe–station angle of 120 deg with a 0-deg horizon mask (Fig. 6).

- (4) One-way doppler shift and doppler shift rate at 2295 Mc for launch azimuths of 96 and 99 deg for a typical station (Figs. 7 and 8).

Antenna axis investigation. The purpose of the antenna axis investigation was to determine the angular error for

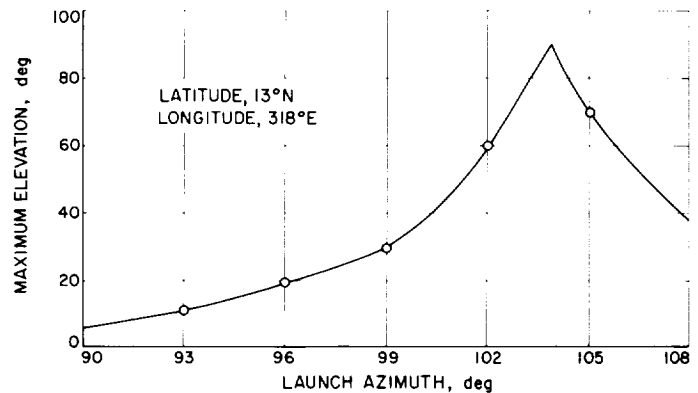


Fig. 1. Maximum elevation angle versus launch azimuth, Station 1

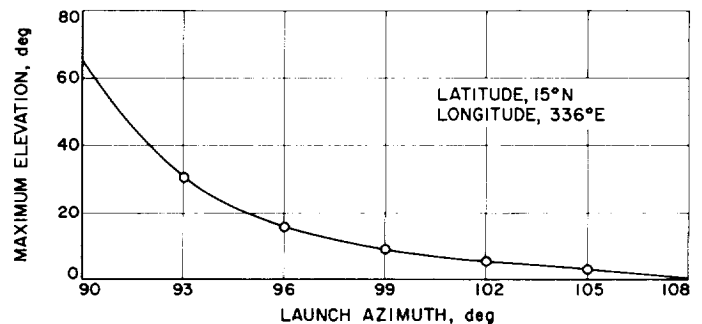


Fig. 2. Maximum elevation angle versus launch azimuth, Station 2

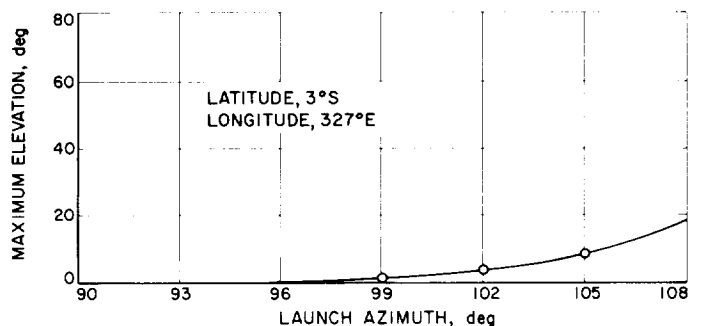


Fig. 3. Maximum elevation angle versus launch azimuth, Station 3

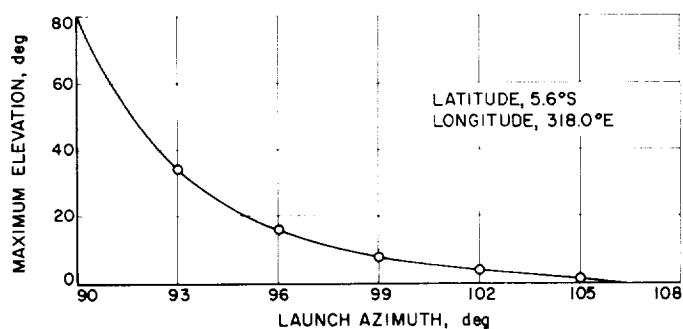


Fig. 4. Maximum elevation angle versus launch azimuth, Station 4

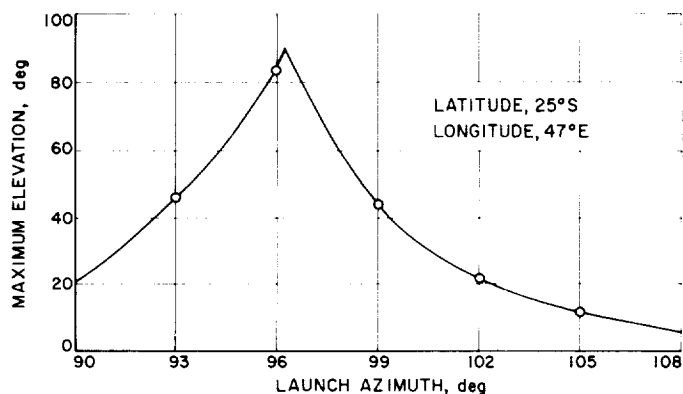


Fig. 5. Maximum elevation angle versus launch azimuth, Station 5

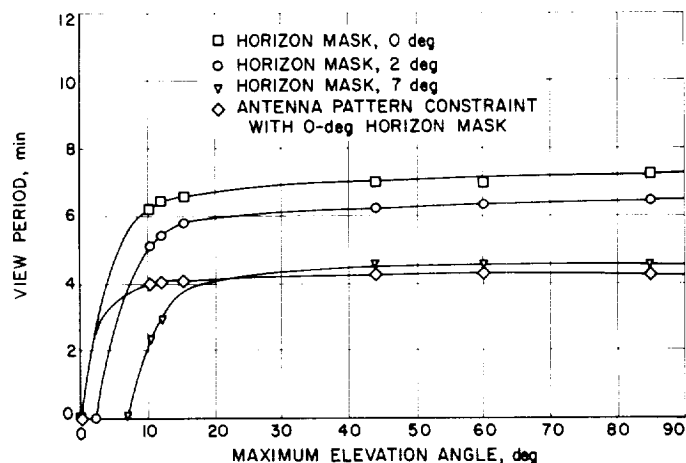


Fig. 6. View period versus maximum elevation angle, nominal station

an azimuth-elevation antenna mount. It was assumed that the mount would be rotated in one plane only; i.e., the elevation plane would be fixed at a given angle (depending on launch azimuth) and the mount would be

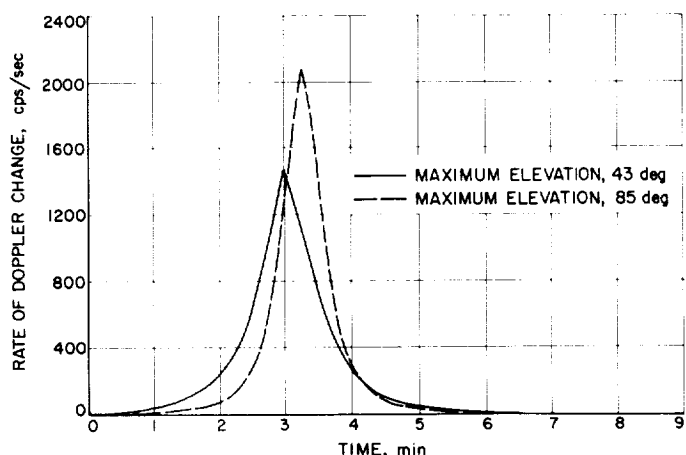


Fig. 7. Rate of doppler shift versus time, Station 5

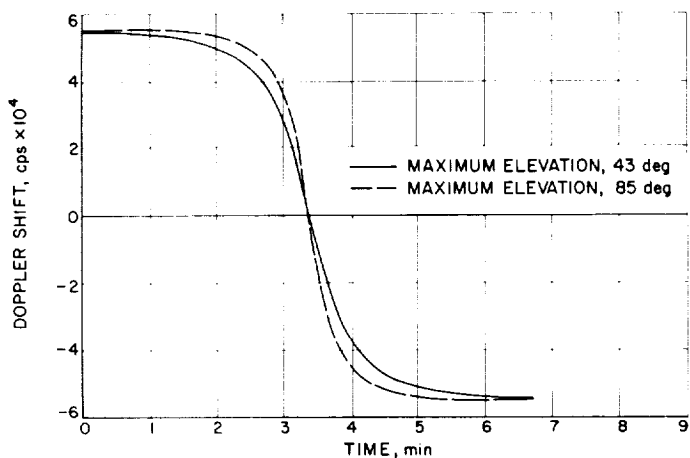


Fig. 8. S-band doppler shift versus time, Station 5

rotated through the azimuth plane. It was also assumed that it was possible to tilt the azimuth plane from 0 to 90 deg. In other words, the antenna mount would have two degrees of freedom (azimuth and elevation), one of which would be preset to some value for a given trajectory.

In the computational procedure, azimuth (σ_m) was rotated to the value corresponding to the maximum elevation angle. The azimuth plane was then tilted to the maximum elevation angle minus $\Delta(\gamma_m)$. The quantity $\Delta(\gamma_m)$ is an empirically determined value, with a magnitude of approximately 2 deg, which will minimize the elevation error when tracking in a tilted azimuth plane. The angular tracking error in elevation, $\Delta\gamma_i$, was computed as follows:

$$\Delta\gamma_i = \tan^{-1} \left\{ \frac{v_i}{[(\lambda'_i)^2 + (\mu'_i)^2]^{1/2}} \right\}$$

where

$$\begin{bmatrix} \lambda'_i \\ \mu'_i \\ \nu'_i \end{bmatrix} = \begin{bmatrix} \cos \sigma'_i & \sin \sigma'_i & 0 \\ -\sin \sigma'_i & \cos \sigma'_i & 0 \\ 0 & 0 & 1 \end{bmatrix} \begin{bmatrix} \cos \gamma_m & 0 & \sin \gamma_m \\ 0 & 1 & 0 \\ -\sin \gamma_m & 0 & \cos \gamma_m \end{bmatrix} \\ \times \begin{bmatrix} \cos \sigma_m & \sin \sigma_m & 0 \\ -\sin \sigma_m & \cos \sigma_m & 0 \\ 0 & 0 & 1 \end{bmatrix} \begin{bmatrix} \cos \gamma_i \cos \sigma_i \\ \cos \gamma_i \sin \sigma_i \\ \sin \gamma_i \end{bmatrix}$$

where

σ_m = azimuth angle in the local horizontal plane of maximum elevation angle

γ_m = maximum elevation angle minus $\Delta\gamma_m$ in the local horizontal plane

$$\sigma'_i = \tan^{-1} \left(\frac{\mu_i}{\lambda_i} \right)$$

where

$$\begin{bmatrix} \lambda_i \\ \mu_i \\ \nu_i \end{bmatrix} = \begin{bmatrix} \cos \gamma_m & 0 & \sin \gamma_m \\ 0 & 1 & 0 \\ -\sin \gamma_m & 0 & \cos \gamma_m \end{bmatrix} \begin{bmatrix} \cos \sigma_m \sin \sigma_m & 0 \\ -\sin \sigma_m \cos \sigma_m & 0 \\ 0 & 0 & 1 \end{bmatrix} \\ \times \begin{bmatrix} \cos \gamma_i \sin \sigma_i \\ \cos \gamma_i \sin \sigma_i \\ \sin \gamma_i \end{bmatrix}$$

The above computations were performed for elevation angles ranging from 10 through 85 deg. Results indicated that the maximum elevation error which would occur, when tracking in azimuth only, was less than 5 deg for each of the maximum elevation angles considered.

Based on these results (Figs. 9 through 11), it appears that a 10-deg antenna beamwidth may be sufficient. However, before a definite conclusion can be reached, the effect of a long or short booster burn must be considered.

3. System Integration and Engineering

a. S-band system integration. Layout designs have been completed for the DSIF antenna cage, the equipment location requirements in the S-band wing of the Pioneer Station, and the equipment installation in the Pioneer staging area Butler building. With these critical layouts completed, cable lengths can now be determined.

Work is continuing on the intersubsystem electrical signal compatibility design, and selection of groups of conductors into cables is now being conducted.

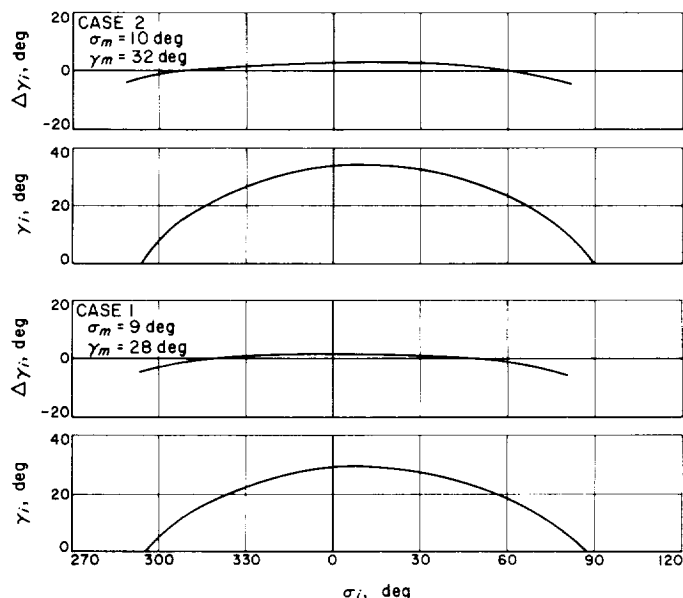


Fig. 9. Antenna axis study, suitcase telemetry, elevation angle and elevation error versus azimuth, Cases 1 and 2

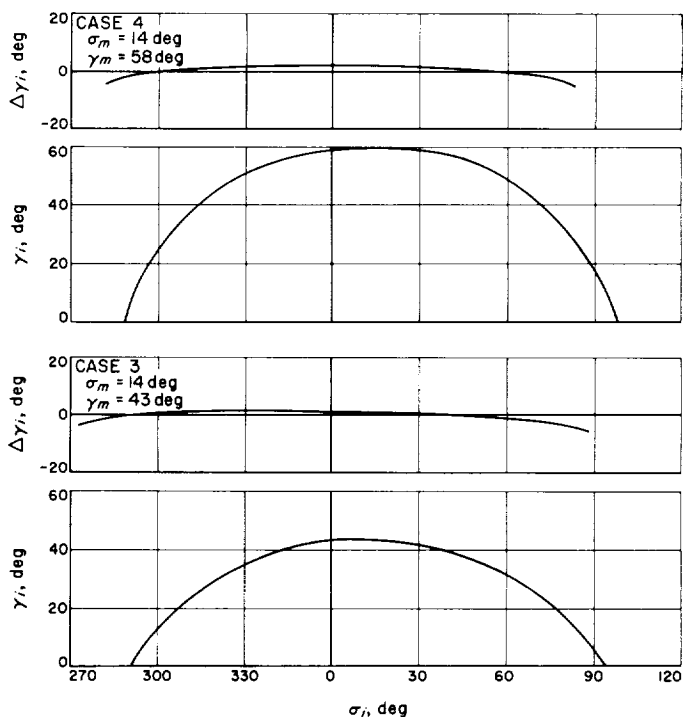


Fig. 10. Antenna axis study, suitcase telemetry, elevation angle and elevation error versus azimuth, Cases 3 and 4

Preliminary design work has been completed and a proposal submitted for incorporation of a mission-oriented equipment patching system for incorporation into the DSIF Stations.

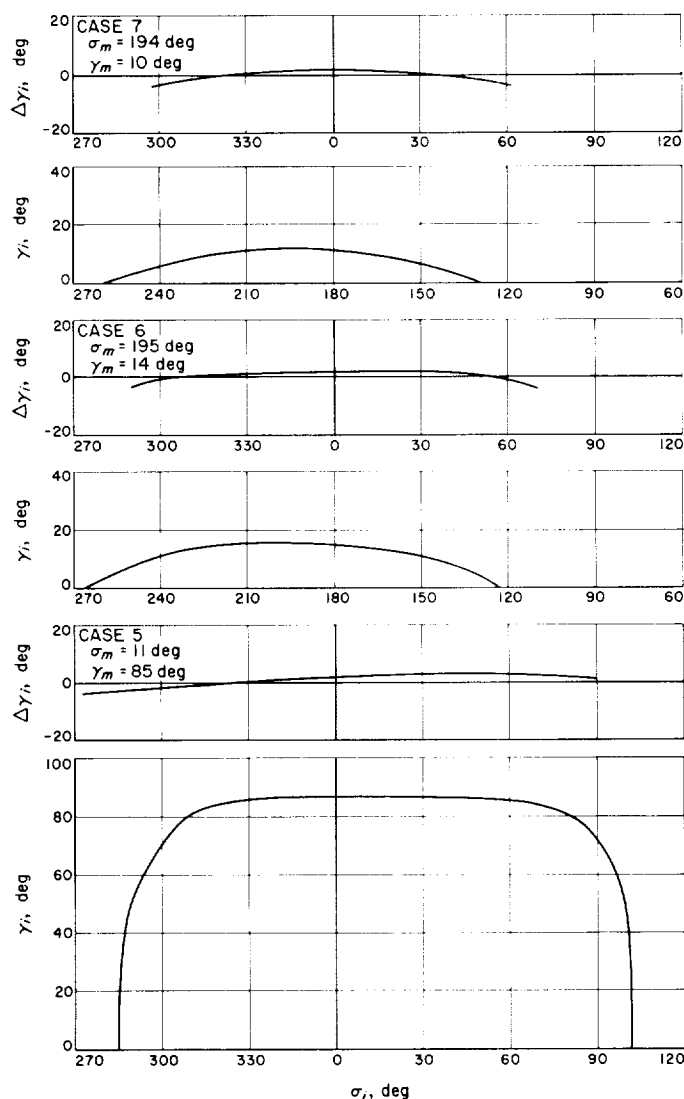


Fig. 11. Antenna axis study, suitcase telemetry, elevation angle and elevation error versus azimuth, Cases 5, 6, and 7

Specification 8907, a general requirements specification for DSIF equipment, is being updated, and all appropriate reference subspecifications will be listed therein. Work is progressing on the indentured S-band system specification lists for both support specifications and the actual equipment specifications. A new specification is being prepared as a control document for the preparation of test plans for subsystem testing.

Acceptance test procedures for the Goldstone Duplicate Standard 1964 S-band systems and subsystems are now being written; as of February 1, approximately 50% of the subsystems tests have been completed in rough draft form.

b. Spacecraft test facility. A plan for the implementation of a general spacecraft test facility to be located at the Goldstone antenna range has been produced. The plan proposes the use of a radio-transparent igloo at the Goldstone antenna range to house the spacecraft, which will then be capable of communicating with the Pioneer facility over a radio path via the Pioneer collimation tower. The path loss between the antenna range and Pioneer Station has been measured at approximately 194 db. This approximates the attenuation of an Earth-Moon path and should be satisfactory for most tests. A supplier for the radio-transparent igloo is soon to be chosen. Additional facilities for support equipment are being considered.

c. Radio frequency interference (RFI). To substantiate the low RFI factor of fluorescent lighting at the DSIF Stations, a series of measurements was made of the radio frequency radiation from typical fluorescent light installations. These measurements showed that the radiation from properly designed and installed fluorescent lights is generally below the relevant RFI specification for the DSIF system. However, it was decided that further measurements were required, and plans were formulated for outfitting the DSIF Stations with both fluorescent lights and emergency incandescent lighting in case the fluorescent lights should prove to be a significant source of interference.

B. Tracking Data Monitoring Program

1. Program Improvements

The Tracking Data Monitoring Program is presently operational and was used extensively by the Tracking Data Analysis facility during the *Ranger 6* mission. The purpose of this program is to provide real-time reduction of tracking data received from the DSIF Stations.

The hardware implementation, which includes teletype and plotter interface electronics, has been completed, and the equipment has been operating satisfactorily.

Use of the program under operational conditions has brought about a more thorough understanding of problem areas within the program. As a result, modifications

are being made which will allow the program to be used in a much more efficient manner. Also, the use of the program through an entire mission has brought to light a few program bugs which include logic errors and precision problems.

To use the program in a more efficient manner, the number of input parameters will be canned so that a number of them will become constants within the program. This will allow the program to be initialized by the operator in much less time and will also reduce the chances of input errors.

Another type of modification which is being implemented is the addition of various output routines. These options allow typewriter outputs of various computed quantities, such as average first or second differences, predicted doppler, and raw data inputs, and will be flexible enough to allow rapid changes of the program so that almost any computed quantity can be output upon request.

A scheme to reject blunder points had been coded prior to the *Ranger 6* mission, but since program checkout was not completed in time, this section of the program was not operational.

During the mission, it was found to be advantageous to output received doppler in cycles per second rather than continuous count during critical portions of the flight. Therefore, a program modification was initiated to output these values with the appropriate time labels. It was also found that if the plotter was not operational, the residuals from the comparison program were lost. Coding is presently being performed which will allow a standard residual output to the typewriter in case of plotter failure.

The real-time portion of the Data Condition Code (DCC) Log Program has been completed and is operational. It was not used for the *Ranger 6* mission because the nonreal-time program, which reads the tape generated by the DDC Log Program, has not been completed.

Used in conjunction with the monitoring program is a prediction program written for the SDS 920 computer. This program computes doppler predictions for a given station. Input parameters include the pertinent injection conditions, station number, and Greenwich Mean Time (GMT) for the beginning and end times of the prediction period. The method used for the prediction computation is described in Ref. 2.

The monitoring program is composed of the following three basic computational areas:

- (1) Comparison of predictions to received tracking data.
- (2) Computation of doppler variance.
- (3) Data Condition Code Log.

These three areas of the program are performed through use of an executive control program which initializes the various routines as needed, provides the necessary logic to check the incoming data, and provides the required input-output subroutines. Since all computation is dependent upon the receipt of tracking data, the program is essentially clocked by the interrupts received from the teletype input hardware. A basic flow diagram of the Read Teletype Data Program is shown in Fig. 12.

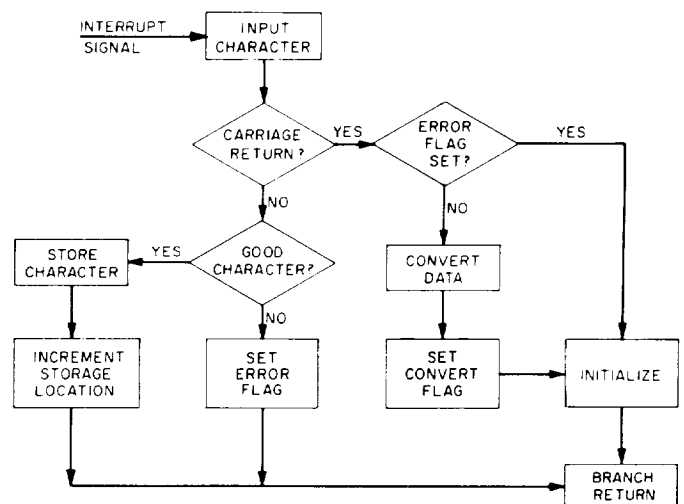


Fig. 12. Read Teletype Data Program, flow diagram

The Executive Control Program, after executing the basic initialization, waits for the Read Teletype Data Program to set the convert flag. A flow diagram of the Executive Control Program is shown in Fig. 13.

Fig. 14 shows a typical typewriter output computed during the *Ranger 6* mission. The first six quantities are input parameters required for the basic initialization. These quantities are:

Line 1 = epoch in seconds.

Line 2 = approximate time that first interpolation can occur.

Line 3 = TS = sample rate, seconds.

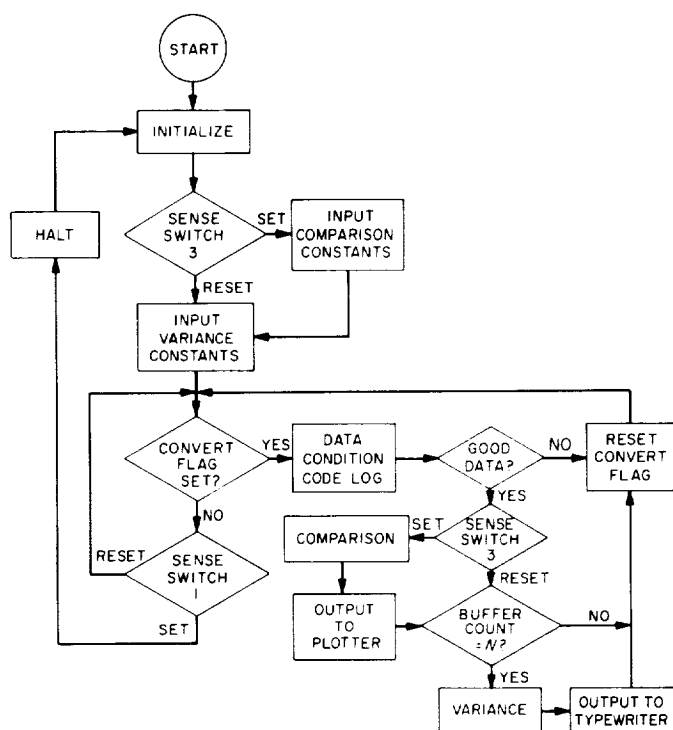


Fig. 13. Executive Control Program, flow diagram

Line 4 = ND = number of differences for variance computation.

Line 5 = P = constant for variance computation.

Line 6 = K = number of samples to use in the variance computation.

After the input parameters, there are four types of typical output formats. The first type is a printout of the form:

NOT ENUF DATA

This printout occurs when bad data (illegal format, illegal characters) causes a data skip, and insufficient samples are available to perform the variance computation.

The second type is a printout of the form:

055502 433.000

This printout consists of time (GMT) and the residual between actual and predicted doppler.

The third type is a printout of the form:

* 12 033 060002 2.85775 4.00000

This printout occurs when the variance computation is performed with less than K samples. It consists of station

820100.0
821000.0
TS:860.0000
ND:82.00000
P:80.00000
K:85.00000

NOT ENUF DATA

055502 433.000
055602 424.000
055702 430.000
055802 435.000
060002 435.000

* 12 033 060002 2.85775 4.00000

060102 271.000

NOT ENUF DATA

060902 105.000
061002 108.000

NOT ENUF DATA

061302 119.000
061402 124.000
061502 127.000
061602 131.000
061702 135.000

12 033 061702 .288673

061802 139.000
061902 142.000
062002 147.000

062102 151.000

062302 149.000

* 12 033 062302 .204124 4.00000

062402 163.000

062502 167.000

062602 172.000

062702 176.000

062802 180.000

12 033 062802 .235588

062902 185.000

063002 189.000

063102 193.000

063202 198.000

063302 202.000

Fig. 14. Typical typewriter printout sheet

identification, day of year, time, variance, and N, where N is the number of samples used in the variance computation.

The fourth type is a normal printout of the variance computation which is performed using the correct number of samples. It is of the form:

12 033 061702 .288673

Fig. 15 shows a typical plot of doppler residuals during the *Ranger 6* midcourse maneuver. This plot was produced on-line and shows the change in doppler observed by the Goldstone Tracking Station during the maneuver.

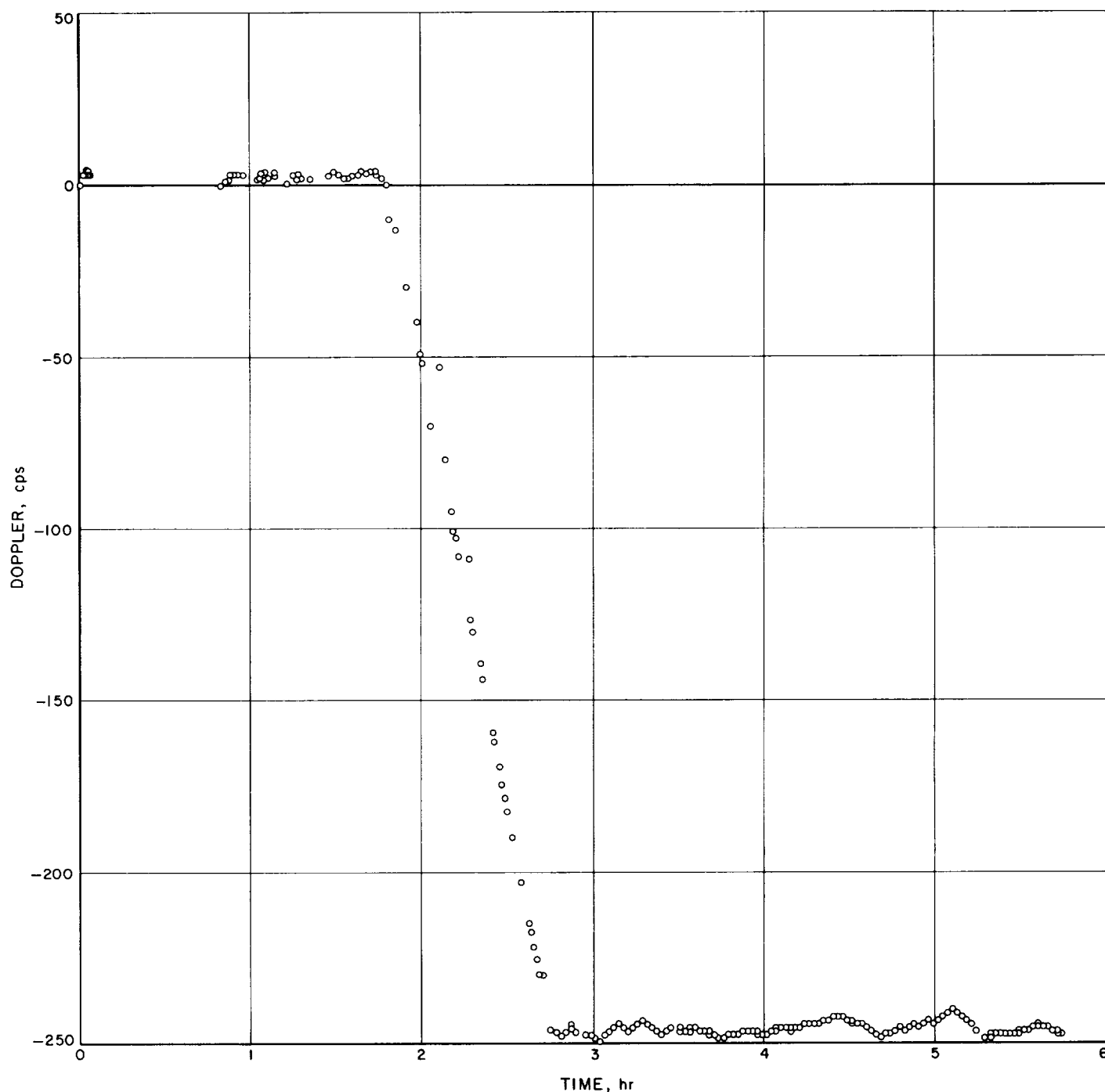


Fig. 15. Typical plot of doppler residuals, 1-sec sample at 5 sec/cm

2. A Trajectory-Independent Method of Estimating the Noise Spectral Density of Tracking Data

A continuing study of tracking data monitoring techniques has led to the examination of schemes for extracting and monitoring data noise by techniques which are

essentially independent of the trajectory or orbit determination program.

One such method of monitoring the tracking data is to monitor the spectral density of the noise on the data. This

approach is analogous to the approach used in analysis of variance, which was first proposed by Sir R. A. Fisher and has become a standard way to monitor statistically independent data. Monitoring the spectrum of the noise is a generalization of analysis of variance to correlated data. The basic assumption is that the noise $N(t)$ of the observed time series $X(t)$ is either covariance stationary or has been transformed so that it is covariance stationary. The observed time series $X(t)$ is then thought of as being the sum of two time series: one deterministic, $M(t)$, and the other purely random, $N(t)$, with mean zero and covariance stationary.

$$X(t) = M(t) + N(t) \quad (1)$$

$$E[X(t)] = M(t) \quad (2)$$

$$E[N(t)N(s)] = R(t-s) \quad (3)$$

Under the above assumptions, it is possible to estimate the spectrum of the noise, using a kernel in L_1 (space of all absolutely integrable functions) provided that there is a method of estimating $M(t)$ without changing the characteristics of the spectrum of the noise. The following scheme was chosen for extracting $M(t)$ from $X(t)$, i.e., $\hat{N}(t) = X(t) - \hat{M}(t)$. Assume that for periods of time less than nine sample points, the velocity of the spacecraft is constant. Then the observed data $X(t)$ can be represented as:

$$X(t) = A + B \cos(\omega_e t + \beta) + N(t) \quad (4)$$

where A is a function of the assumed constant spacecraft velocity, ω_e is Earth rate, and β is the phase of the Earth with respect to the spacecraft. This is rather a simple model and easy to fit in real-time, and for a reasonable range of sample rates will fit the physical problem well. Using the above model for $X(t)$, estimates of $N(t)$ can be produced by numerical differencing. Two estimates using second differences have been examined.

$$\begin{aligned} \hat{N}_1(t) &= X(t+4) - X(t-4) \\ &\quad - 2 \sin(2\omega_e) [X(t+2) - X(t-2)] \end{aligned} \quad (5)$$

$$\begin{aligned} \hat{N}_2(t) &= X(t+2) - X(t-2) \\ &\quad - 2 \sin(\omega_e) [X(t+1) - X(t-1)] \end{aligned} \quad (6)$$

Both of these estimates satisfy Eq. (4) and both are covariance stationary as well.

The estimated covariance function of $\hat{N}_1(t)$ and $\hat{N}_2(t)$ in terms of the estimated covariance function $\hat{R}(\gamma)$ of $N(t)$ is:

$$\begin{aligned} \hat{R}_1(\gamma) &= R(\gamma) [2 + 8 \sin^2(2\omega_e)] \\ &\quad + \sin(2\omega_e) [4\hat{R}(\gamma-6) - 2\hat{R}(\gamma-4) \\ &\quad - 2\hat{R}(\gamma+4) + 4\hat{R}(\gamma+6)] \\ &\quad - [\hat{R}(\gamma-8) + \hat{R}(\gamma+8)] \end{aligned} \quad (7)$$

$$\begin{aligned} \hat{R}_2(\gamma) &= R(\gamma) [2 + 8 \sin^2(\omega_e)] \\ &\quad + \sin(\omega_e) [4\hat{R}(\gamma-3) - 2\hat{R}(\gamma-2) \\ &\quad - 2\hat{R}(\gamma+2) + 4\hat{R}(\gamma+3)] \\ &\quad - [\hat{R}(\gamma-4) + \hat{R}(\gamma+4)] \end{aligned} \quad (8)$$

which can be approximated by:

$$\hat{R}_1(\gamma) = 2\hat{R}(\gamma) - [\hat{R}(\gamma-8) + \hat{R}(\gamma+8)] \quad (9)$$

$$\hat{R}_2(\gamma) = 2\hat{R}(\gamma) - [\hat{R}(\gamma-4) + \hat{R}(\gamma+4)] \quad (10)$$

The final question to be answered is: how does the spectrum of $\hat{N}_1(t)$ and $\hat{N}_2(t)$ differ from the spectrum of $N(t)$?

$$\hat{\phi}_1(\lambda) = \int_{-\infty}^{\infty} \hat{R}_1(\gamma) k(\gamma, \lambda) d\gamma \quad (11)$$

$$\begin{aligned} \hat{\phi}_1(\lambda) &= 2 \int_{-\infty}^{\infty} \hat{R}(\gamma) k(\gamma, \lambda) d\gamma - \int_{-\infty}^{\infty} \hat{R}(\gamma-4) k(\gamma, \lambda) d\gamma \\ &\quad - \int_{-\infty}^{\infty} \hat{R}(\gamma+4) k(\gamma, \lambda) d\gamma \end{aligned} \quad (12)$$

but

$$\begin{aligned} 0 &\leq \left| \int_{-\infty}^{\infty} \hat{R}(\gamma) + \alpha k(\gamma, \lambda) d\gamma \right| \\ &\leq \int_{-\infty}^{\infty} |\hat{R}(\gamma) + \alpha k(\gamma, \lambda)| d\gamma \rightarrow 0 \end{aligned} \quad (13)$$

monotonically in α with λ fixed for $k(\gamma, \lambda) \in L_1$. Therefore, as $\alpha \rightarrow \infty$, $\phi_1 \rightarrow \phi$. Similar arguments apply to ϕ_2 . It is possible to form an improved estimate of the spectrum of $N(t)$ by computing $\hat{\phi}_1(\lambda)$ and $\hat{\phi}_2(\lambda)$ from $R_1(\lambda)$ and $R_2(\lambda)$, respectively, and extrapolating to the limit in α . Similarly, the cross spectrum between $\hat{N}_1(t)$ and $\hat{N}_2(t)$ could be computed, thereby giving an improved estimate of the spectrum over $\hat{\phi}_1(\lambda)$ or $\hat{\phi}_2(\lambda)$. This will take more than twice the time to compute so that the added accuracy may not be feasible in real-time.

Experience with *Mariner 2* data has shown that both $\hat{N}_1(t)$ and $\hat{N}_2(t)$ give good estimates of the spectrum of $\hat{N}(t)$ and differ insignificantly from the spectra produced by conventional trend-moving schemes.

C. Pointing Errors Due To Quadripod Leg Distortions Of New Truss Type Quadripod At Echo Station

The pointing errors being sought are in hour angle and declination angle or $\Delta\psi$ and $\Delta\delta$ for the 85-ft polar mounted antenna located at the Goldstone Echo Station. These pointing errors are confined to dead and live gravity loading and involve the movement of the focal point with respect to the box girders; pedestal distortions are not considered. A cartesian system that moves with the antenna is oriented so that, with $\psi = \delta = 0$ deg, X points East, Y is colinear with the polar shaft, and Z points outward. Because of radial symmetry, it is only necessary to solve for ΔX_0 and ΔZ_0 , these quantities being the linear deflections of the focal point with the antenna oriented so that the gravity vector is in the X- and -Z-direction, respectively. Note that $\Delta Y_0 = \Delta X_0$. By applying proper Euler rotations to the antenna in any of the previous positions, the components of the gravity vector for an arbitrary ψ, δ position are:

$$P_x = \cos \phi \sin \psi$$

$$P_y = \cos \phi \cos \psi \sin \delta - \sin \phi \cos \delta$$

$$P_z = -\cos \phi \cos \psi \cos \delta - \sin \phi \sin \delta$$

where ϕ is the latitude (35.30° North for this case) and P_x is the component in the X-direction etc.

From the above we obtain

$$\Delta X = P_x(\Delta X_0), \quad \Delta Y = P_y(\Delta Y_0), \quad \Delta Z = P_z(\Delta Z_0)$$

and from the antenna dimensions these quantities are converted into $\Delta\psi$ and $\Delta\delta$.

$$\Delta\psi = \frac{57.29578 \Delta X}{519 \cos \delta + 264}$$

$$\Delta\delta = 0.1104 \Delta Y \text{ in degrees}$$

The Structural Analysis Interpretive Routine (STAIR) Program³ (Ref. 3) was used in the solution for ΔX_0 and ΔZ_0 . The program's outstanding feature is that a pin connected structure made up of prismatic bars can be solved by this method without the necessity of inverting a large matrix. This makes it particularly useful for a structure such as the antenna with the truss type quadripod which has more than 1000 joints. Solution of a structure with only 75 joints by one of the conventional methods will exhaust the core capacity of an IBM 7090, but STAIR can be used to solve a structure with as many as 3900 joints. The application of STAIR to this problem involved 180 joints and 528 axial members, and only that part of the antenna structure considered necessary for the final output was used, since the deleted portion has a compensatory effect. A slight disadvantage of STAIR is that, since the structure must be pin jointed and stable, imaginary members must be added to the actual structure where required and yet done in such a manner that the structure solved by STAIR will hardly differ from the actual structure.

The results from STAIR were:

$$\Delta X_0 = \Delta Y_0 = 0.1474 \text{ in.}$$

$$\Delta Z_0 = -0.0179 \text{ in.}$$

for the case of dead load and 1150 lb of live load (including 950-lb hyperbolic reflector) which means maximum angular errors of:

$$\Delta\psi = 0.0263 \text{ deg } (\psi = 90 \text{ deg}, \quad \delta = 80 \text{ deg})$$

$$\Delta\delta = 0.0133 \text{ deg } (\psi = 0 \text{ deg}, \quad \delta = 90 \text{ deg})$$

Also:

$$\Delta X_0 = \Delta Y_0 = 0.1089 \text{ in.}$$

$$\Delta Z_0 = -0.0163 \text{ in.}$$

for the case of dead load and 450-lb live load, which means maximum angular errors of:

$$\Delta\psi = 0.0195 \text{ deg } (\psi = 90 \text{ deg}, \quad \delta = 80 \text{ deg})$$

$$\Delta\delta = 0.0098 \text{ deg } (\psi = 0 \text{ deg}, \quad \delta = 90 \text{ deg})$$

³ S. Katow and K. Bartos, "JPL-STAIR Load Program," Technical Memorandum, May 1963.

Comparison with the older type of telescoping pipe quadripod shows an increase in accuracy of 25% based on a live load of 650 lb.

D. *Mariner C* 100-kw Transmitter

Under certain operating conditions, it has been determined that a ground transmitter power of 100-kw continuous wave (CW) will be required for the *Mariner C*

Project. A preliminary description of this transmitter was given in Ref. 4.

1. *Klystron Amplifier Subsystem*

The contract negotiations have been completed for the amplifier subsystem, and the contract has been awarded to Energy Systems Incorporated, Palo Alto, California. The contract with Energy Systems Inc. is essentially an assembly contract with all of the major components supplied by JPL. Since the amplifier subsystem is not operational without the complete transmitting system, the final tests of the assembly will be made in the transmitter test area at the Goldstone Venus site. The amplifier subsystem is scheduled for delivery June 1, 1964.

References

1. "Project Engineering," *Space Programs Summary No. 37-25*, Vol. III, p. 12-13, Jet Propulsion Laboratory, Pasadena, California, January 31, 1964.
2. "Trajectory Program for On-Site Computers," *Space Programs Summary No. 37-25*, Vol. III, pp. 13-14, Jet Propulsion Laboratory, Pasadena, California, January 31, 1964.
3. "Structural Analysis Interpretive Routine," *Lincoln Laboratory Manual No. 48*, Massachusetts Institute of Technology, March 1962.
4. "*Mariner C* 100-kw Transmitter," *Space Programs Summary No. 37-25*, Vol. III, pp. 18-19, December 31, 1963.

IV. Research and Development

A. Ground Antennas

1. Precision Drive System for 30-ft Antenna

The 30-ft Az-El antenna of the Goldstone Venus site was originally procured under JPL Specification 6203A, a performance specification for a relatively high angle rate mount suitable for ranging system experiments performed by tracking Earth satellites. The antenna fulfilled specification requirements as demonstrated by the acceptance test data reported in Ref. 1.

Last summer we attempted to use the 30-ft antenna for X-band radio astronomical measurements in connection with our program of AAS oriented pattern and gain testing and calculation. This use required exceedingly good low-speed operation. A field modification to improve the azimuth axis low-speed performance made during the experiments obtained marked improvement; however, in the course of the experiments, the azimuth drive system was damaged.

At that time three corrective plans were considered:

- (1) Plan 1 was to restore the antenna to the pre-accident condition.
- (2) Plan 2 was to make a drive system modification providing adequate advanced experimental operational performance for 1 to 3 yr after completion.
- (3) Plan 3 was to make a very advanced drive system modification which would provide performance aimed at matching the ultimate capability of the antenna structure.

Studies were made in order to select the best plan. The original pointing and tracking specification, related design loads, and the strength capability of the structural-mechanical axes were reviewed. Deflection characteristics of the axes as complete systems were calculated. The deflection data were used to develop a table of pointing and tracking specifications for significant environmental conditions. Schematic diagrams, cost estimates, time schedules, and comparative evaluations for two alternate servo drive system arrangements have been developed.

Based upon the study results and the conclusion that such an approach would provide the most applicable analysis and testing work for related work in the Advanced Antenna System, Plan 2 has been adopted. JPL will do the system design and integration using commercially supplied components throughout. The design

embodies a two-speed drive system in azimuth and elevation patterned after the azimuth axis of the Goldstone Venus site 85-ft Az-El antenna with some detail engineering improvements obtained from operating experience and advancement in component art. The block diagram is as shown in Fig. 1. Each drive unit has an output pinion supported by an outboard bearing engaging the axis bull-gear. In high-speed mode, the high-speed hydraulic motor drives the pinion through the primary gear reducer. In low-speed mode, the low-speed hydraulic motor is clutched in with an additional gear reducer to drive the output pinion, and the high-speed hydraulic motor is short-circuited hydraulically. An electromechanical disk brake is mounted on the input shaft of the primary gear reducer. Two of the drive units described are provided on each axis for reasons of backlash removal and gear tooth loading.

The servo is a second-order system employing hydraulic pressure and motor rate feedback. In each of the separate high- and low-speed systems, a single electrohydraulic servo valve controls the two hydraulic motors involved in the particular drive mode.

The hydraulic supply system is conventional in design, consisting of reservoir, constant pressure variable volume pump direct connected to an induction electric motor. Taking advantage of a margin in flow capacity, the noise

level of the existing unit will be appreciably reduced by a reduction in motor speed; also noise reduction will be obtained by shock mounting and isolating components by means of hoses.

One standard problem with a high-speed mount (maximum 6 deg/sec provided for the ranging experiments) is providing a mechanical counter for operator console display and as a backup for the precision readout. Conventional mechanical counters reading in hundredths of a degree have a continuous duty rating of about 2 deg/sec. Also most mechanical counters exhibit a serious velocity lag even at relatively low axis rates. An analytical and experimental investigation of the mechanical counter problem has provided a suitable solution which will be implemented on the 30-ft antenna.

2. Antenna Instrumentation

a. Summary. A transportable instrumentation system is being developed for use in research and development testing of the structural and mechanical properties of large ground antennas. It will be used initially on the 30- and 85-ft antennas, and later on the 210-ft-diameter Advanced Antenna System (AAS). In addition to developing the necessary instrumentation for making measurements on the future 210-ft AAS, the data derived is continuously applied to validate the design analysis techniques being

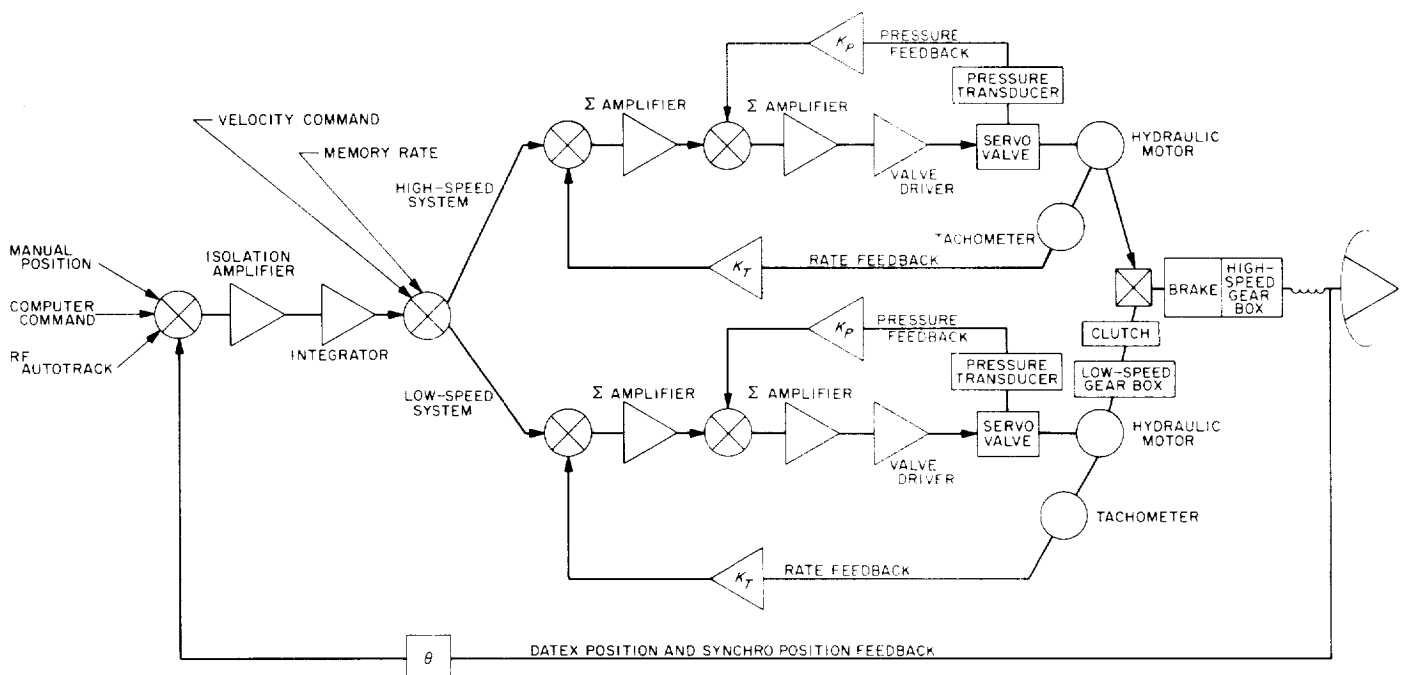


Fig. 1. Block diagram of wide-speed-range drive system for 30-ft antenna

employed in the AAS Project. There is a detailed description of the instrumentation system in Ref. 2, and progress reports in subsequent issues. The system was first used for structural and thermal testing conducted as part of the 85-ft Az-El antenna resurfacing work during July and August 1963, the preliminary results of which appear in Ref. 3. Additional equipment was added to the system prior to the last test series, accomplished during January and February of 1964.

b. Recent work. Critical antenna time prevented extensive structural testing of the Az-El antenna after the resurfacing operations in August 1963; recently, the series of tests outlined in Ref. 4 were conducted. As mentioned in Ref. 4, a special scanner was added to monitor the wire span temperatures of the extensometers in order to provide temperature correction as part of the data scan program information for the data analysis. Thus, all these data appear on the printed data sheets as well as on the special punched paper tape for later computer analysis. The raw data, after editing, labeling and coding on the Flexowriter, is computer processed using special computer programs which are being worked out to provide rapid data reduction of this raw data.

The punched tape can also be fed into a data plotter which will be installed in the data trailer. For future field operations the data tape can be fed into the plotter for "quick-look" plots immediately following each data scan.

Of the six tests outlined in Ref. 4, four were successfully carried out in the recent measurements on the Venus site 85-ft Az-El antenna. Two tests were omitted:

- (1) Continuous recording of extensometer signals during antenna movement in elevation to zenith to horizon was not possible because of weather conditions during the test period.
- (2) Vibration measurements to determine environmental data for reflector mounted electronic equipment were not possible because of weather conditions and of delay in equipment delivery.

A cursory examination of the raw data from these recent tests has been made and shows that the information to be derived from these tests should be good. Further data reduction is underway and will be reported in the next *Space Programs Summary*.

3. Radio Astronomical Techniques

a. Summary. The techniques of using radio stars for calibrating the operational antennas of the DSIF are be-

ing tested. Prior to the launching of *Ranger 6*, a measurement of the gain of the L-band antenna at the Echo Station was made using radio source techniques. To analyze the measurement, data collected during the testing of the 960-Mc Cassegrainian installation (Refs. 5, 6) were used to evaluate the Echo Station antenna. By comparing radio source temperatures as measured on the two antennas, the difference of gain of the two antennas is obtained; and from the previous determination of the Cassegrainian antenna gain, the gain for the Echo antenna is derived. The gain of the Echo antenna determined in this way is approximately 45.6 db.

b. Recent work. On the nights of January 8 and 9, 1964, gain measurements were made of the Goldstone Echo Station 85-ft antenna using radio astronomical techniques. The DSIF L-band receiver system with a maser and parametric amplifier was used as a total power radiometer. The antenna was driven by the coordinate converter computer, and the boresight was checked before each temperature measurement by the techniques discussed in Ref. 7. Because of receiver instability problems, it was found necessary to use the Y-factor technique to measure system temperature difference while aiming the antenna at the source and then a few degrees away from the source. The Y-factor is defined as $Y = (T_s + T_r/T_s)$, where T_s is the system temperature and T_r is the gas tube temperature. The difference temperature is the

$$\Delta T = T_r \left(\frac{1}{Y_1 - 1} - \frac{1}{Y_2 - 1} \right)$$

where Y_1 is the ratio on source and Y_2 is the ratio off source. The accuracy of the measurement is then seen to be linearly dependent on the accuracy of the calibration of the noise tube. It is also dependent upon the assumption that the source contribution is the only variable in the measurement of Y_1 and Y_2 ; i.e., the receiver system temperature is assumed to be stable, and antenna temperature changes due to sidelobe effects are negligible. The gas tube contribution was calibrated using an ambient load and a nitrogen cooled load. These loads were not carefully calibrated. Considering all the system measurement sources of error, a tolerance of approximately ± 1 db is placed on the measured absolute value of ΔT for celestial sources.

The effective temperature difference, ΔT , measured for the Crab Nebula referred to the Echo antenna Radiation Inc. feed output was 96°K as compared to 93.9°K for the Cassegrainian antenna (Ref. 5), a +0.4-db difference. The

measured average of Cassiopeia was 305°K compared to 338°K for the Cassegrainian antenna (Ref. 5), a -0.1-db difference. However, there were fewer measurements of Cassiopeia made, and the low temperature of the gas tube contribution compared to the total system temperature probably made this measurement less accurate than the measurement of Crab Nebula. Also, the elevation angles for Cassiopeia measurements were low, further reducing the accuracy.

The gain of the 960-Mc Cassegrainian antenna is 45.6 db (Ref. 6); the uncertainties of that gain and of the absolute value of ΔT must be combined so that the maximum gain uncertainty in the Echo antenna determination is probably larger than ± 1 db. Based on these data, we quote the tentative gain 45.6 ± 1.5 db for the Echo antenna at 960 Mc.

It is planned to make additional measurements with better calibrated equipment soon at the Echo Station.

4. Radio Calibration Techniques

a. Summary. Radio astronomical techniques have been employed at the Goldstone Station Venus site for the calibration of the 85-ft Az-El antenna. This antenna has been calibrated for pointing accuracy and effective antenna area by using the signal received by several intense radio sources. Boresight measurement procedures have been described in Refs. 7, 8, and 9; measurement of effective antenna area and antenna gain are described in Refs. 7, 10, and 11. In measuring radiometric quantities, radio-frequency terminations immersed in a cryogenic bath are employed as thermal noise standards.

Recently, the Cassegrainian cone was removed from the 85-ft antenna to facilitate antenna structural measurements. During that time, the insertion loss of the cone transmission line was measured, and evaluation of the cryogenic loads was started.

b. Recent work. The Cassegrainian antenna cone was removed from the Venus site 85-ft antenna to facilitate structural measurements. During this period, insertion loss measurements, which are critical for temperature measurements, were performed on all transmission lines in the planetary radar. In Ref. 10, insertion loss of the original Venus site Cassegrainian transmission line was presented and is shown in Table 1. Since those measurements were made, several changes in the transmission line system have been made. The MCS waveguide switch used in the polarization basket and the MCS transmit-

receive switch were replaced with Bogart switches because of their greater power handling capabilities, as discussed in Ref. 12. It was not possible to make insertion loss measurements at that time because of schedule commitments. However, estimates of loss were made and appear in Table 1.¹

Table 1. Insertion loss of Venus site Cassegrainian transmission line

Transmission line	Original measurement, db	Modification estimate, db	Final measurement, db
Feedhorn throat	0.120 ± 0.01	0.105 ± 0.1	Arm A, 0.092 ± 0.01 Arm B, 0.099 ± 0.01
Helium load output flange (coax or waveguide) to input of maser	Coaxial flange, 0.10 ± 0.01	Coaxial flange, 0.10 ± 0.01	Waveguide flange, 0.060 ± 0.005
Nitrogen load output flange (coax or waveguide) to input of maser	Coaxial flange, 0.10 ± 0.01	Coaxial flange, 0.10 ± 0.01	Waveguide flange, 0.073 ± 0.005

The cone was again modified for lunar radar work by addition of an MCS switch in the nitrogen load line as discussed in Ref. 13. The original configuration of the cone and the associated losses and temperatures are shown in Fig. 2. The current configuration and losses are shown in Fig. 3. A comparison of original measurements, intermediate estimates, and final measurements are given in Table 1.

The insertion loss measurements were made with the audio frequency substitution measurement set described in Ref. 14. The total estimated error for the helium and nitrogen transmission lines is ± 0.005 db, for the antenna transmission line ± 0.010 db.

When the radio tracking operations were concluded, the cryogenic loads were removed from the cone and sent to JPL. These loads are now being radiometrically compared to the waveguide helium load described in Ref. 15. Using this comparison technique, it is possible to avoid the requirement for a precise loss measurement of a waveguide to coaxial transition, because the effective temperatures are compared at the waveguide output flange.

The initial temperature comparisons indicated that the loads had deteriorated in field use. It was necessary to

¹ Data taken from "Antenna Feed and Polarizer 1963," JPL Planetary Radar Report (to be published).

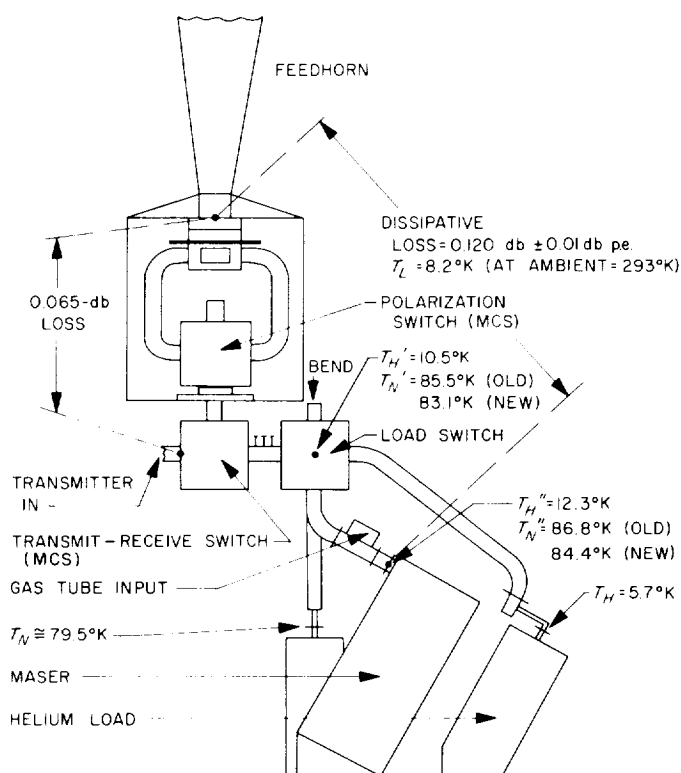


Fig. 2. Original insertion loss and temperature measurements

dismantle, clean, and repair the loads that were in use at Goldstone. It appears that a periodic check of these loads is desirable. The results of the temperature comparison will be presented in the next *Space Programs Summary*.

5. 85-ft Az-El Antenna, Reflector Resurfacing

a. Summary. The reflector surface of the Venus site 85-ft Az-El antenna was replaced with a higher accuracy surface. The purpose of the work is to provide data on correlation of reflector surface accuracy with radio frequency performance, and provide a reflector surface suitable for future X-band frequency experiments including 210-ft AAS model tests.

Measurements of the surface accuracy were made by the supplier (Rohr Corp.) in the plant prior to delivery and installation on the antenna. Recently, measurements have been made of the panels on the antenna. The data have not yet been analyzed.

b. Recent work. Prior to preparation of the specifications for the resurface job, studies were conducted at JPL of various materials and design concepts for antenna sur-

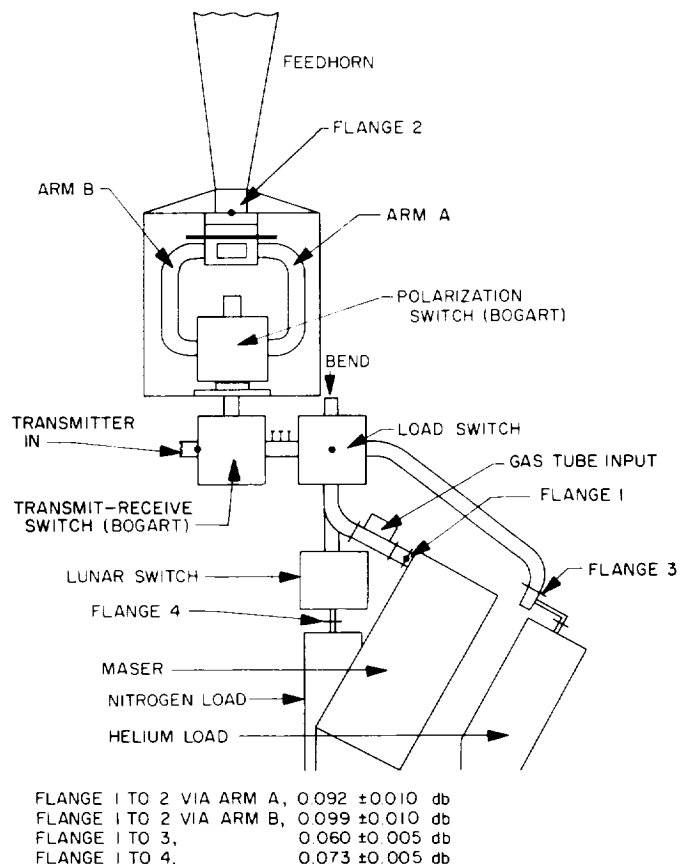


Fig. 3. Recent insertion loss measurements

face panels potentially useful in future applications in the DSIF 85-ft antennas and the AAS. The objective was to develop a surface panel meeting the following requirements:

- (1) The panel must accept without permanent deformation the load of a 300-lb man standing on one foot.
- (2) The panel must satisfy the manufacturing tolerance specifications for an X-band reflector surface (defined as 0.087-in. rms total surface error in operating environment).
- (3) The panel must be stiff enough to meet the dead-load deflection specifications for an X-band dish.
- (4) The panel must survive, in tolerance for an X-band reflector, a hailstorm producing hailstones with diameters up to 1 in.
- (5) The panel must be of equal weight or lighter than the existing 85-ft-diameter DSIF antenna solid surface panels (2.4 lb/ft^2 of reflector surface).

- (6) The panel configuration must have either a solid surface or a perforated surface with perforations equal to or smaller than $\frac{1}{8}$ in. in diameter.
- (7) The panel must have small thermal gradients and associated thermal deformations.

The specifications for the manufacture of the panels reflected the above requirements. Related information is contained in Refs. 16, 17.

For a total operational reflector accuracy of 0.087-in. rms, 0.031-in. rms was specified as allocated to the reflector panels which was, in turn, subdivided in the following way:

Item	3- σ error (inches $\times 10^{-3}$)	1- σ error (inches $\times 10^{-3}$)	σ^2 (inches $\times 10^{-6}$)
Manufacturing tolerance	60	20	400
Dead-load deflection	36	12	144
Wind-load deflection	54	18	324
Erection tolerance	30	10	100
Thermals	9	3	9

This gives a total summation of σ^2 errors of 977×10^{-6} in., a total 1- σ value of 0.031 in., or an approximate peak of 0.093 in. These figures apply in an operational wind up to 25 mph.

The present effort was limited to resurfacing of the antenna reflector; the actual full performance capability of the antenna will not be available until the reflector backup structure is stiffened appropriately. That job is planned for the future.

In order to provide a surface capable of meeting the listed requirements, the surface of the panels was constructed of 7178 T-6 aluminum 0.072 in. thick. The material has a 25% porosity. Perforations are 0.125-in.-diameter holes (absolute). The surface is coated with a special high reflectance flat white paint to provide a low (near ambient) thermal gradient at the focal point of the reflector. The panel substructure was constructed of formed (zee section) 7178 T-6 aluminum, 0.050 in. thick.

We have taken data describing the as-built, as-installed condition of the surface panels. The panels were field set at 45-deg elevation; adverse environmental conditions were

such that allowances had to be made for wind loading during the alignment and measurement of the surface.

The specifications required that the installed panel accuracy be 0.031 in. rms in winds up to 25 mph. Because of unpredictable errors apparently caused from hysteresis in the reflector backup structure in winds exceeding 5 mph, it was determined that, for field installation, the wind-load environment must be less than 5 mph to provide sufficiently accurate measurement and setting of the panels.

The results of the manufacturer's in-plant testing and the field erection tests are shown below:

Item	1- σ error (inches $\times 10^{-3}$)	σ^2 (inches $\times 10^{-6}$)
Manufacturing tolerance (from in-plant measurements)	16.5 ^a	272.2
Dead-load deflections (from in-plant measurements)	3.4	11.8
Wind-load deflections (from in-plant measurements)	5.7	32.5
Erection tolerance (from field measurements)	30.1	907.8

^aThe inspection data of the surface panels as provided by the manufacturer was reduced by a JPL computer run (Run 3034, February 20, 1964).

This gives a total summation of σ^2 errors of 1224×10^{-6} in., a total 1- σ value of 0.035 in. The panel manufacturing tolerance and dead-load and wind-load deflection characteristics considerably exceeded the specified requirements. The erection tolerance, as previously stated, was larger than expected because of what appeared to be hysteresis in the reflector structure, which is not within the panel suppliers cognizance. This problem is being studied. Some recent measurements on the 85-ft Az-El reflector structure are reported in Sec. IV-A-2 (Antenna Instrumentation) of this SPS issue. The measurements consisted of:

- (1) Extensometer measurements recording structural dead- and wind-load deflections of the reflector, Cassegrainian system, and quadripod in various elevation attitudes.
- (2) Optical measurements of the reflector surface accuracy in various attitudes of elevation without the Cassegrainian cone. The measurements were conducted under near ideal environments.
- (3) Measurements were made of the paraboloidal contour of the antenna surface panels by means of a paraboloid test fixture.

The in-plant measurements on the panel included simulated wind and walking load on the panels; these measurements are discussed below.

Wind load. The largest panel, approximately 5 ft², was set up for test, supported at its mounting points. Thirteen dial indicators were suspended across the face of the panel for measurement of deviations from zero reference when applying a load. Three separate distributions of load tests were conducted simulating wind loads of approximately 25 to 60 mph.

Test No.	Deflection, in. rms	Peak deviation, in.	Peak permanent deformation, in.
1 (2 lb/ft ²)	0.0057	0.012	0.00
2 (5 lb/ft ²)	0.0150	0.030	0.00
3 (10 lb/ft ²)	0.0320	0.061	0.001
Total area = approx. 25 ft ² .			

Walking load. 300-lb-man load measurements were made with the same panel and setup. A man weighing 190 lb carrying 110 lb of shot walked over given areas on the face of the panel, and deflections were recorded in the same manner as in the wind-load tests. The peak deflection was 0.250 in. with no permanent deformation of the panel.

Fig. 4 shows the completed surface panel installation. The dark lines along the edges of the panels are areas left unpainted, with primer only, to permit placement of

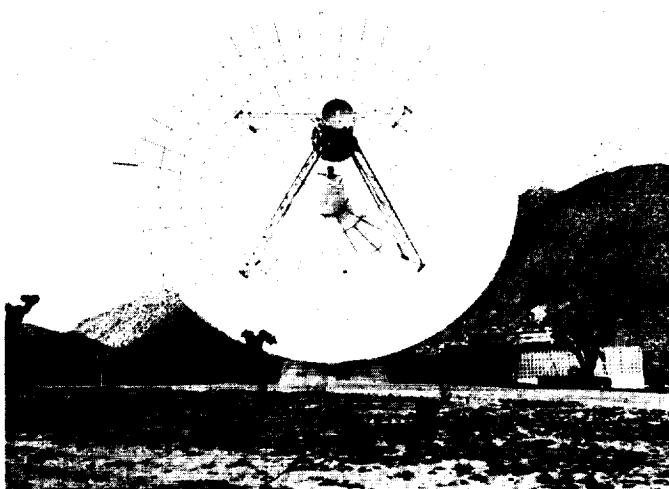


Fig. 4. 85-ft Az-El antenna with new accurate surface

aluminum tape which increases the reflective surface area. Fig. 5 shows the instrumentation setup at the vertex of the reflector for the recent measurements of the surface panel targets. Fig. 6 shows the paraboloid test fixture in place on the reflector during the recent measurements. Recent tests of the antenna gain at 2.4 Gc show an approximate 0.4-db increase with the new surface as compared to the gain with the old surface (Ref. 18).

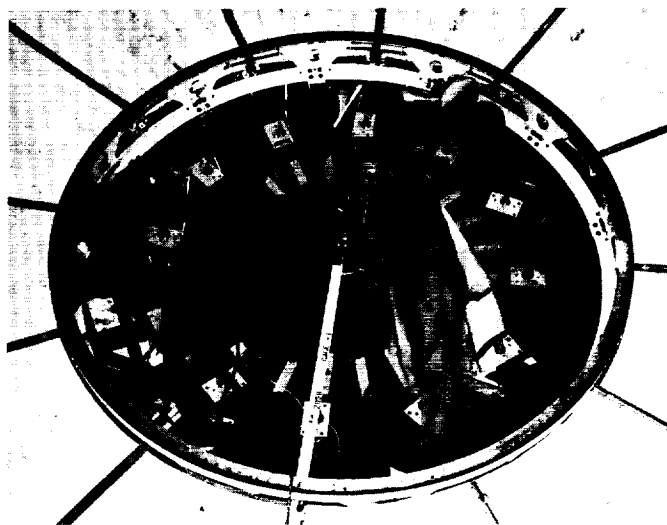


Fig. 5. Surface panel adjustment and measurement instrumentation setup

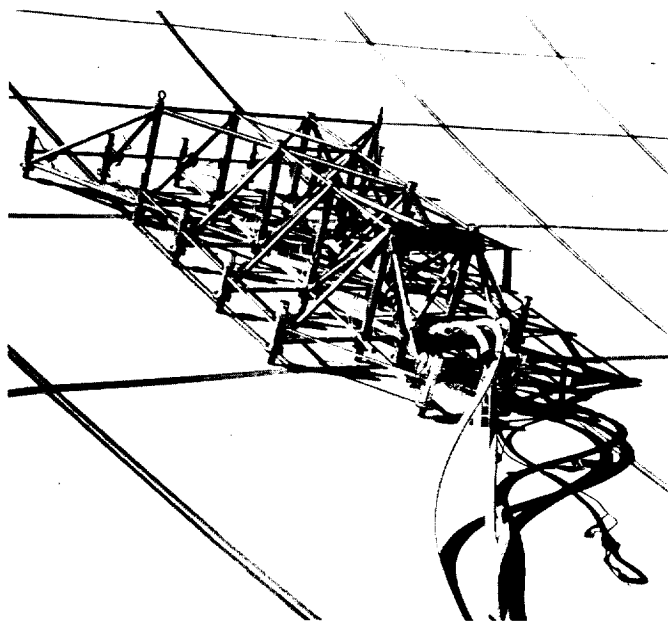


Fig. 6. Dish contour measurement test, paraboloid test fixture

B. Planetary Radar Project

1. 100-kw S-Band Transmitter

a. Introduction. The period covered by this report began with the cessation of Venus and Jupiter tracking operations and ends with the final preparations for the resumption of planetary radar tracking. This interval of time between missions has been utilized to effect major improvements, perform system and subsystem tests, and enhance the reliability and serviceability of the transmitter (Ref. 19).

The specific items treated herein are the installation of new crowbar electronics units, the test of repeated crowbar firings to observe transient phenomena and reliability, the movement of two major pieces of rotating machinery, the reinstallation and automation of the transmitter high-voltage dc water load, tests and improvements made on the klystron RF instrumentation, and measurements of klystron harmonic radiation.

b. Crowbar electronics. Unsatisfactory performance, unreliable operation, and inaccessibility have provided ample cause for the complete replacement and repackaging of the several chassis which comprise the crowbar electronics. These units are located in the high-voltage dc output cubicle. This major assembly is part of the 55,000-v klystron power supply. The three units which constitute the crowbar electronics consist of the crowbar positioning chassis, the crowbar auxiliary power supply, and the crowbar trigger chassis. New replacement units were built with increased safety factors, mechanical improvements, and increased serviceability features. The old units were removed and modified for use as emergency spares. The new units are mounted in a wall cabinet (Fig. 7) where ease of observation, adjustment, and servicing are assured.

c. High-voltage crowbar tests. The operation of the high-voltage power supply crowbar has recently been a topic of critical study. The switching time, reliability, and electrical stresses during the transient period are of concern to studies of klystron life, high-voltage rectifier life, and over-all system performance. In addition, design information can be produced from crowbar transient observations which will affect future systems and components such as the high-voltage, solid-state rectifier presently in the final stages of completion (Ref. 20).

A synchroscope was adjusted for single-sweep operation, and a camera was fitted to the cathode-ray tube. The internal sweep trigger, after initiating the synchroscope

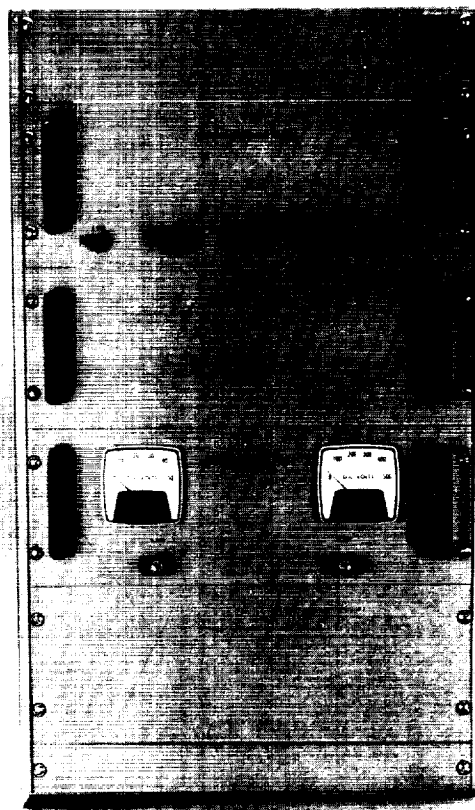


Fig. 7. Crowbar electronics units shown installed

sweep, was directed to a pulse generator which produced a 3000- μ sec pulse approximately 10,000 μ sec after the receipt of its trigger. The 3000- μ sec output pulse was then injected into the crowbar logic chassis located in the transmitter control cabinet to serve as an artificial klystron fault current. The vertical amplifier of the synchroscope was then connected to the current shunt which carries the current flowing from the high-vacuum rectifier positive return bus to the high-voltage L-C filter and system ground. Since the crowbar arc-gap is located on the load side of the high-voltage L-C filter, the voltage developed across the shunt will correspond to the high-voltage rectifier current during normal operation and also during crowbar.

The crowbar operation, time delay, and rectifier current transient phenomena were recorded by using the camera and synchroscope in a special, multiple time exposure process. [Refer to Fig. 8(a), (b), and (c).] The synchroscope and pulse generators were adjusted so that the inception of the artificial fault at the crowbar electronics corresponded to the end of the first centimeter of horizontal sweep. This was done specifically to observe

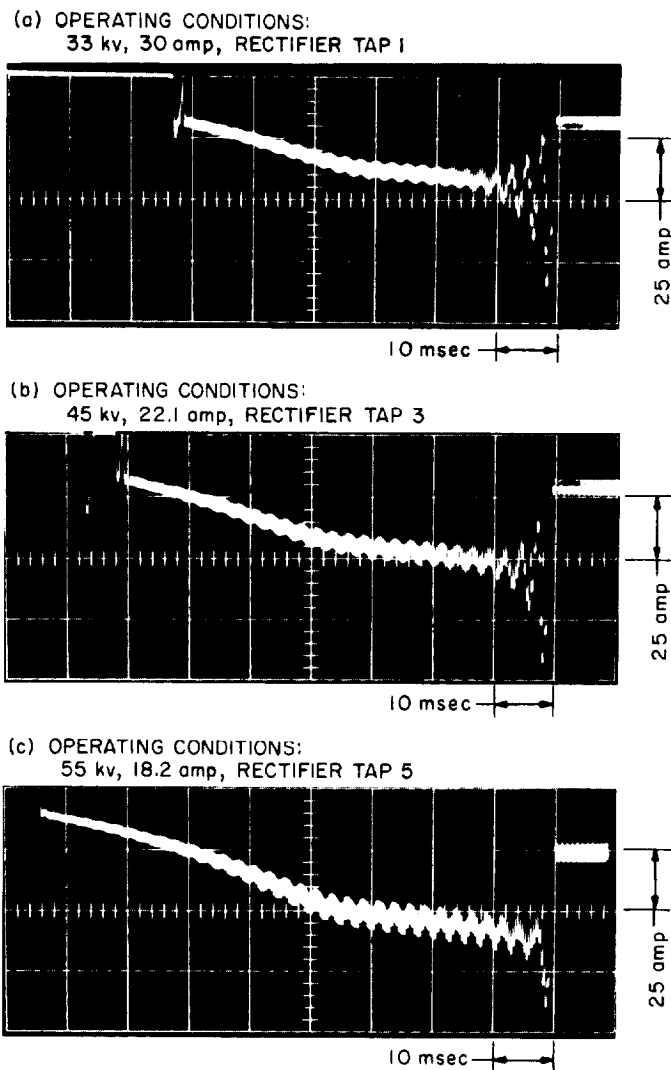


Fig. 8. Current discharge waveforms seen by the rectifier tubes during crowbar operation

the current before and after crowbar, as well as to determine the exact instant the transient began. The high-frequency ripple noted in the pictures is due to the expected current ripple from the three-phase, 400-cycle rectifier when connected to the L-C filter.

The power supply was adjusted for 1-Mw output into the dc water load at each of the voltage settings. However, the series limiter had to be used in the 55,000-v test to keep the water-load voltage drop to 45,000 v. Unreliable operation was experienced when the dc water-load voltage drop approached 53,000 v. The power supply was then manually crowbarred ten times to indicate any deterioration or variation of performance. The three selected power supply settings used were 33,000 v at 30 amp,

45,000 v at 22.1 amp, and 55,000 v at 18.2 amp. These three voltage settings correspond to taps 1, 3, and 5, respectively, on the power transformer secondary. (Fig. 8 shows typical waveforms.)

The evaluation of the test resulted in placing surge-protecting capacitors across the 400-v crowbar auxiliary power supply. In addition, the crowbar spark plug was cleaned, the glass insulator was replaced, and the high-voltage gap distance was reduced.

d. Relocation of the transmitter building rotating machinery. The 220-v, 400-cps auxiliary motor generator and the amplidyne unit for the control of the field of the high-voltage, 400-cps generator were originally installed in the transmitter control building. These two equipments produce considerable noise and heat in the building which is used by personnel to control the transmitter and to perform emergency and routine maintenance on the equipment. The high outside air temperature in the desert area, together with limited building air-conditioning, have made conditions intolerable for the personnel and a hazard to the performance and reliability of the equipment.

The two rotating machinery units were moved to the hydromechanical building, which is approximately 30 ft from the transmitter building. The required electrical conduit pipes and cement mounting pads were previously laid before transmitter shutdown (Figs. 9 and 10). This location affords protection for the equipment from the hazardous desert climatic elements, such as sand and rain storms, while solving the problems of noise and heat in the transmitter control room.



Fig. 9. 220-v, 400-cps auxiliary generator

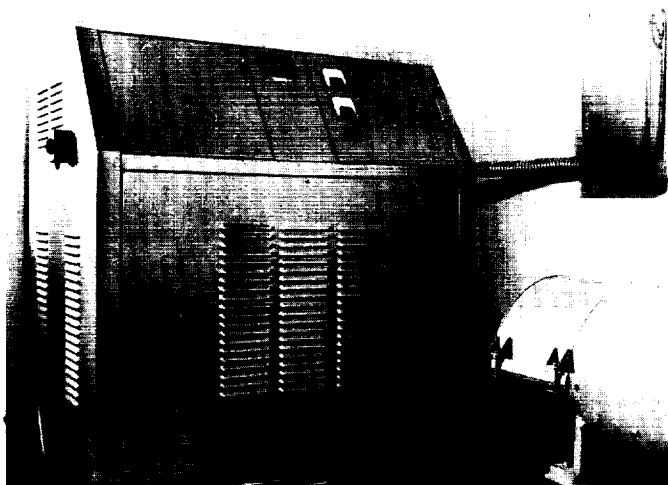


Fig. 10. Transmitter amplidyne unit

e. Relocation and automation of the high-voltage dc water load. The 55,000-v dc power supply is a complex unit which must be tested and adjusted as an independent subsystem to ensure proper operation and to avoid damage to itself and the other components of the transmitter system. The high-voltage dc water load was designed to fulfill this requirement.

The operation of the unit depends upon the passage of current from the center rod, insulated for 55,000 v, to the grounded cylindrical housing via the intervening high-resistivity water. The resistance is changed by sliding a cylindrical plastic "mask" in or out of the grounded metal housing, thereby effecting a change in the virtual area of the electrodes in contact with the electrolyte.

The water load has recently been moved from a temporary location on the floor of the cone storage room to a location on the wall 15 ft above the floor and immediately below the dc output cubicle of the 55,000-v power supply (Fig. 11). This removes the high-voltage hazard to personnel and removes the physical obstruction in the cone storage room. A reversible electric motor was attached to the lead screw which moves the plastic "mask" when load resistance changes are necessary. Limit switches to protect the motor and a remote control panel, installed on the transmitter control panel, have been provided for convenient operation.

f. Improvements made in the 100-kw klystron instrumentation. The Varian VA-858 100-kw klystron is instrumented for remote indication of transmitted RF power, reflected RF power, and drive RF power. During the course of the previous mission, considerable errors

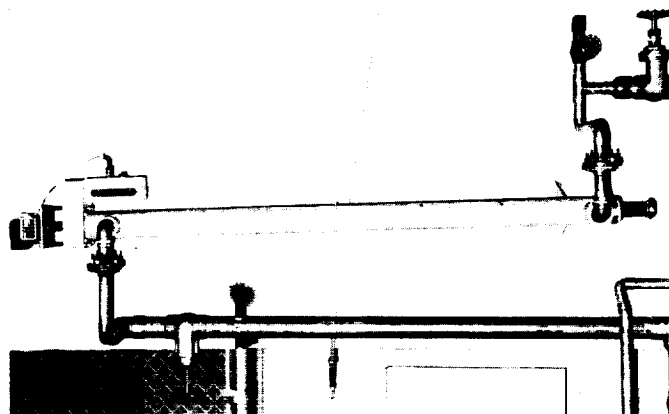


Fig. 11. High-voltage dc water load

were encountered during each postcalibration measurement. These errors appeared as discrepancies between the indicated power and the actual power as measured at the klystron using calorimetric power measuring equipment.

The RF calibration attenuators, which are located between the klystron and the RF power bridge providing the remote meter indications, were suspected of changing with temperature. These RF attenuators were subsequently removed and tested in a temperature chamber. Their variations with temperature were prohibitively large and their replacement was considered mandatory. Another type of RF attenuator was given the same temperature test. These units showed a marked improvement and were, therefore, installed in the Venus transmitter klystron housing in place of the original units. (See part d of this article.)

g. Transmitter harmonic power. Harmonic power from the experimental 2388-Mc transmitter was measured using the Tiefert Mountain Facility (Ref. 21). A Polarad FIM receiver was located at Mt. Tiefert, and the 85-ft Az-El antenna was accurately oriented on the center of the receiving horn (Fig. 12). The VA-858 klystron was tuned for high efficiency, and a low-pass filter was placed in the exciter input to reduce possible exciter contribution to the harmonic output. The antenna switches were positioned as shown in Fig. 13, and the results of the measurements are given in Table 2. The antenna was rotated 90°N and 90°S of the boresight line for the fundamental frequency, 2388 Mc, to determine if there was any offset in the boresight line for the harmonics. The main lobe for the third harmonic, 7164 Mc, was 0.118°N of the boresight line for fundamental frequency. The main lobes for the second and fourth harmonics were in line with the fundamental frequency boresight.

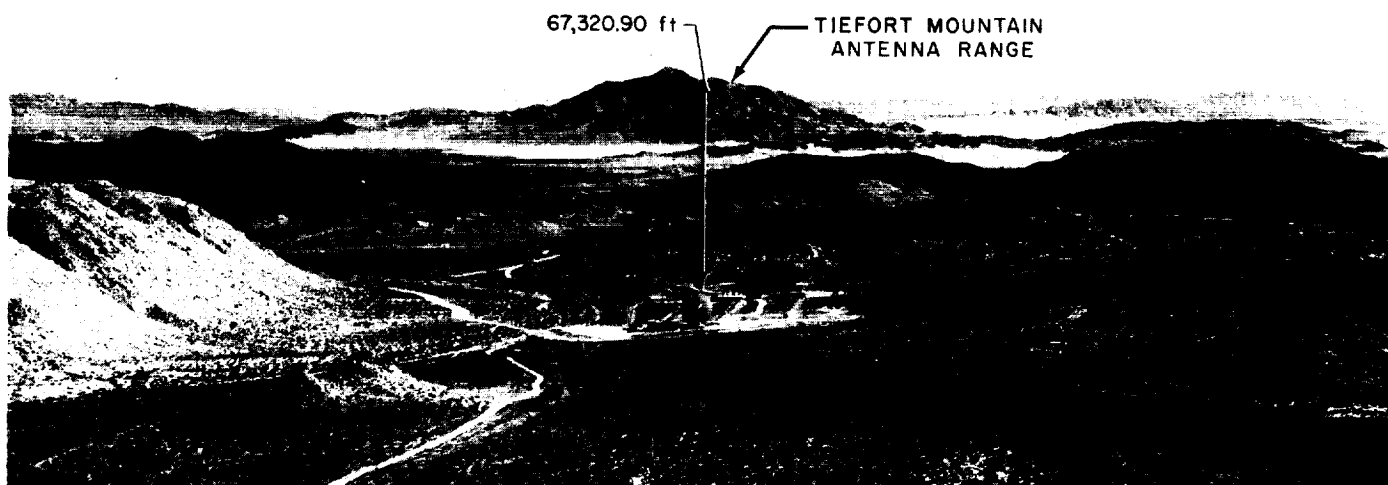


Fig. 12. Tiefert Mountain antenna range

h. RF switch isolation. The test setup for measuring the harmonic power described above provided an excellent opportunity to obtain additional measurements of the RF switch isolation. Previous measurements are described in Ref. 22. The transmitter power of 94.5 kw (+79.75 dbm) was directed into the water load with the switches as shown in Fig. 14; the results are given in Table 3.

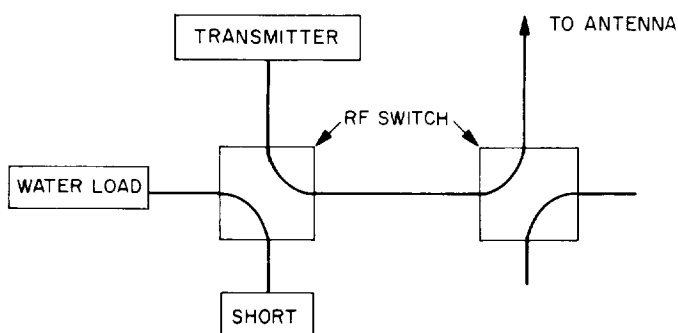


Fig. 13. Switch position for harmonic measurements

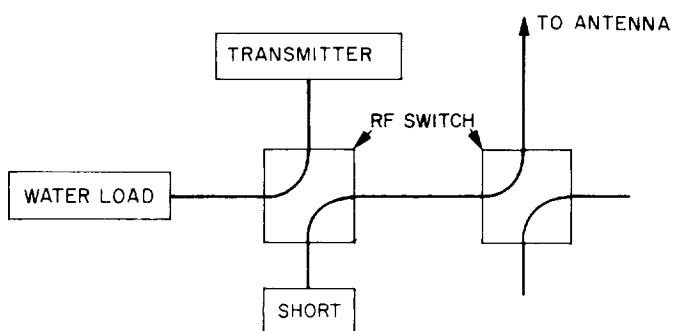


Fig. 14. Switch position for isolation measurements

2. Nine-Channel Autocorrelator

Construction of a nine-channel autocorrelator has been completed, and the unit installed at the Venus site, Goldstone, California. This instrument processes in real-time the signal received by the planetary radar receiver. The equipment is contained in one cabinet rack as shown in the photograph of Fig. 15. All the logic cards are mounted in two slideout frames located in the bottom half of the rack. The top half of the rack contains the control panel and two power supplies.

a. Function. The nine-channel autocorrelator extracts from the received composite signal those signal components which are reflected from nine adjacent planetary

Table 2. Transmitter harmonic power

Harmonic	Frequency, Mc	Transmitter power		Harmonic power below fundamental, db
		kw	dbm	
Second	4776	90.5	79.56	42
Third	7164	94.9	79.77	47
Fourth	9552	94.5	79.75	72

Table 3. RF switch isolation

Frequency, Mc	Isolation, db
2388	87.24
4776	34.5
7164	37.0
9552	34.5

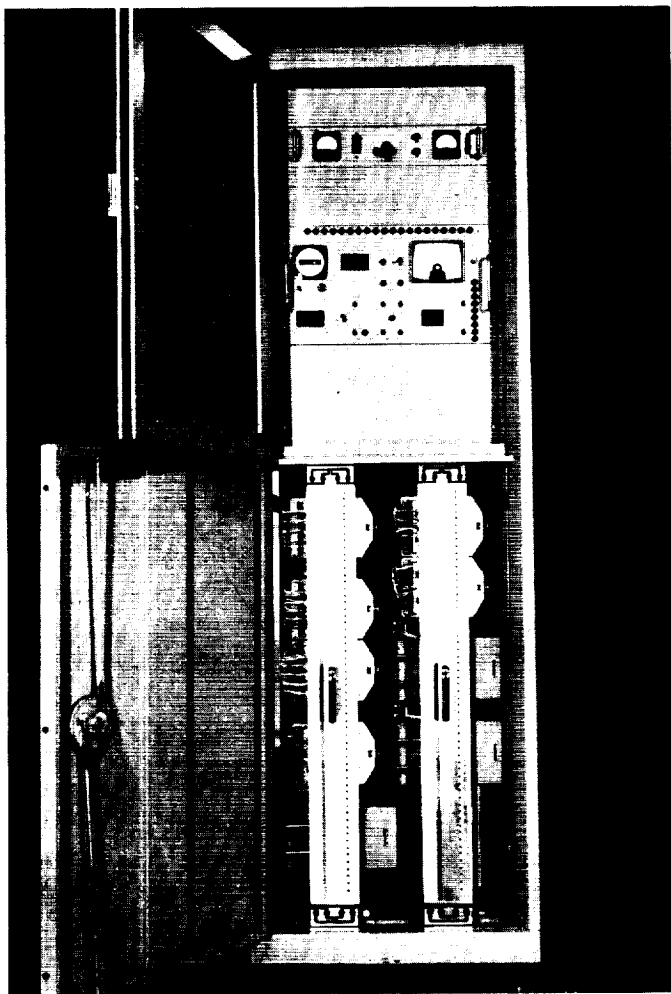


Fig. 15. Nine-channel autocorrelator

range zones. The autocorrelation functions of the extracted signal components are then each continuously compiled in a separate channel. This process of signal component extraction is made possible by first biphase-modulating the transmitted signal with a pseudonoise (PN) code. Each received signal component is modulated by a different phase of this PN code depending upon the signal time-of-flight to its range zone. When the composite signal is demodulated by a given phase of the PN code, the signal component whose modulation is in phase with the demodulating code becomes a narrow bandwidth signal. The remaining signal components remain wide-band and are suppressed by filtering. Each of the nine channels, therefore, demodulates the received composite signal with a different phase of the PN code, passes the result through a narrow-band filter, and continuously compiles the autocorrelation function of the selected signal component. Further details of this process are discussed in Ref. 23.

b. System operation. Shown in the system block diagram of Fig. 16 are the major groups of internal logic plus the two pieces of associated external equipment, the general purpose stored program computer, and the X-Y recorder. The receiver IF signal at 15.625 kc is processed by the nine channels whose outputs go to the computer.

Control of the autocorrelator by the computer is accomplished by means of a series of binary coded computer commands. These commands are decoded by the command decoder logic from which they are routed to either the autocorrelation control and output logic, the digital-to-analog (D/A) converter, or the pen control logic. Commands to the autocorrelation control and output logic perform such functions as starting and stopping correlation, and outputting the accumulator storage one bit at a time simultaneously from each of the nine channels.

After receiving the accumulator information from the channel outputs, the computer can then compute the power spectrum for each channel. These curves are plotted by means of commands to the D/A converter and pen control logic. The D/A converter provides position information for both the x and y axes of the X-Y recorder, and the pen control logic permits the computer to raise or lower the X-Y recording pen on the recording paper.

The timing and sampling signal logic provide accurate logic timing signals and input signal sampling periods. High accuracy is obtained by tying the logic to an atomic standard by means of the synthesized 1-Mc reference signal.

The PN generator provides the nine phases of the PN demodulating code. It is slaved to the code generator which modulates the transmitted signal by means of two synchronizing signals: the code bit rate clock and the word detect signal. The clock signal causes the PN code to be generated bit by bit, and the word detect signal aligns the code so as to be generally in phase with the desired received signal components.

The front panel display logic permits the operator to read out the value of any of the 51 autocorrelation terms in any of the nine channels.

c. Channel description. Fig. 17 is a block diagram of a typical channel. The receiver IF signal goes to a phase switch which is controlled by the particular phase of the PN code to that channel. Phase switching involves passing the signal either normally or inverted according to

whether the PN code is true or false. This causes the in-phase signal component to become narrow band and leaves the out-of-phase signal components wide band.

The output of the phase switch goes to a filter, which is constructed as a plug-in unit so that different filter bandwidths may be used for the different planetary radar

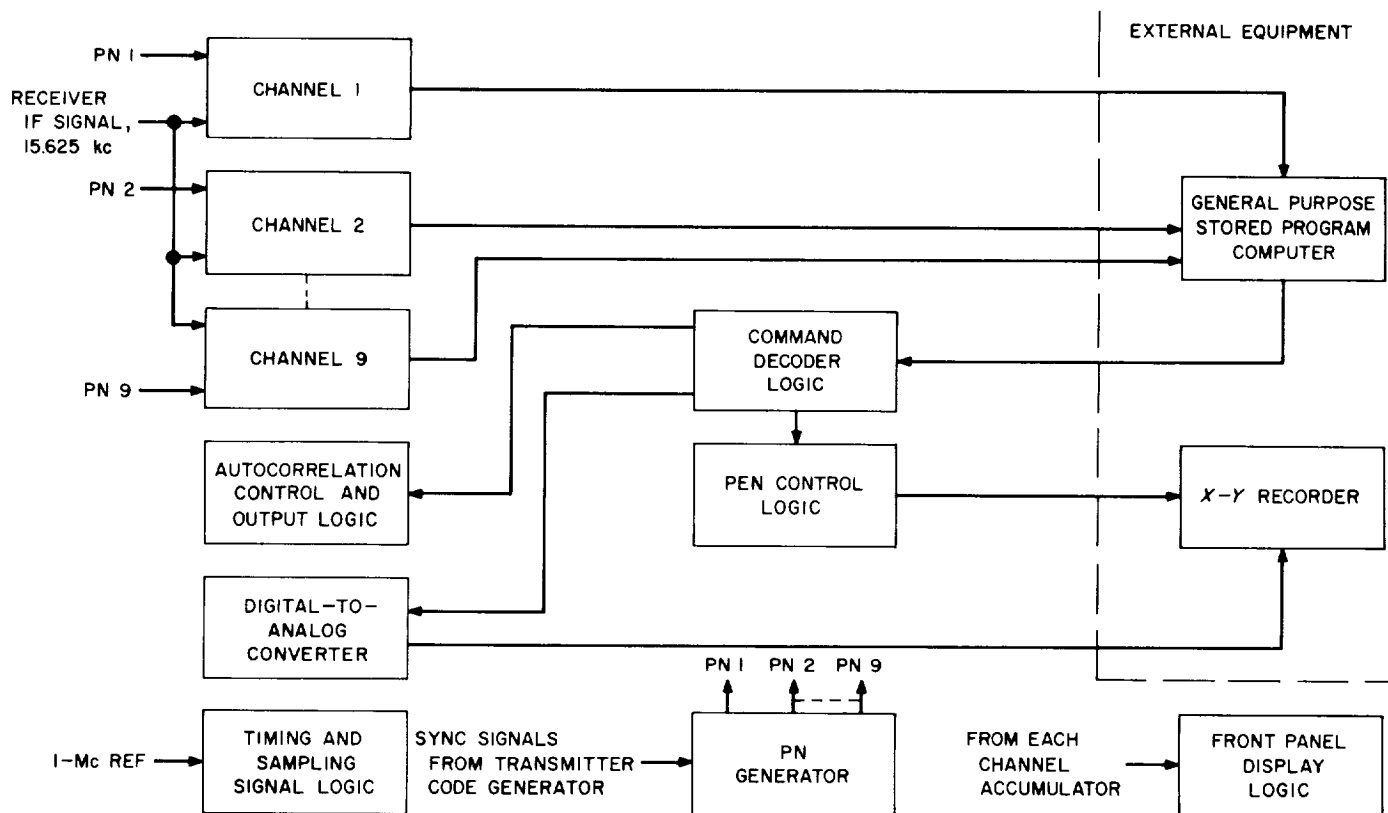


Fig. 16. System block diagram

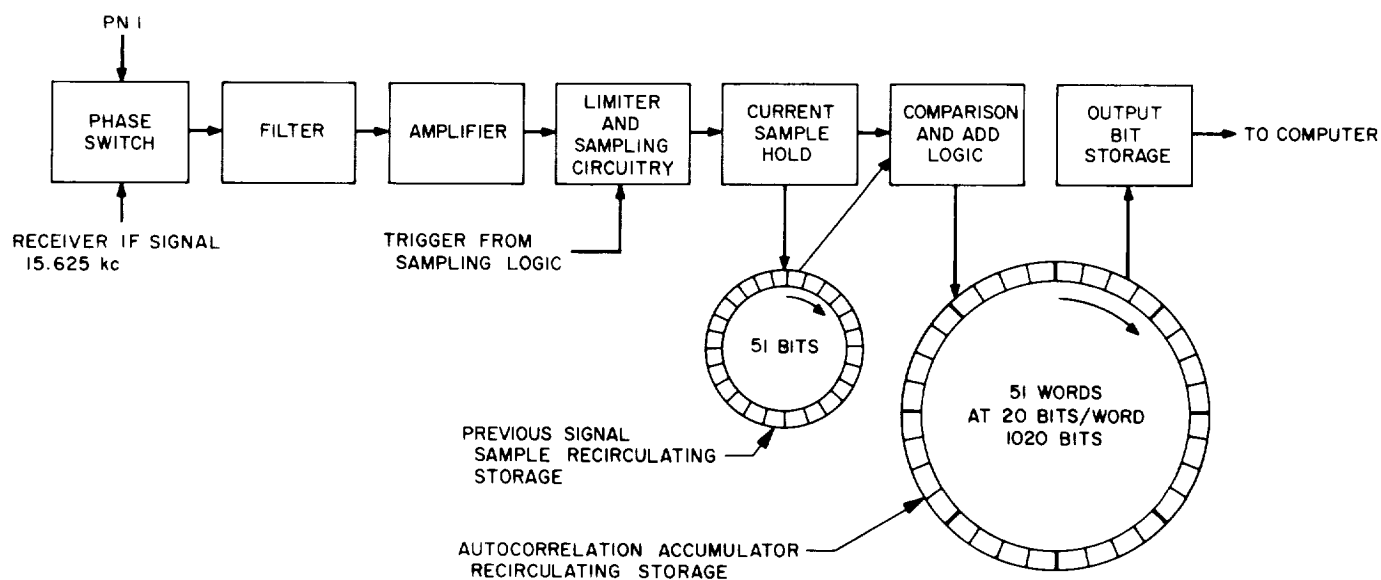


Fig. 17. Block diagram of typical channel

experiments. Typical filter bandwidths range from 400 to 25 cps, and have a center frequency of 15.625 kc. The action of the filter on the out-of-phase signal components is to cause them to look like noise which only slightly adds to the rest of the system and galactic noise of the received composite signal.

The amplifier is used to match the high output impedance of the limiter and sampling circuitry. This circuitry consists of a signal amplifier and a triggered flip-flop. Trigger signals from the sampling logic cause the flip-flop to set or reset according to whether the input signal is positive or negative. Information from the sampling circuitry goes to the current sample hold flip-flop which receives the signal sample when the recirculating registers are correctly aligned and holds this sample during the accumulating process.

A record of the 50 previous samples plus the current sample is contained in the 51-bit recirculating storage register. Each time the current sample hold receives information from the sampling circuitry, the 51-bit register is precessed and the new sample information entered.

The outputs from the current sample hold and 51-bit register go to the comparison and add logic which compares the sample hold output to each twentieth bit in the 51-bit register. If agreement exists, the corresponding 20-bit word on the 1020-bit line is incremented by one count. At the end of 1020 μ sec, the 51-bit register has recirculated 20 times. Since 51 is relatively prime to 20, all 51 bits will have been compared to the current sample hold.

Thus, the 1020-bit storage register contains the 51 autocorrelation coefficients (lags), each of which occupies 20 bits of storage. Since each lag is formed by observing the twentieth bit positions on the 51-bit line, consecutive word positions on the 1020-bit line correspond to twentieth bit lag numbers taken modulo 51. As a result, consecutive words on the 1020-bit line contain lag numbers 0, 20, 40, 9, 29, 49, 18, etc.

The output bit storage, under command of the computer, consecutively selects the 1020 bits of the 1020-bit line, one bit per computer command. The first bit selected is the least significant bit of lag 0, followed by the next least significant bit, etc. After lag 0 is read out, the next lag to be read out is lag 20 as discussed above.

d. Front panel controls. Fig. 18 is a photograph of the front panel controls and displays. These controls and

displays are used for machine setup, operation, readout of internal parameters, and verification of correct performance. Arrangement of the controls conform where possible to the principle of functional grouping.

The ac power group consists of an on-off toggle switch, power indicator light, and elapsed time meter. The toggle switch activates a relay which, in turn, supplies power to the equipment.

The display group on the upper half of the panel consists of the 20 indicator lights, digit switch, zero lag light, 200-deg meter, and adjacent meter controls. The 20 indicator lights display the 20 bits of information in any lag of any channel as selected by the digit switch. Least significant bits are on the left and most significant bits are on the right. The left decade of the digit switch selects the channel as read directly from the dial. The right two decades select the lag using a special code determined by the internal logic. During normal operation, the zero lag should be monitored because it will have the highest count. The decade code for lag 0 is 50, and when the lag decades are set to this number the zero lag indicator will light. The 200-deg meter reads the output of a special D/A converter whose inputs are the six most significant bits of the display. Calibration of the meter is done by reading either all ones or all zeros into the D/A converter with the toggle switch to the left of the meter. Full-scale meter deflection is set by the potentiometer on the right side of the meter.

Input signal sampling is controlled by the sampling period digit switch located on the lower left corner of the panel. The actual period between sample pulses is found by taking the decimal equivalent of the switch dial, which reads in octal notation, and multiplying by 20 μ sec. Dial readings for proper operation will be within the range of 63 to 1776, corresponding to a sampling period range of 1020 to 20,440 μ sec.

To the right of the sampling period digit switch is the group of controls associated with X-Y recorder. The XY D/A test toggle switch puts all ones or all zeros into the XY D/A converter. This permits setting up the scale limits on the X-Y recorder using the recorder zero and sensitivity controls. The pen controls permit manual operation of the pen. When the pen is down, the pen down indicator will light. These control functions are duplicated by the computer, and therefore not used during operation.

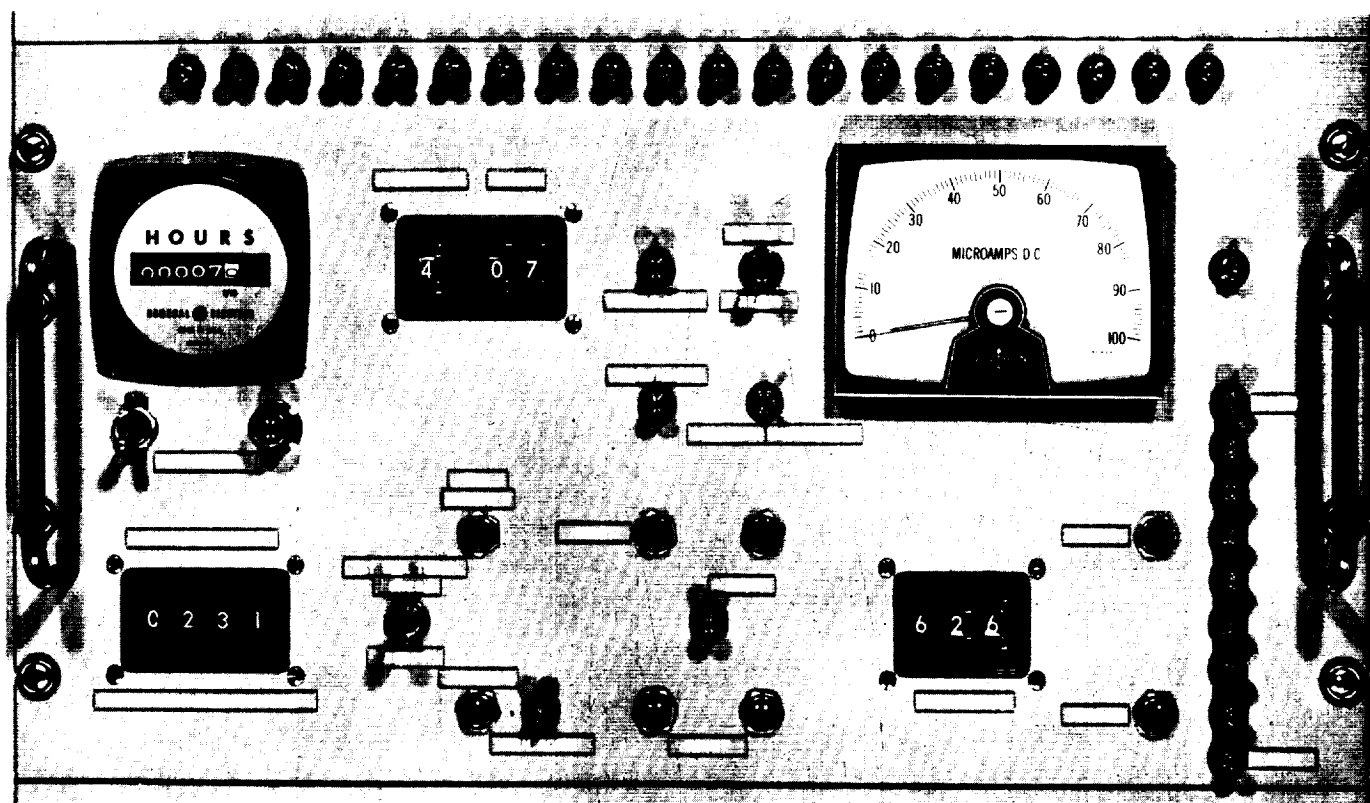


Fig. 18. Front panel controls

Adjacent to the recorder controls is the prime autocorrelator control group. The start pushbutton puts the autocorrelator in the operate mode, and the stop pushbutton puts the autocorrelator in the stop mode. When the autocorrelator is stopped, the stop indicator will light and sampling will be inhibited. The start and stop functions are normally controlled by the computer. Beneath the stop indicator are two red reset pushbuttons. These act only when the autocorrelator is stopped, and only when both buttons are depressed at the same time. This is to help guard against accidental loss of information due to possible operator error. Resetting the autocorrelator puts zeros in the 1020-bit accumulator memories, and also in the 51-bit storage registers.

The PN delay digit switch selects the code word to which the PN generator will be set in response to the word detect synchronizing signal from the transmitter coder. In effect, this permits inserting a constant phase delay between the transmitter coder and PN generator. Since the word detect signal detects all ones, zero delay occurs with a switch setting of 777.

The vertical group of indicators on the right side of the panel monitors the channel outputs to the computer. The

load pushbutton puts the first bit of each channel into the output bit storage flip-flop. This bit is the least significant bit of the zero lag. The test pushbutton puts all ones in the output storage flip-flops.

An additional function not previously discussed has been incorporated in the nine-channel autocorrelator. In some experiments it may be desired to subtract the autocorrelation function of pure noise from the autocorrelation function of signal plus noise under the command of an external keying signal. The autocorrelator can accept such a command signal, and during the subtract cycle will count *disagreements* between the current sample hold and previous signal samples, except for the zero lag. The keyed-internal toggle switch in the center of the control panel inhibits the external keying signal when turned to the internal position. When the switch is in the keyed position and the keying signal has put the autocorrelator in the subtract mode, the subtract light will be on.

e. Conclusion. The nine-channel autocorrelator has been completely tested in the laboratory. Installation in the field and preliminary field testing have also been successfully concluded. During operation the unit is completely controlled by the computer with the exception of

the reset function. This exception was incorporated to compel a minimal amount of operator control over the experiment. Additional logic has been provided in the autocorrelator to permit computer control of the reset function should this be desired in future operations.

C. Ranging and Tracking System Development

1. Microwave System Design Performance

a. Introduction. Over-all system performance of the monostatic satellite and lunar radar (MSSLR) versus cost is investigated for various alternative microwave feed line arrangements. The system will utilize the existing 30-ft antenna and will operate at S-band (2388 Mc). The feed line will connect an apex mounted monopulse feed,

via the quadripod legs, to the transmitting and receiving equipment located in the electronics cage. It is proposed to use an existing S-band apex monostatic feed which was matched originally at 2295 Mc and which will therefore have to be modified and retuned to 2388 Mc.

b. Transmitter system. The transmitter power P_t reaching the antenna (Fig. 19) is:

$$P_t = (P_x - P_c - P_{sw} - P_L - P_D) \\ = 71.1 - 0.01 - 0.04 - 0.102 - 0.14 = 70.81 \text{ dbm}$$

where

$$P_x = \text{transmitter output power} = 13 \text{ kw} = 71.1 \text{ dbm}$$

$$P_c = \text{back-forward power coupler loss} = -0.01 \text{ db}$$

$$P_{sw} = \text{waveguide switch loss} = -0.04 \text{ db.}$$

$$P_L = \text{line loss using WR 430 oxygen-free, copper waveguide (Table 4)} = -0.102 \text{ db}$$

$$P_D = \text{duplexer loss} = -0.14 \text{ db}$$

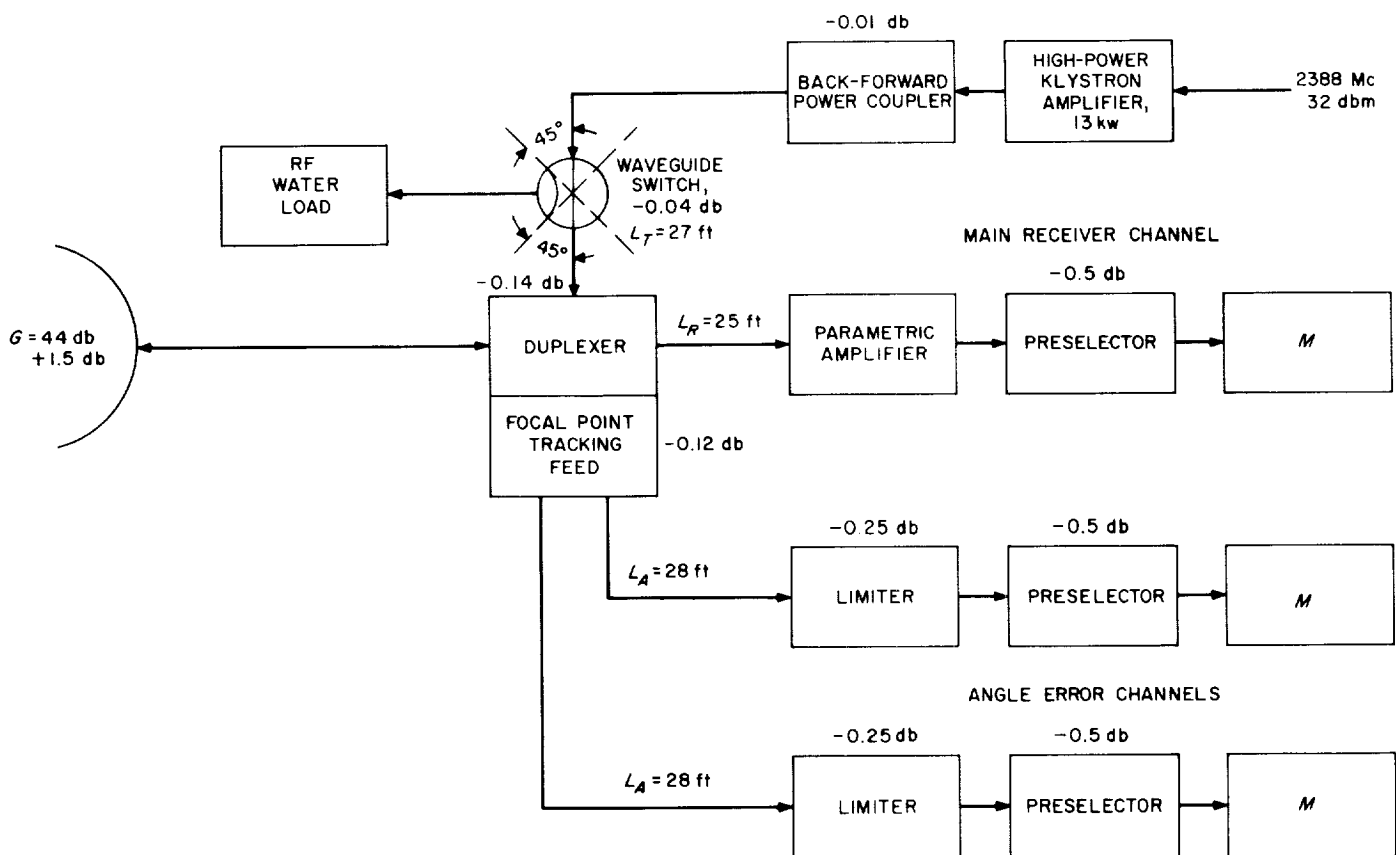


Fig. 19. Microwave feed system

Table 4. System capability

Target	Range at		σ/R^4 at		S/N ratio (db) at	
	Zenith	Horizon	Zenith	Horizon	Zenith	Horizon
6-in.-diameter Vanguard	400	3000	9.83×10^{-26}	3.07×10^{-29}	+ 3.5	- - 31.5
36-in.-diameter satellite	500	3500	1.45×10^{-24}	6.05×10^{-28}	+ 15.2	- 18.6
135-ft-diameter Echo II	800	4500	4.45×10^{-22}	4.37×10^{-25}	+ 40.05	+ 10

The effective radiated power, P_{eff} is:

$$P_{eff} = P_t + G$$

$$= 70.81 + 42 = 112.81 \text{ dbm}$$

where G = antenna gain = 42 db (estimated). The received signal strength s is:

$$s = \frac{P_{eff} G \lambda^2 \sigma}{(4\pi)^3 R^4} \text{ watts}$$

where

$$\lambda = \text{signal wavelength} = 300/2388 = 0.1255 \text{ m}$$

$$R = \text{target range in meters}$$

$$\sigma = \text{apparent radar cross-section of target}$$

$$= \pi r^2 h \text{ where } r = \text{radius of target in meters and}$$

$$h = \text{reflectivity of target}$$

Table 4 indicates the value of σ/R^4 for various targets at zenith and at the horizon assuming a reflectivity $h = 1$. Since only 25% of the radiated power will appear in the carrier, the received carrier strength is:

$$s = 112.81 - 6 + 42 - 50.64 + 10 \log \left(\frac{\sigma}{R^4} \right) \text{ dbm}$$

$$= 98.17 + 10 \log \left(\frac{\sigma}{R^4} \right) \text{ dbm}$$

c. Receiver system. The receiver noise temperature $t_{(receiver)}$ for the main channel, from Fig. 19 is:

$$t_{(receiver)} = t_A + t_D + t_L + \frac{t_{(main)}}{G_{(D+L)}} \text{ } ^\circ\text{K}$$

where

$$t_A = \text{antenna temperature} = 30^\circ\text{K}$$

$$t_D = \text{duplexer loss } 0.14 \text{ db, temperature} = 10^\circ\text{K}$$

$$t_L = \text{feed line loss temperature from Table 5}$$

$$t_{(main)} = 411^\circ\text{K from Table 6}$$

$$G_{(D+L)} = \text{gain between antenna and main channel input}$$

$$\text{or } t_{(receiver)} = 40 + t_L + \frac{411}{G_{(D+L)}} \text{ } ^\circ\text{K}$$

Similarly, the receiver noise temperature $t_{(tracking)}$ for each of the angle error channels, from Fig. 19 is:

$$t_{(tracking)} = 40 + t_L + t_{FPT} + \frac{t_{(angle)}}{G_{(D+L+FPT)}} \text{ } ^\circ\text{K}$$

where

$$t_{FPT} = \text{tracking feed loss temperature} = 0.12 \text{ db} = 8^\circ\text{K}$$

$$t_{(angle)} = \text{noise temperature angle error channel from Table 6} = 2147^\circ\text{K}$$

$$G = \text{gain between antenna and angle error channel input}$$

or

$$t_{(angle)} = 48 + t_L + \frac{2147}{G_{(D+L+FPT)}} \text{ } ^\circ\text{K}$$

Table 7 (lines 1 and 2, respectively) summarizes the cost and performance of alternative feed line arrangements from the detailed breakdown (Table 5). The over-all receiver noise temperatures for the main and angle error channels have been computed and entered on line 3, from which it would appear that the best compromise would be to use Helix 561 for the receiving channels.

This yields a noise temperature of 516°K for the main channel and 2542°K for each of the angle error channels. Using a 20-db directional coupler (instead of 10 db) for noise figure instrumentation in the parametric amplifier

Table 5. Microwave feed for 30-ft antenna

Description	Decibel loss per 100 ft	Price per foot	Loss, db	Unit price	Cost, dollars	T , °K (feedline)
Transmitter						
Two 10-ft lengths WR 430 waveguide	0.3		0.060	425	950	
One 5-ft length WR 430 waveguide	0.3		0.015	335	335	
One 2-ft length WR 430 waveguide	0.3		0.006	281	281	
Three elbows			<u>0.021</u>	245	<u>735</u>	
Total			0.102		2301	
Main receiver channel						
(a)						
Two 10-ft lengths WR 430 waveguide	0.3		0.060	425	950	
One 3-ft length WR 430 waveguide	0.3		0.009	300	300	
One 2-ft length WR 430 waveguide	0.3		0.006	281	281	
Three elbows			<u>0.021</u>	245	<u>735</u>	
Total			0.096		2266	7.0
(b)						
25-ft length 1½-in.-diameter Helix 561	1.15	2.98	0.29	75	75	
MCS waveguide to coax transition			<u>0.02</u>	285	<u>285</u>	
Total			0.31		360	21.0
(c)						
25-ft length 7/8-in.-diameter Helix 560	2.50	1.33	0.63	34	34	
Total (including transition)			0.65		319	47.0
(d)						
25-ft length 1½-in.-diameter Styroflex	1.4	3.19	0.35	80	80	
Total including transition			0.37		365	26.0
(e)						
25-ft length 7/8-in.-diameter Styroflex	2.6	1.44	0.65	36	36	
Total including transition			0.67		321	48.0
Angle error channels (two)						
(a)						
28-ft length 1½-in.-diameter Helix 561	1.15	2.98	0.32	84	168	
Total including transition			0.34		738	24
(b)						
28-ft length 7/8-in.-diameter Helix 560	2.50	1.33	0.70	38	76	
Total including transition			0.72		646	53
(c)						
28-ft length 1½-in.-diameter Styroflex	1.4	3.19	0.39	90	180	
Total including transition			0.41		750	29.0
(d)						
28-ft length 7/8-in.-diameter Styroflex	2.6	1.44	0.73	42	84	
Total including transition			0.75		654	55.0

(Fig. 20), the main receiver noise temperature would improve to 418 deg (based on 0.15-db directional coupler loss).

Also, eliminating the preselectors from the angle error channels (Fig. 19), the noise temperature for each of these channels would improve to 1957°K.

Table 6. Receiver noise temperature

Component	Noise temperature, °K	Noise temperature contribution	
		Main channel, °K	Angle error channel, °K
Parametric amplifier (Fig. 20)	211	281	
Input limiter loss, 0.25 db			
Input directional coupler loss, 0.75 db			
Cabling and connector losses, 0.25 db			
Total input losses, 1.25 db	97	97	
Output directional coupler loss, 0.75 db			
Output isolator loss, 0.50 db			
Output cabling and connection losses, 0.3 db			
Total output losses, 1.3 db	101	1.3	
Mixer plus IF noise figure, 8 db	1540	31	2050
Preselector loss, 0.5 db	35	0.63	
Angle error channel limiter loss, 0.25 db			
Cabling and connector losses, 0.5 db			
Total input losses, 1.25 db	97		97
Total noise temperature		411	
Main channel $t_{(main)}$			
Angle error channels $t_{(angle error)}$			2147

d. Receiver power sensitivity. Power sensitivity of main channel = $Kt_s B$ where

K = Boltzmann's constant = 1.38×10^{-23} joules/°K

t_s = system noise temperature

= $t_{(receiver)} + t_{(target)}$

B = bandwidth = 100 cps

For 50% keying and assuming the noise contributed by the cool sky is negligible with respect to the receiver noise:

$$\begin{aligned} \text{Receiver threshold} &= \frac{Kt_{(receiver)} B}{2} \\ &= \frac{1.38 \times 10^{-23} \times 418 \times 100}{2} \text{ watts} \\ &= 2.89 \times 10^{-19} \text{ w} = -155.4 \text{ dbm} \end{aligned}$$

and signal-to-noise ratio S/N will be:

$$\begin{aligned} S/N &= 98.17 + 10 \log \frac{\sigma}{R^4} + 155.4 \text{ db} \\ &= 253.57 + 10 \log \frac{\sigma}{R^4} \text{ db} \end{aligned}$$

which is plotted in Fig. 21 for the 6-in. *Vanguard* and typical 36-in.-diameter satellites and 135-ft-diameter *Echo II* between zenith and horizon. The differences between alternate feed systems are too small to plot in Fig. 21.

2. Monostatic Satellite and Lunar Radar Synchronous Sideband Detector

a. Introduction. As discussed in a previous report (SPS 37-25, Vol. III, p. 47; note correction p. 49, $T_1/T_2 = 0.98$ not 0.5%), the subsystem designed for odd-order keying sideband lock detection is ineffective on "even" even-order sidebands and requires a predetection bandwidth wider than is optimum for the main receiver channel. Means of extending detection capability to *all* sidebands, including even-order which arise due to time asymmetry in the IF signal, and the feasibility of an auxiliary wide-band IF channel for the sideband detector have been investigated during this reporting period.

b. Even-order sideband detection. Whereas odd sideband detection is obtained by correlating the received

Table 7. Cost/performance summary

Description	Microwave feed line				
	WR 430	Helix		Styroflex	
		561	560	1 7/8-in. diameter	7/8-in. diameter
Main channel	2266	360	319	365	321
1. Feed line cost, dollars	0.096	0.31	0.65	0.37	0.67
2. Feed line loss, db		516	579	528	583
3. Receiver noise temperature, $t_{(receiver)}$, °K	481				
Angle error channels					
1. Feed line cost, dollars (both channels)		738	646	750	654
2. Feed line loss, db (each)		0.34	0.72	0.41	0.75
3. Receiver noise temperature, $t_{(tracking)}$, °K		2542	2790	2587	2813

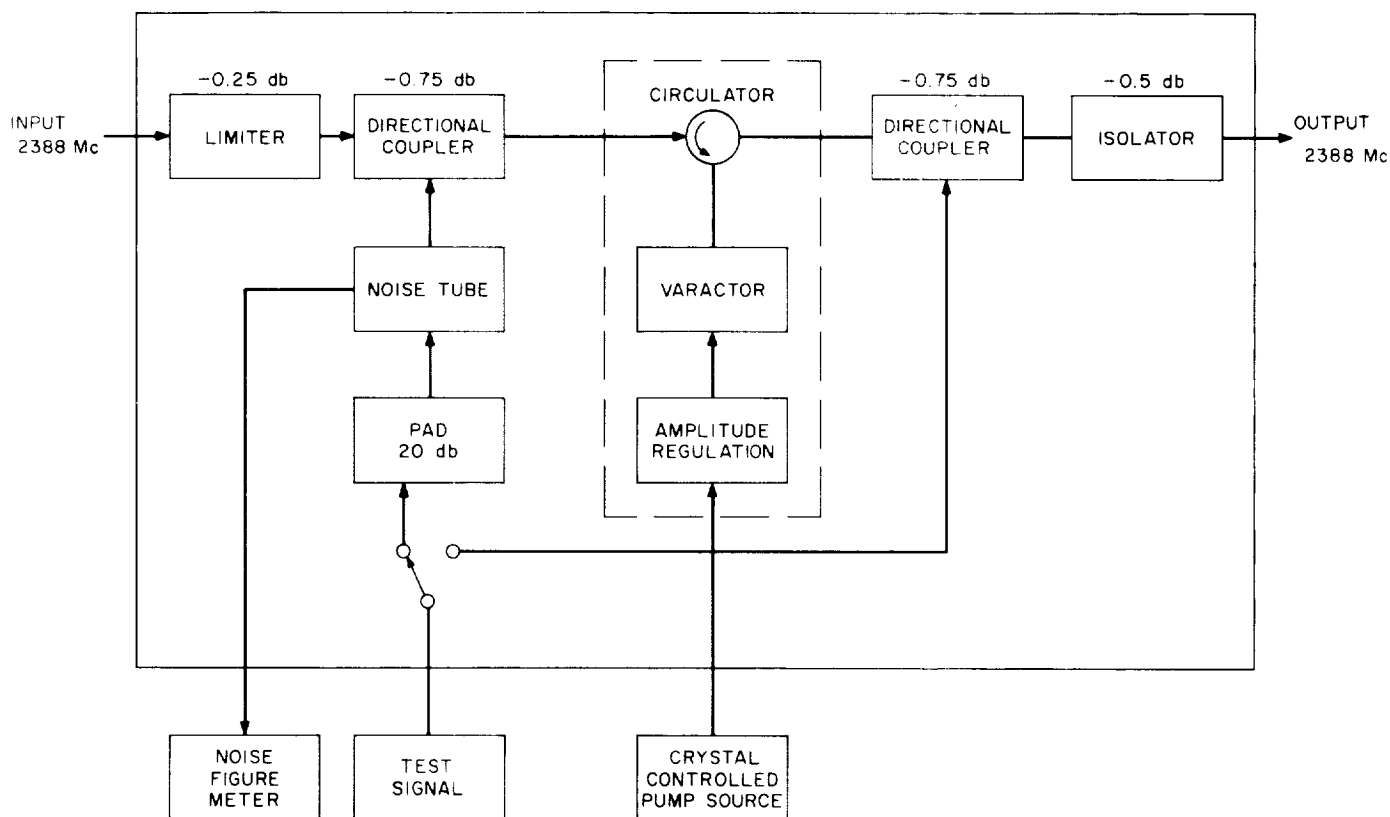


Fig. 20. Parametric amplifier system

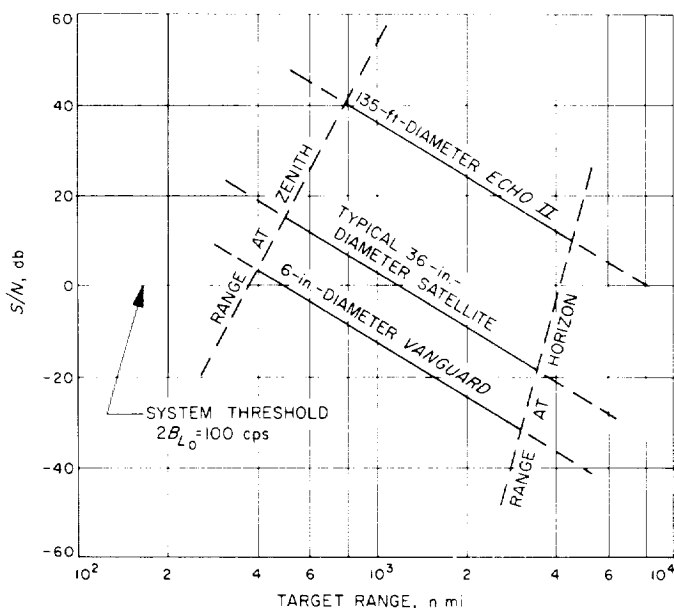


Fig. 21. System capability

signal with a square wave modulated reference signal (thus possessing a spectrum of odd and *only* odd keying sidebands), even-order sideband detection should be feasi-

ble through synthesis of an even-order modulated reference. Readily synthesized low-frequency waveforms of the proper spectra include ramps whose fundamental frequency equals twice and four times the keying rate. Since a ramp in time represents a frequency spectrum containing *all* harmonics of the fundamental having amplitudes inversely proportional to order of harmonic, a twice keying rate ramp contains all *even*-order keying sidebands, and the four times keying rate ramp contains all "*even*" even-order keying sidebands. As noted in the cited report, the odd-order detector produces correlation at the "*odd*" even-order sidebands. This results from the fact that the pure odd order reference is, in effect, modulated by a similar waveform (the signal) but delayed 90 deg with respect to the keying fundamental. The significance of this phenomenon is that it is not *necessary* to duplicate "*odd*" even-order protection in the solution of the "*even*" even-order problem. Although investigation has included the twice keying rate ramp, as well as several other less promising variations, attention here will be focused on the four times keying rate ramp.

The analyses and experiment have been based upon ramp phase modulation of the detection reference with

an index of ± 90 deg, which is equivalent to that used in the square wave or step modulated detector. Contemplation of this mechanization leads to two problems: (1) linear, wide-angle phase modulation and (2) presence of significant carrier power in the resulting spectrum. The significance of the presence of the carrier is that a sideband detector of this nature would tend to label a carrier lock as being that of a sideband. Even if the required phasing produced a correlation null for the carrier, any amount of dynamic phase error experienced by the main loop would tend to reject a valid carrier lock. Although once carrier lock is obtained (satellite acquisition normally occurs at a time of minimum rate error) the sideband detector could be disabled, a more straightforward and reliable solution appears to be that of removing the carrier component from the phase modulated reference prior to correlation with the signal. The principal problem in the design of a carrier rejection filter is that of preserving the phase of the low-order sidebands.

For purposes of system evaluation of even-order sideband solutions, an existing wide-angle modulator design has been adapted including the addition of a carrier rejection filter. The latter consists essentially of a wide-band operational amplifier with a 455-kc crystal in the

feedback path. The modulator is capable of producing extremely linear modulation at indices approaching ± 180 deg per time delay multivibrator stage. Fig. 22 shows the principal functions of the modulator.

Table 8 reveals the spectra of the several waveforms of interest. The interval "S" indicates the nominal "on" time of the received signal. Note that waveforms A through D all are phased such that a step occurs at the 90-deg point of the received signal square wave corresponding to "S." Columns B and D indicate the sidebands for which detection is expected for step and ramp modulation, respectively. Recalling that multiplication of periodic signals corresponds to algebraic addition of phase angles, Column D may be interpreted as B shifted two sideband numbers, noting that D differs from B only in the addition of 4×90 deg in the interval "S" which corresponds to 180 deg of the keying waveform. The performance data of a sideband detector utilizing waveform C is shown in Fig. 23 superimposed upon the previously reported data for the waveform A detector. The desired immunity to carrier detection as a sideband lock was achieved with a 12-db margin under least favorable phasing conditions. The dephasing of the two fourth-order sidebands, as evidenced in Fig. 22, is attributed to the carrier rejection filter.

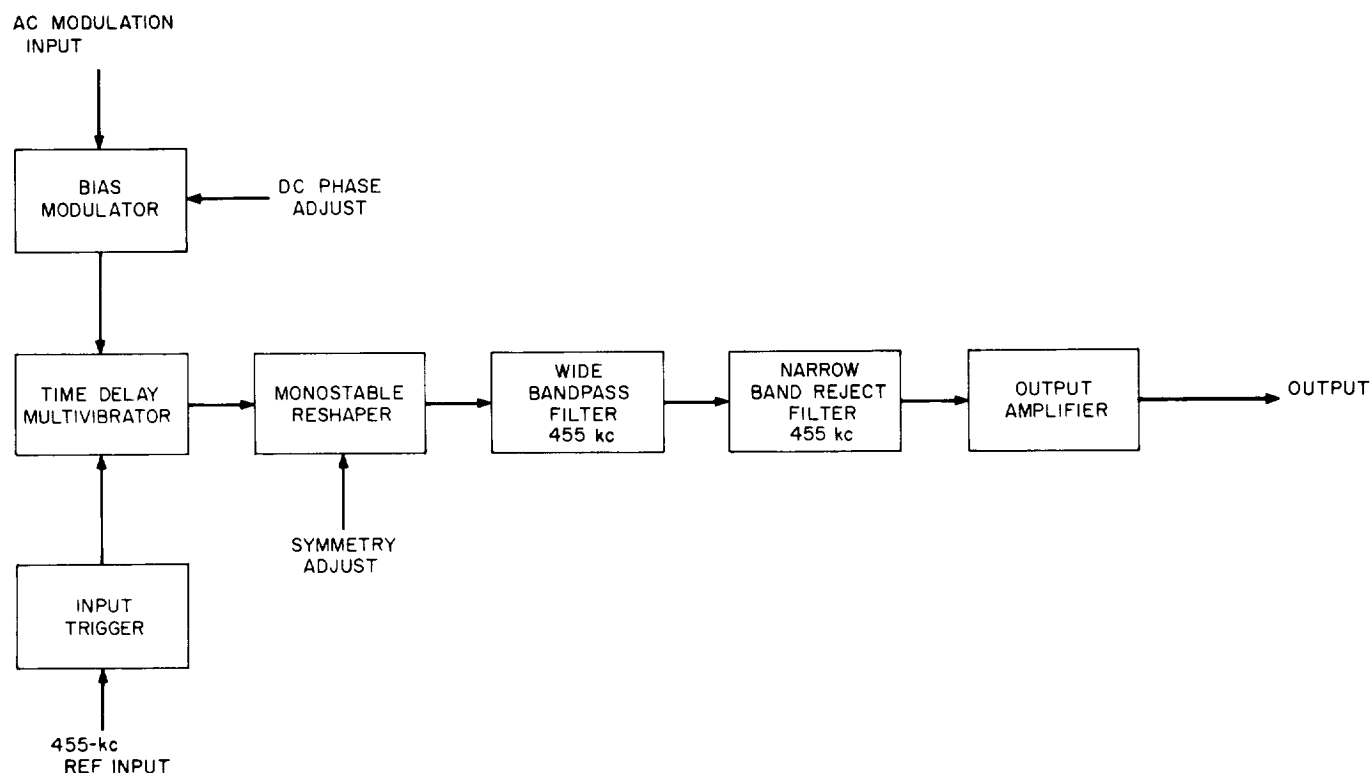



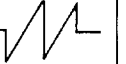


Fig. 22. Wide-angle phase modulator

Table 8. Modulation waveforms and spectra

	A	B	C	D
				
	± 90 -deg step modulation spectrum	"A" ampli- tude modulated by signal "S"	± 90 -deg ramp modulation spectrum	"C" ampli- tude modulated by signal "S"
Sideband number				
10		x		
9	x	x		x
8			x	x
7	x	x		x
6		x		
5	x	x		x
4			x	x
3	x	x		x
2		x		
1	x	x		x
0			x	[x]
1	x	x		x
2		x		
3	x	x		x
4			x	x
5	x	x		x
6		x		
7	x	x		x
8			x	x
9	x	x		x
10		x		

[] Carrier to be eliminated.

c. *Sideband detector implementation.* While the methods described in the preceding paragraphs may be used in a "ramp" detector whose logical output is combined in an "or" fashion with the output of the "step" detector to provide a composite "sideband lock" indication and control, hardware complexity might be reduced (to one each modulator, phase shifter, and detector, instead of two each, plus additional common input and output devices) by combining the reference spectra prior to modulation. The principal questions involved in such an alternative are:

- (1) In what relative phase should the spectra be combined?
- (2) What effective modulation index should be used for each component?

The answers to these questions are presently under investigation. Also under study are the 455-kc (IF) phasing problems first encountered with the "step" detector

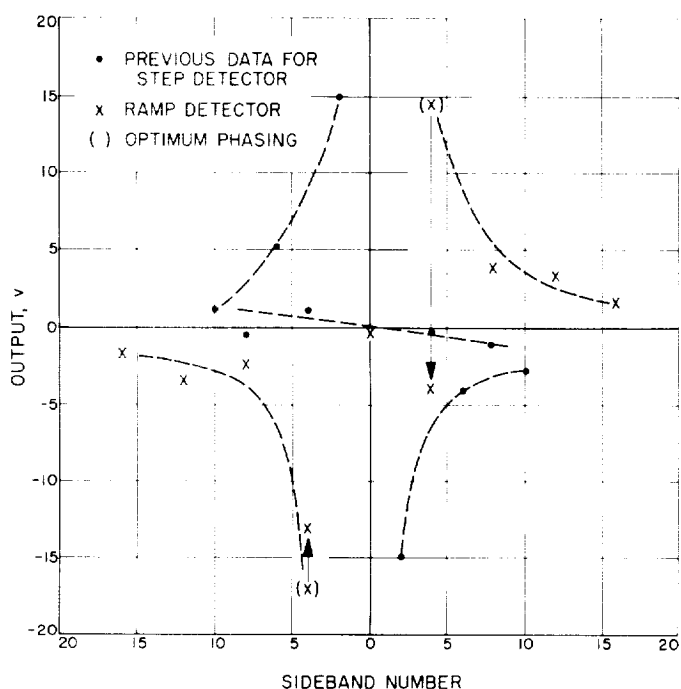


Fig. 23. Even-order sideband detector performance

and complicated by the possibility of the separate wide-band IF channel and of the "ramp" detector.

The data of Fig. 24 was obtained by locking the receiver sequentially to each indicated sideband and noting the optimum phasing required to produce [a] maximum output in narrow-band channel (taken to indicate the sideband phase relative to the carrier, as "seen" by the main loop) and [b] minimum output in wideband channel (when compared to [a], interpreted as a measure of differential phase shift between the channels).

Interpretation of the data of Fig. 24 is difficult. First, the phase shift of the narrow channel has been independently measured to be approximately 100 deg per sideband (of Fig. 24) over the passband corresponding to $\pm 3\frac{1}{2}$ sidebands. This figure greatly exceeds most trends evidenced within this band. Second, while the trends of the odd sidebands of *both* channels approximate the known phase slope of the wideband channel (approximately 3.6 deg per sideband over ± 25 sidebands), it is difficult to imagine how the performance of the *main* channel could be affected by the *auxiliary* channel.

The odd-order data indicates reasonably constant phasing both with sideband number and between channels, but the even-order results show trends more nearly related to the steep phase characteristic and band limiting

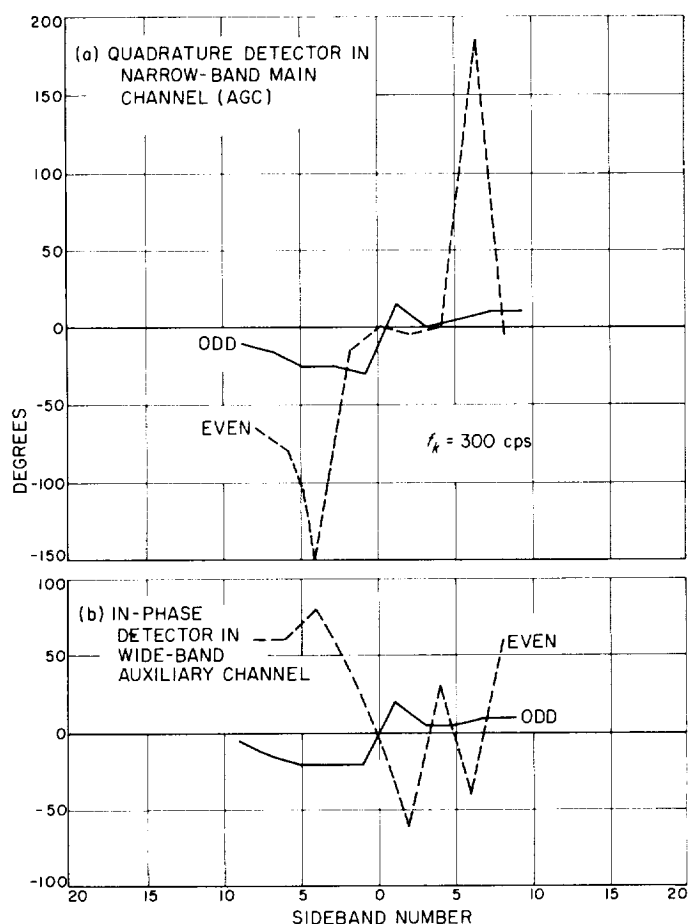


Fig. 24. Optimum phasing for synchronous detectors

of the main channel. This phase discrimination between odd and even sidebands must evidently be caused either by the phase structure of the received signal or by the mechanism of even-order lock and not by the phase versus frequency characteristics of the channels as such.

3. Monostatic Satellite and Lunar Radar Receiver Module Development

a. Introduction. The monostatic radar, as depicted in Fig. 66 of SPS 37-24, Vol. III, will make use of many modules and subsystems similar or identical in design to those of previous systems. While this similarity affords maximum flexibility and ease of evolution of new systems, there are frequently unique requirements in a given configuration and also opportunity for "standard" module revision. One example of each is discussed in the following paragraphs.

b. Solid-state, high-power limiter. The relatively high (hundreds of cycles per second) keying rate required for

a monostatic satellite radar does not afford time for receiver protection by means of waveguide switching as is done currently in planetary work. The design (Ref. 24) provides for isolation of the receiver from the transmitter in the following manner. Referring to Fig. 25, it is planned to reduce the approximately 10-w duplexer leakage to tolerable levels in the receiver by means of solid-state limiters. Although only the carrier reference channel is shown in the figure, the receiver mixers in the antenna angle error channels will be similarly protected. The requirements on the duplexer feed for receiver protection are also shown in detail in Fig. 25.

Present planning calls for use of an orthogonally circularly polarized tracking feed (Ref. 24, Fig. 27), which inherently includes a duplexing function. While the VSWR of the feed proper *may* not be explicitly measurable, the effect of internal mismatches are of interest in the receiver protection problem.

A limiter with the following principal performance specifications has been procured for evaluation:

Operating frequency	2388 \pm 5 Mc
Input power	16 w, maximum
Output power	16 mw, maximum
Low-level insertion loss	0.2-db nominal, 0.5 db absolute maximum
Low-level phase stability	\pm 1 deg, short term maximum
Duty cycle	0 to 100%
Spike leakage duration	1.0 μ sec, maximum
Spike energy	0.5 erg, maximum

The design consists of a two-stage, solid-state diode limiter furnished in a coaxial connector package. Preliminary

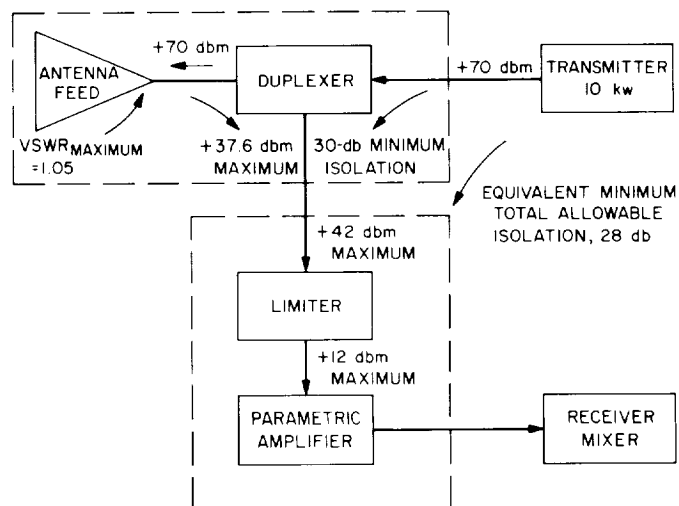


Fig. 25. Monostatic radar receiver protection

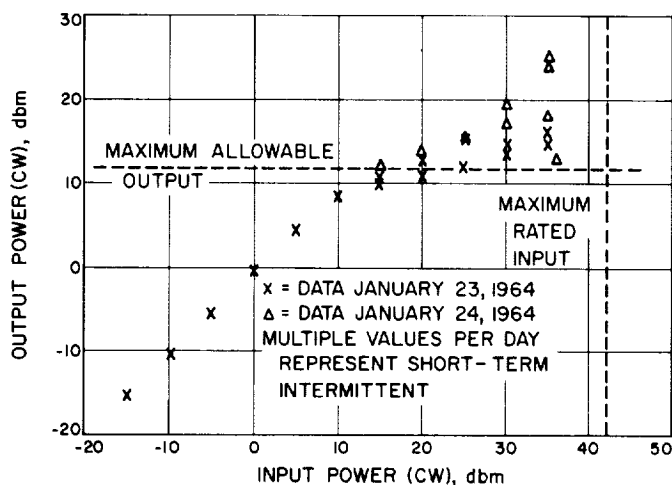


Fig. 26. Solid-state, high-power limiter

evaluation indicates a low-level (receiving) insertion loss of 0.15 db and a limiting characteristic indicative of an acceptable design. However, the evaluation unit exhibited an intermittent condition as evidenced by Fig. 26. The procurement of a quantity sufficient for the operating system awaits resolution of this problem with the supplier.

c. Integrated mixer preamplifier. In each of the three tracking channels, an S-band mixer with preamplifier follows the limiter (parametric amplifier in the case of the carrier reference). A survey of commercially available mixer/preamplifiers has been made with the intention of improving packaging size and availability as compared with the JPL design used previously. A quantity of the selected model has been procured. The design makes use of three miniature tubes as compared with four subminiatures in the JPL design. The size reduction is obtained primarily in the coaxial hybrid mixer and in the interconnection with the preamplifier.

The measured performance (Table 9) compares favorably with the previous design, particularly with regard to bandwidth which is required to pass ranging modulation.

Table 9. Comparison of measured performance characteristics

Characteristics	LEL preamplifier	JPL preamplifier
Input frequency, Mc	1700 to 2400	2388
Output frequency, Mc	30	30
Bandwidth, Mc	8 ^a	2
Conversion gain, db	41.5	48 ^b
Noise figure, db	8.5	9.3

^aRated value.
^bComparison unit with grounded AGC input.

While the JPL design is capable of some 15 db more gain at an elevated bias input, the lower gain figure is deemed adequate. Although gain control of the preamplifier is not contemplated for use with systems requiring the modest dynamic range of Earth satellites and planets, the bias performance of the subject unit has been evaluated. Fig. 27 compares the conversion gain of the test unit with that of the AGC grounded JPL mixer and preamplifier combination. Noise figure data is presented in Fig. 27. In order to avoid measurement uncertainties related to a preselector and associated interconnections, the single sideband noise figure was inferred by adding 3 db to the value obtained by direct measurement at the mixer input.

Slightly offsetting the physical advantages of the integrated mixer/preamplifier is the need for external shielding and additional line filtering required to meet JPL interference specifications.

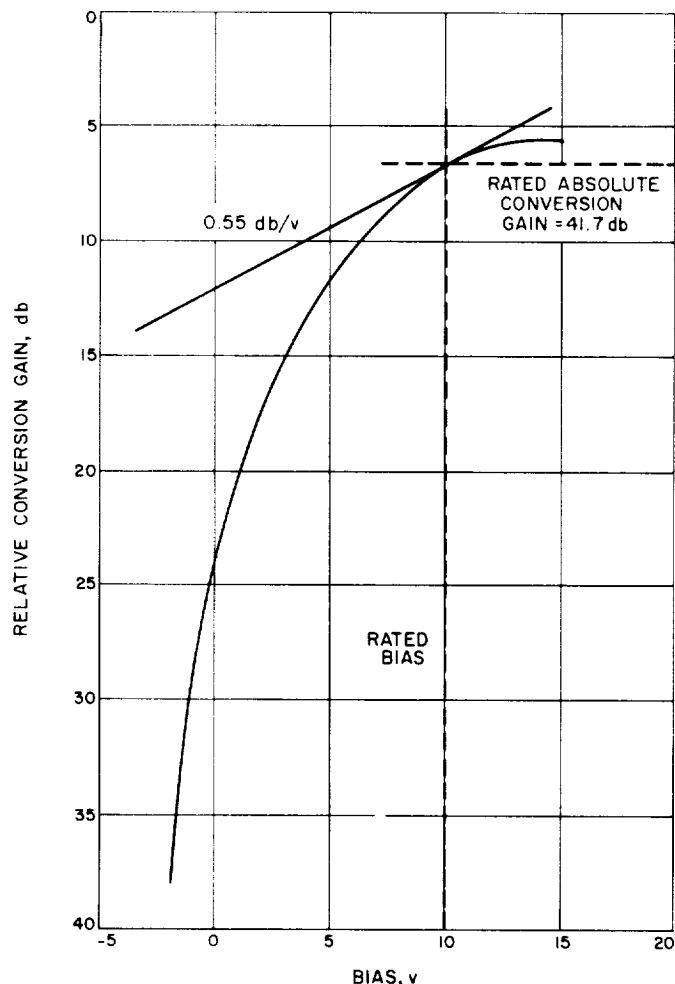


Fig. 27. Integrated mixer preamplifier bias sensitivity

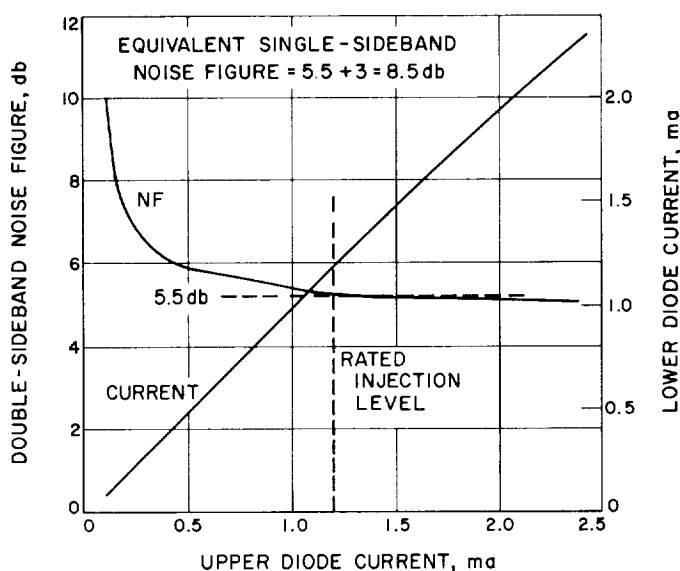


Fig. 28. Integrated mixer preamplifier noise figure and dc mixer balance

4. 10-kw S-Band Transmitter

a. Introduction. The 10-kw, S-band, 2.388-Gc transmitter is being built at JPL as reported in Ref. 25. The design will incorporate many of the better features of the old 10-kw transmitter as well as the present 100-kw S-band transmitter at GTS. Four areas of study have been, or are being, performed in conjunction with the design of the 10-kw transmitter. They are discussed in the following paragraphs.

b. Beam modulator. The beam modulator will electronically switch the klystron beam voltage *on* and *off* at rates up to 1000 cps with duty rates from 0 to 100%. Voltage rise and fall times are required to be 10 μ sec or less. The beam voltage must be switched off during the receive cycle because of the residual beam noise generated in the klystron with only the klystron drive off. The rapid switching rates necessary for a satellite tracking radar precludes using a conventional waveguide switch to direct this noise power, approximately 10 mw, into a suitable load.

Presently an engineering and cost study is being made to determine whether the beam modulation should be built by JPL rather than by outside contract; the contract bids for building the device according to JPL specifications were considerably more than the original estimate, and the technical proposals seemed unnecessarily complicated. A possible course would be JPL design and outside fabrication.

c. Bombarder power supply. The transmitter incorporates a three-phase, full-wave rectified bridge (Fig. 29) rated at 2000 v dc at 125 ma to provide cathode heating through diode action between filament and cathode of the klystron. Previously each diode stack was required to withstand the 2000 peak inverse voltage. Transients caused by the beam modulator turning the 17-kv beam voltage *on* and *off* at rates up to 1000 cps will require the diode stacks to hold off the 17-kv beam voltage. The transients will be caused by the 200-pf stray capacitance of the filament and bombarder transformers charging up to the full 17 kv during beam voltage *on* time. During *off* time, this capacity will develop a peak inverse voltage of 17 kv across the right-hand diode stacks. New diode stacks will be designed for a working voltage of at least 17 kv and will have resistors and capacitors in parallel with the diodes to ensure even voltage distribution during both steady and transient conditions.

The diode stacks of the old 10-kw system were a constant source of trouble. Although the old system did not have a beam modulator, a similar transient state occurred during planetary radar work as a high-speed vacuum switch was used to remove the beam voltage at the end of a transmitter run. The voltage transients described above were probably responsible for the breakdown of the diodes which was experienced periodically.

d. Variable attenuators. The variable attenuators used to set the klystron RF forward and back power meter

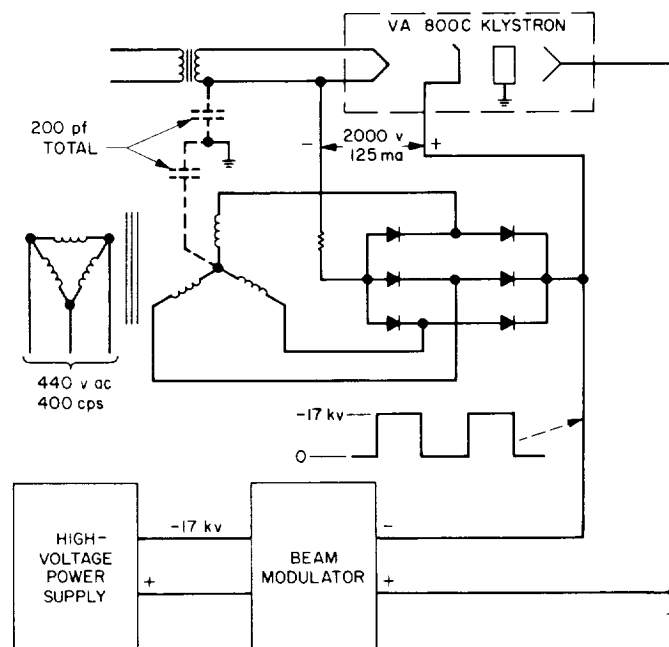


Fig. 29. Simplified schematic bombarder power supply

levels must be stable to permit accurate power measurements. The variable attenuators used on the 100-kw S-band transmitter at the Venus site were suspected of being temperature sensitive. These attenuators were checked in a test oven and the results are shown in Fig. 30, curves A and B. Attenuator B varied 2.3 db in the important temperature range of 60 to 120°F. Also shown in Fig. 30 are curves for C and D which are tests of the attenuators to be used in the 10-kw transmitter system and as replacements in the 100-kw system. The 10-kw transmitter attenuators will be mounted in a constant temperature oven to ensure stability with the widely varying ambient temperatures at GTS.

e. Beam power supply. The 10-kw transmitter will use the same power supply and control unit that was used on the *Echo* and planetary radar transmitter. Although the power supply was very reliable in operation, it had not been tested for volt-ampere characteristics since it was built. It was also desirable to know the internal impedance of the power supply so this can be considered in the design of the beam modulator; present plans call for the beam modulator to have internal beam voltage regulation circuits.

Fig. 31 shows the volt-ampere characteristics of the power supply determined from recent tests at Goldstone. The full rated capacity of 17 kv at 2.7 amp could not be obtained because of inadequate primary wire capacity during the temporary setup.

f. Test procedure. A dc water load with a variable length center electrode was used as a variable load; cir-

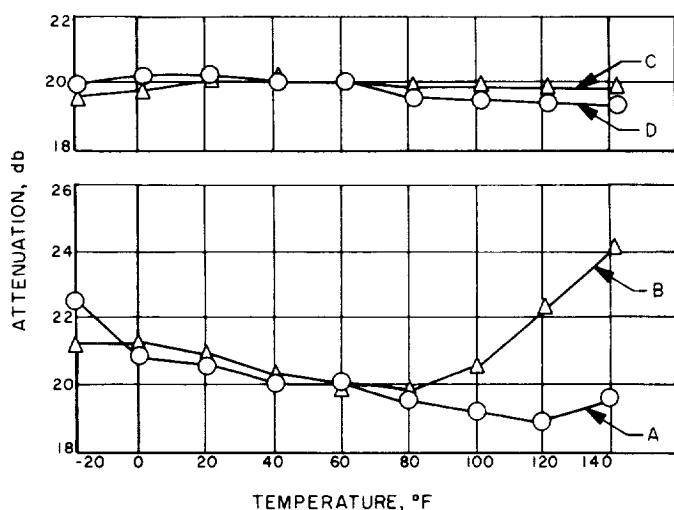


Fig. 30. Attenuator variation with temperature

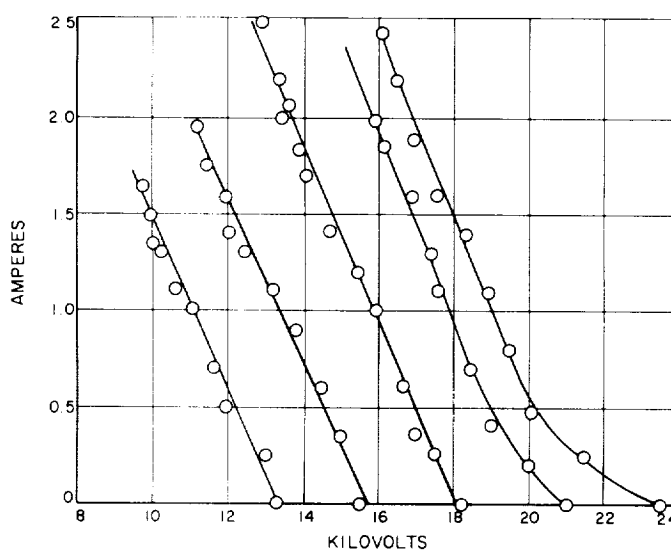


Fig. 31. 10-kw S-band transmitter power supply characteristics

culating distilled water was used as the resistive dissipating material. The power supply contains an Inductrol which makes the output voltage continuously variable. The power supply was adjusted for a no-load voltage; the water load was then connected and varied from maximum to minimum resistance. The voltage and current were then recorded at various load resistances.

The slopes of the volt-ampere lines are nearly constant, which indicates that the dc internal impedance of the power supply is nearly constant at about 2300 ohm for normal loads.

5. Ranging Coders

The monostatic keyed radar program is intended to provide a model for a DSIF S-band tracking system. Four coders are required: two form the range-gate subsystem; the remaining two are used for target-ranging. The design of these ranging coders is the subject of this article.

Since the system is to function at a maximum target range of 8000 km, it is possible to specify the minimum acceptable code length. An assumption is made that the code period should at least equal the round-trip time. The unit of range measurement is the microsecond; therefore, the required length p can be found from the following relationship.

$$p = \frac{2R}{c} = 53,300 \quad (1)$$

In Ref. 26, it is shown that a multiple component code offers a significant advantage over a single component code during the acquisition phase. This saving in acquisition time is expressed as

$$\frac{T'_{acq.}}{T_{acq.}} \simeq np \frac{1-n}{n} \left(\frac{\Delta c'}{\Delta c} \right)^{-2} \quad (2)$$

where $T'_{acq.}/T_{acq.}$ is the ratio of the acquisition time for an n -component code of period p to that of an equivalent length single component code. The ratio $\Delta c'/\Delta c$ is a measure of the relative correlation distinguishability for the two cases. Furthermore, the optimal acquisition ratio ($T'_{acq.}/T_{acq.}$) occurs when

$$4 < n < 5 \quad \text{for } p = 53,300$$

and the ratio is approximately 4×10^{-3} for $n = 5$. Since n is constrained to integer values, a five-component code was selected for use in the monostatic radar project.

The optimal component length is given by

$$v_i = (p) \frac{1}{n} \simeq 9 \quad (3)$$

At this point a working system is forced to depart from the optimal for several reasons. First, the five components must all be relatively prime. Second, certain sequences are easier to generate than others making their inclusion highly desirable. Finally, all current ranging systems include a clock component which is basically a sequence of length two. Given these restraints the following components were selected

$$\begin{aligned} v_1 &= 2 \quad (\text{clock}) \\ v_2 &= 7 \\ v_3 &= 11 \\ v_4 &= 15 \\ v_5 &= 23 \end{aligned}$$

The period provided by the above components is

$$p = (v_1 v_2 v_3 v_4 v_5) = 53,130 \quad (4)$$

which, for all practical purposes, is equal to the desired length. The number of steps required during the acquisition phase is given by the sum of all non-clock components

$$s = (v_2 + v_3 + v_4 + v_5) = 56 \quad (5)$$

The monostatic radar project requires two ranging coders: one provides the transmitted signal; the other acts as a local reference for the received signal. Though the coders are identical on the component level, they differ in the combinatorial techniques employed. Also, the transmitter coder can be synchronized to the receiver coder; and each component in the receiver coder can be shifted by one bit position at a time to facilitate acquisition. Shifting of the various components is accomplished by two basic methods. The first, employed in the 7, 11, and 15 coders, involves repeating a word vector to lengthen the code and deleting a vector to shorten the code. The word vectors are always a part of the main sequence. The second method, which is used in the length 23 coder, utilizes word vectors which are not a part of the main sequence. The procedure is to force the coder to a particular word vector outside of the sequence. When the coder finally returns to the main sequence, it will have been advanced or retarded by the desired amount. Some of the techniques used in shifting the various components differ from those employed in the past. These departures will be explained more fully in the description of each coder.

Both the length 7 (v_2) and the length 15 (v_4) components are generated by maximal length sequence generators defined, respectively, by the polynomials

$$x^3 + x + 1$$

and

$$x^4 + x + 1 \quad (6)$$

Fig. 32 illustrates the mechanization of the length 7 component and is representative of the method employed in the length 15 coder. Fig. 32(a) depicts the transmitter component coder which consists of two active stages and a unit delay. The second active stage facilitates in-phase synchronization with the receiver component coder. During the synchronization phase, code bits are transferred from the first stage of the receiver coder to the second stage of the transmitter coder. This results in an identical time-series sequence emerging from the second stage of both component coders.

The receiver component coder differs from the other in its ability to lengthen or shorten the sequence by one bit. Table 10, which shows all possible word vectors, will illustrate the method. A word detector indicates the existence of the 101 vector and, in the presence of a shift command, provides an input to the appropriate shift generator. To shift right (i.e., lengthen the sequence) the 111 vector is repeated by inserting an extra 1 into the first stage. The modified sequence is shown in the second column of

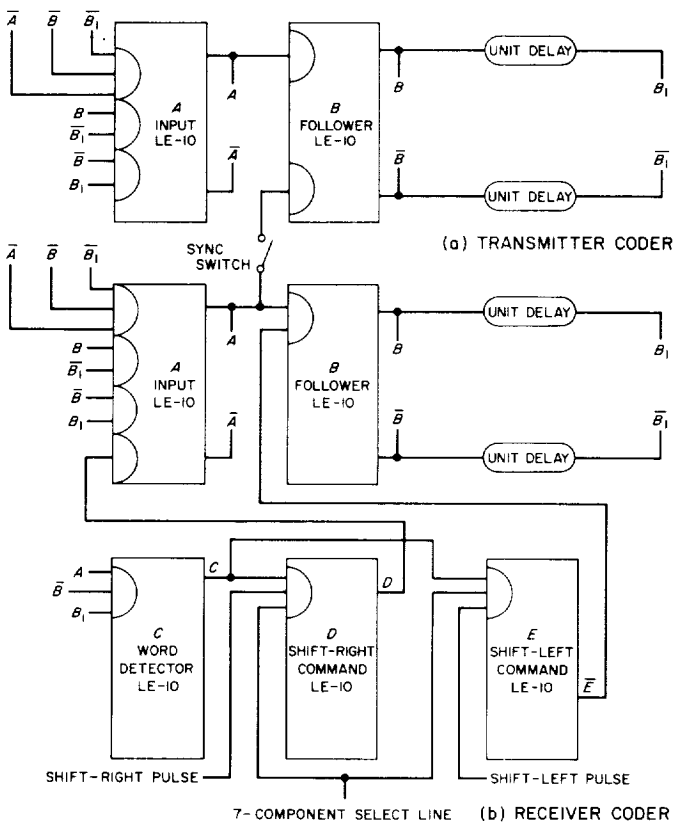


Fig. 32. Length 7 component coders

Table 10. To shift left (i.e., shorten the sequence) the 011 vector is skipped. The resulting sequence is shown in the third column of Table 10. The shift-left process represents a slight departure from the techniques employed in the past. Heretofore, it has been customary to inhibit the first stage when the all ones vector occurs, thus going directly to the 011 vector. The present method involves inhibiting the second stage with the result that the 011 vector is skipped and the sequence goes directly to 001. Since the length 15 coder (Fig. 33 and Table 11) is con-

Table 10. Length 7 code

Length	Standard sequence	Shift right	Shift left
1	1 0 1 (word detector)	1 0 1	1 0 1
2	1 1 0	1 1 0	1 1 0
3	1 1 1	1 1 1	1 1 1
4	0 1 1	1 1 1	0 0 1
5	0 0 1	0 1 1	1 0 0
6	1 0 0	0 0 1	0 1 0
7	0 1 0	1 0 0	0 1 0

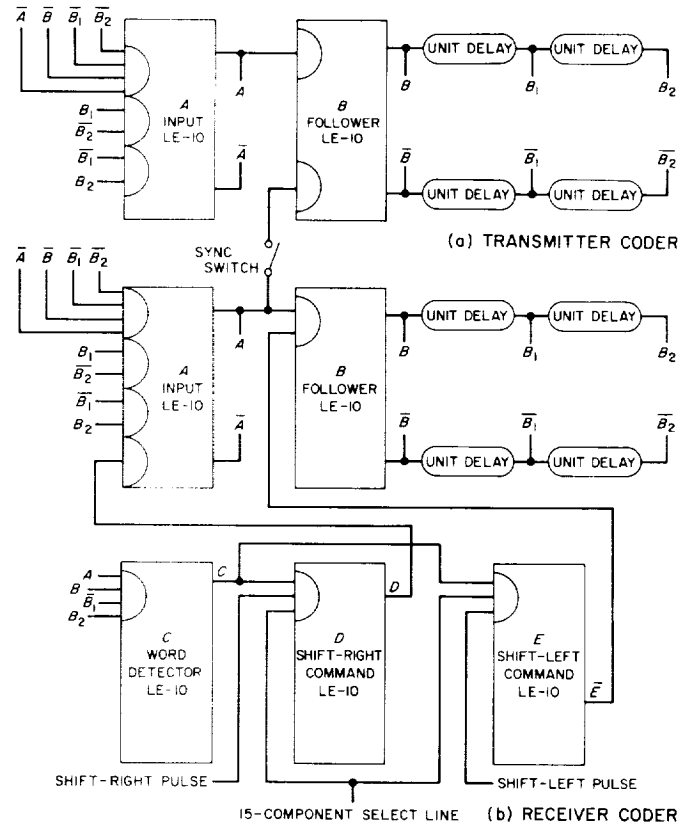


Fig. 33. Length 15 component coders

ceptually identical to the one just discussed, no further commentary will be made.

Table 11. Length 15 code

Length	Standard sequence	Shift right	Shift left
1	1 1 0 1 (word detector)	1 1 0 1	1 1 0 1
2	1 1 1 0	1 1 1 0	1 1 1 0
3	1 1 1 1	1 1 1 1	1 1 1 1
4	0 1 1 1	1 1 1 1	0 0 1 1
5	0 0 1 1	0 1 1 1	0 0 0 1
6	0 0 0 1	0 0 1 1	1 0 0 0
7	1 0 0 0	0 0 0 1	0 1 0 0
8	0 1 0 0	1 0 0 0	0 0 1 0
9	0 0 1 0	0 1 0 0	1 0 0 1
10	1 0 0 1	0 0 1 0	1 1 0 0
11	1 1 0 0	1 0 0 1	0 1 1 0
12	0 1 1 0	1 1 0 0	1 0 1 1
13	1 0 1 1	0 1 1 0	0 1 0 1
14	0 1 0 1	1 0 1 1	1 0 1 0
15	1 0 1 0	0 1 0 1	1 0 1 0

The length 11 sequence generator is more complex than the aforesaid units. Generation, although of the direct logic type, is not accomplished by the simple mod 2 addition of two stages. The length 11 transmitter coder is shown in Fig. 34(a). The generator has five stages, two active and three passive, providing a maximum of 32 possible states. Of these, the 11 states found in the first column of Table 12 form a closed loop in a state diagram. The logic is arranged such that any of the remaining states will eventually lead into the main loop, thus ensuring the proper starting of the coder. Coder synchroniza-

tion is achieved in the previously described manner by transferring the receiver sequence to the transmitter coder.

Mechanization of the receiver coder differs from the transmitter coder in its use of five active stages. These extra active stages considerably simplify the shifting procedure. Formerly, the process used in shifting the length 11 coder has been to leave the main loop of the state diagram by forcing the coder to a particular word vector.

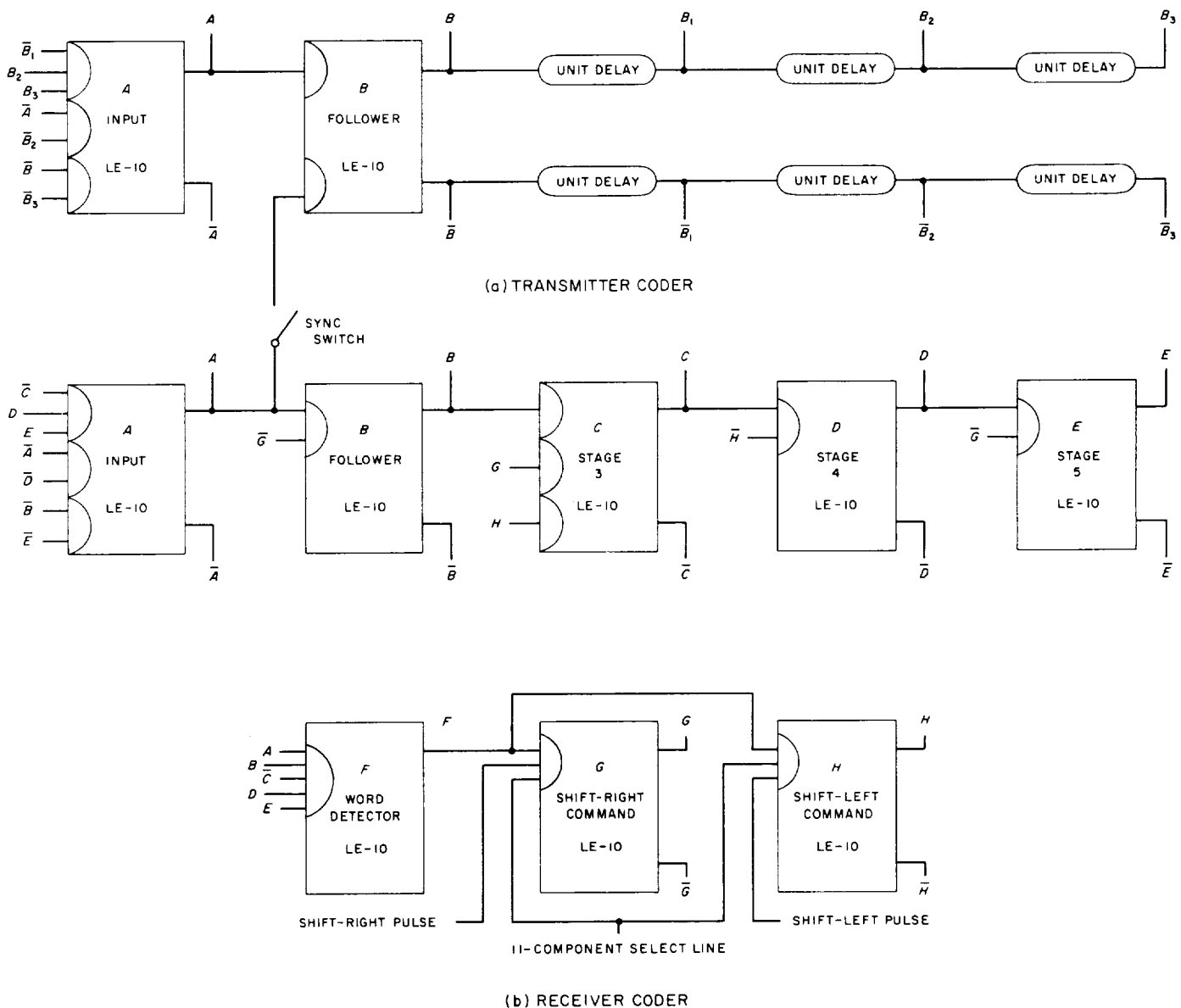


Fig. 34. Length 11 component coders

Table 12. Length 11 code

Length	Standard sequence	Shift right	Shift left
1	1 1 0 1 0 (word detector)	1 1 0 1 0	1 1 0 1 0
2	0 1 1 0 1	0 1 1 0 1	0 1 1 0 1
3	1 0 1 1 0	1 0 1 1 0	1 0 1 1 0
4	1 1 0 1 1	1 0 1 1 0	1 1 1 0 1
5	1 1 1 0 1	1 1 0 1 1	0 1 1 1 0
6	0 1 1 1 0	1 1 1 0 1	0 0 1 1 1
7	0 0 1 1 1	0 1 1 1 0	0 0 0 1 1
8	0 0 0 1 1	0 0 1 1 1	1 0 0 0 1
9	1 0 0 0 1	0 0 0 1 1	0 1 0 0 0
10	0 1 0 0 0	1 0 0 0 1	1 0 1 0 0
11	1 0 1 0 0	0 1 0 0 0	1 0 1 0 0

When the sequence returned, it had been shifted by the desired amount. It was found that, by employing five active stages to facilitate the insertion or deletion of the appropriate bits, the coder could be simplified. Thus, shifting is accomplished by repeating or skipping word vectors within the main loop. Another advantage of this

direct method is that it facilitates coder servicing. The operation of the shifting mechanism is obvious and it eliminates the need to refer to state diagrams. The word detector recognizes the 11010 vector, and at a shift-right command causes a repetition of the 10110 vector. The second column of Table 12 illustrates the new sequence. A command to shift left deletes the 11011 vector, and the resulting sequence is indicated in column 3 of Table 12.

The length 23 coders are the most complex of the group. Two stages of logic and a six-stage generator are required to produce the code shown in Table 13. As in the length 11 code, all other states eventually lead to the main loop. Both transmitter and receiver coders [Fig. 35(a) and (b)] are identical, and synchronization is accomplished in the forementioned manner.

The shifting technique is most easily demonstrated by a state diagram (Fig. 36). To shift right, the code vector 00 100001 is modified to 00 000001 by inhibiting the first generator stage. (The two leftmost digits in the word vectors represent the logic stages while the remaining six are the actual sequence generator.) The new vector is not in the main loop, and when the sequence finally does return

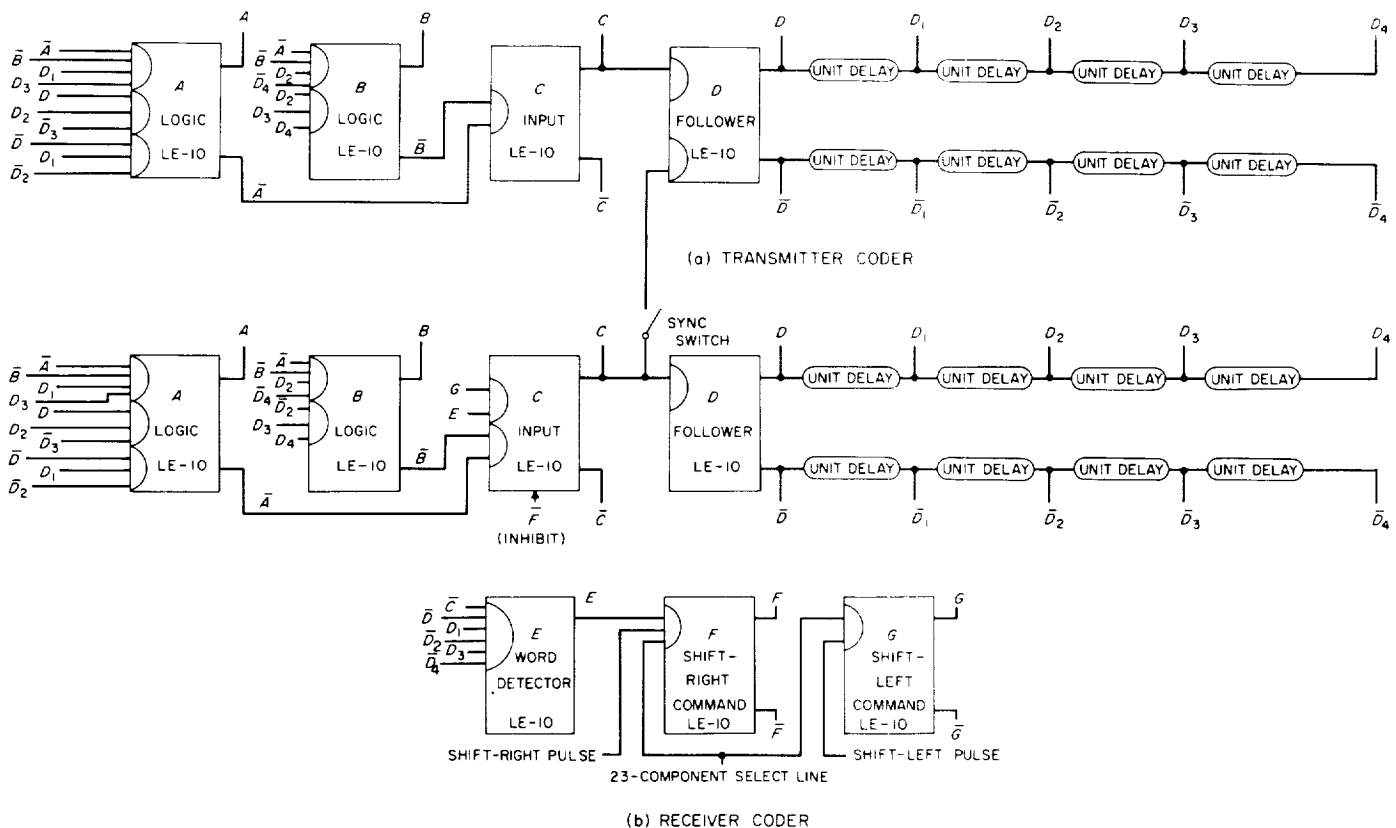


Fig. 35. Length 23 component coders

Table 13. Length 23 code

Length	Standard sequence	Shift right	Shift left	Length	Standard sequence	Shift right	Shift left
1	1 0 0 0 1 0 1 0 (word detector)	1 0 0 0 1 0 1 0	1 0 0 0 1 0 1 0	13	1 1 1 1 0 1 0 1	0 0 1 0 1 0 1 1	1 0 0 1 1 0 1 0
2	1 0 0 0 0 1 0 1	1 0 0 0 0 1 0 1	1 0 0 0 0 1 0 1	14	1 0 0 1 1 0 1 0	1 1 1 1 0 1 0 1	0 0 0 0 1 1 0 1
3	0 0 0 0 0 0 1 0	0 0 0 0 0 0 1 0	0 0 1 0 0 0 1 0	15	0 0 0 0 1 1 0 1	1 0 0 1 1 0 1 0	0 0 1 0 0 1 1 0
4	0 0 1 0 0 0 0 1	0 0 0 0 0 0 0 1	0 0 1 1 0 0 0 1	16	0 0 1 0 0 1 1 0	0 0 0 0 1 1 0 1	0 1 1 1 0 0 1 1
5	0 0 1 1 0 0 0 0	0 0 1 0 0 0 0 0	0 0 1 1 1 0 0 0	17	0 1 1 1 0 0 1 1	0 0 1 0 0 1 1 0	0 1 0 1 1 0 0 1
6	0 0 1 1 1 0 0 0	0 0 1 1 0 0 0 0	0 0 1 1 1 1 0 0	18	0 1 0 1 1 0 0 1	0 1 1 1 0 0 1 1	0 0 0 0 1 1 0 0
7	0 0 1 1 1 1 0 0	0 0 1 1 1 0 0 0	1 1 1 1 1 1 1 0	19	0 0 0 0 1 1 0 0	0 1 0 1 1 0 0 1	0 1 1 0 0 1 1 0
8	1 1 1 1 1 1 1 0	0 0 1 1 1 1 0 0	0 0 0 1 1 1 1 1	20	0 1 1 0 0 1 1 0	0 0 0 0 1 1 0 0	0 0 0 1 0 0 1 1
9	0 0 0 1 1 1 1 1	1 1 1 1 1 1 1 0	1 0 1 0 1 1 1 1	21	0 0 0 1 0 0 1 1	0 1 1 0 0 1 1 0	0 1 1 0 1 0 0 1
10	1 0 1 0 1 1 1 1	0 0 0 1 1 1 1 1	0 0 0 1 0 1 1 1	22	0 1 1 0 1 0 0 1	0 0 0 1 0 0 1 1	1 0 0 1 0 1 0 0
11	0 0 0 1 0 1 1 1	1 0 1 0 1 1 1 1	0 0 1 0 1 0 1 1	23	1 0 0 1 0 1 0 0	0 1 1 0 1 0 0 1	
12	0 0 1 0 1 0 1 1	0 0 0 1 0 1 1 1	1 1 1 1 0 1 0 1			1 0 0 1 0 1 0 0	

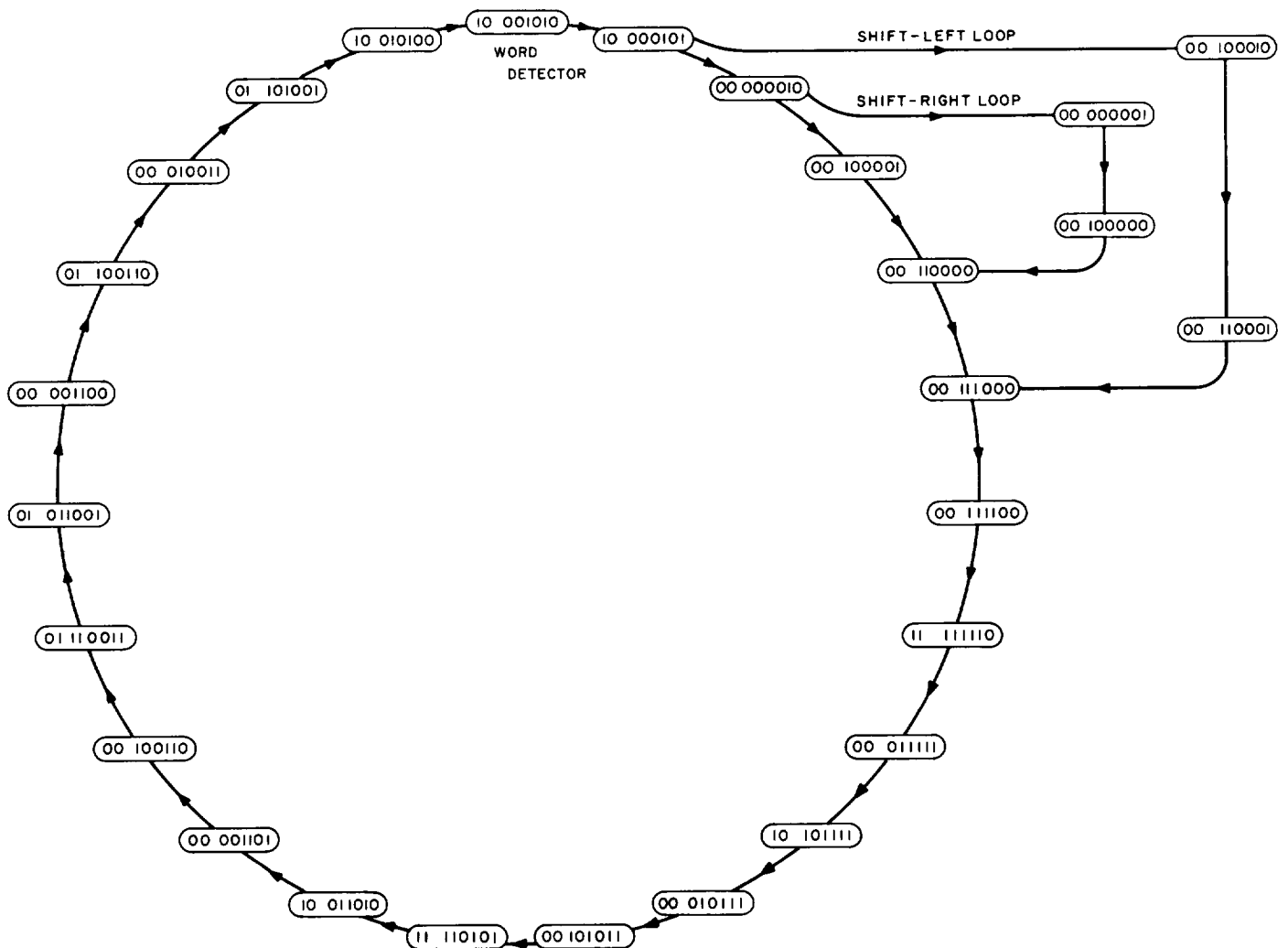


Fig. 36. State diagram for length 23 code

it is retarded by one bit-time. A comparison of the first and second columns of Table 13 will clarify the operation. Conversely, to shift left 00 000010 is modified by the insertion of an additional one to 00 100010. When the sequence returns to the main loop, it is advanced by one bit-time relative to the standard sequence (Table 13, third column).

The full transmitter coder is depicted schematically in Fig. 37. The four component codes and clock are combined according to a modified majority logic originally developed for the Mod II ranging system (Ref. 27).

$$T = v_1 v_2 + \bar{v}_2 \{ [v_3 v_4 + v_4 v_5 + v_5 v_3] \oplus [v_1] \} \quad (7)$$

The combiner output is a time series sequence of length p in which the clock component predominates. A large clock component is desirable during initial clock acquisition when the signal-to-noise ratio may be poor (Refs. 26, 28). An inhibit line on the second stage of the combiner prevents transmission of the code during the synchronization mode. Both the inhibit and the sync line are under the control of the stored program controller (Ref. 28).

The receiver coder is found in Fig. 38. Contrasting with the transmitter combiner, the receiver combiner has four modes of operation which are defined as follows:

- (1) $\bar{v}_2 v_3$
- (2) $\bar{v}_2 v_4$
- (3) $\bar{v}_2 v_5$
- (4) $\bar{v}_2 [v_3 v_4 + v_4 v_5 + v_5 v_3]$

The non-clock components can be individually selected for correlation with the incoming signal. Thus, each component is acquired separately (Fig. 39). When acquisition is complete, the system is switched to the fourth mode and full correlation should be indicated. The clock component is acquired separately in the clock loop and does not enter into the combiner logic. Mode select lines, as well as the shift command lines, are under the control of the stored program controller.

The coders and their associated control subsystems are currently being constructed. A second set of combiners, embodying more optimal properties as described in Ref. 26, will be added in the immediate future. Ref. 28 furnishes a further description of the project.

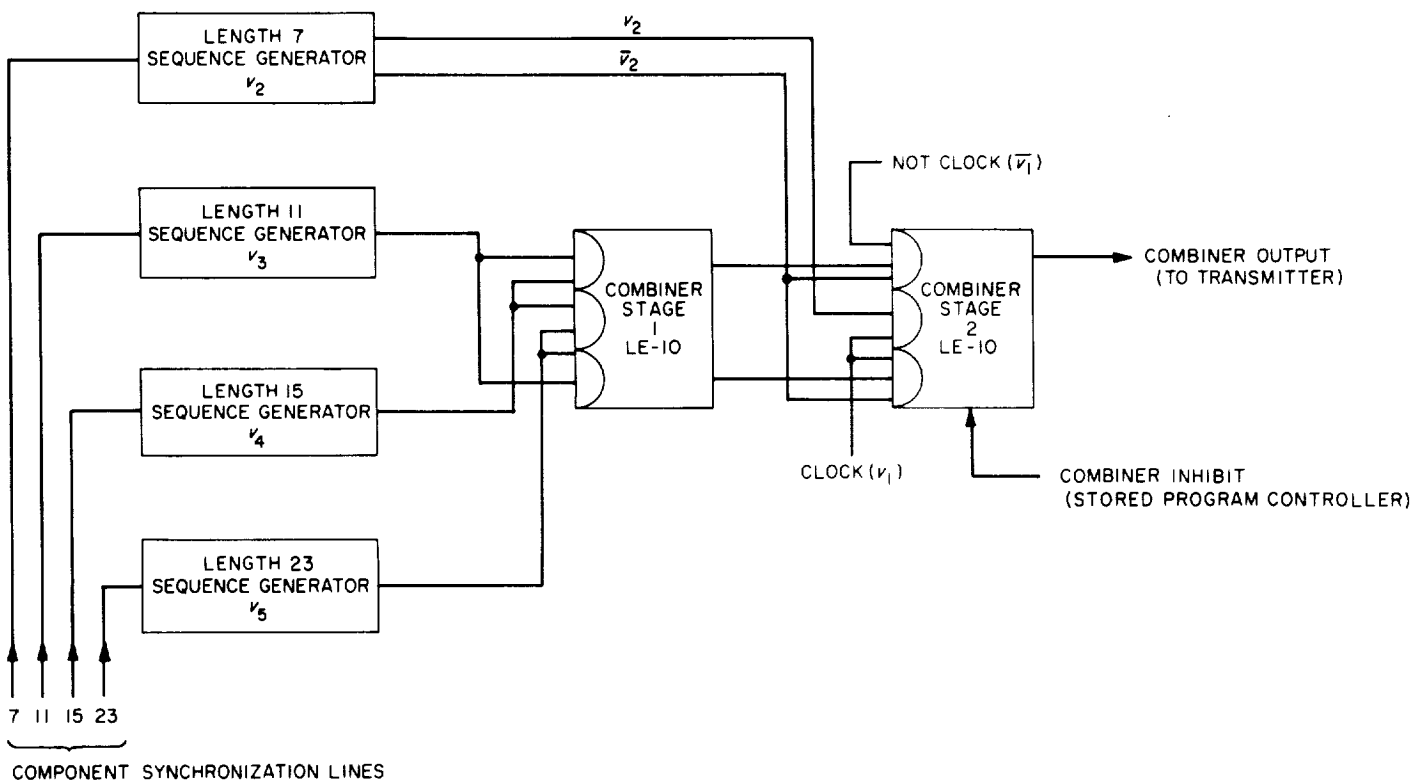
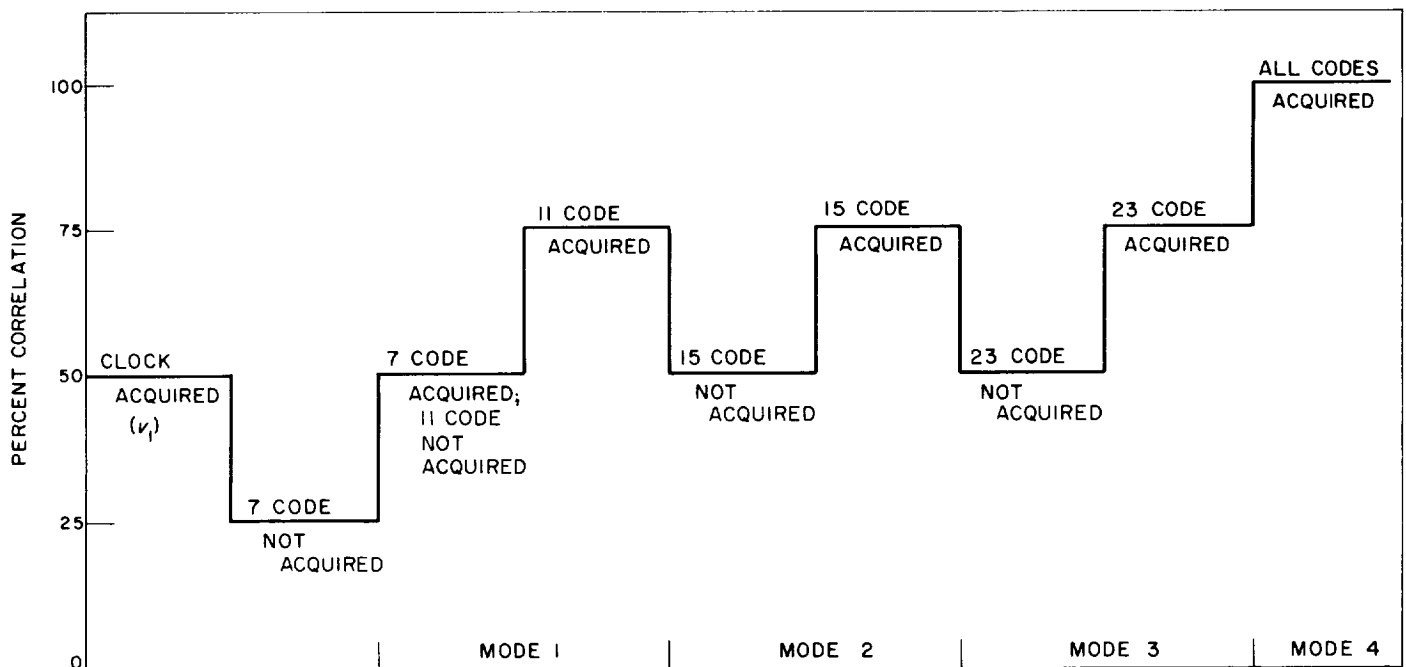


Fig. 37. Full transmitter coder



6. Register Display for Mod III Stored Program Controller (SPC)

The Mod III SPC as installed at the Venus site did not include equipment for the display of the internal registers. Its predecessor, the Mod II SPC, uses an oscilloscope for this purpose. In its original conception, it was thought that the uses of the Mod III would not require an oscilloscope, inasmuch as it was to be part of an operational system used with well-checked programs. For testing and initial checkout, it was thought that the portable scopes available at the Venus site would be sufficient.

The continuing need to check the internal registers of the Mod III SPC during the "debugging" of field-written programs, coupled with the limited availability of portable scopes and the inconvenience of such loosely coupled peripheral devices in that environment has indicated a need for an integral display system.

The philosophy governing the construction of the display was that it should be installed within the Mod III and yet be a self-contained subsystem. Fig. 40 is the block diagram of the subsystem. Selection, timing, and data shifting control circuitry are contained in a T-block located in the input-output area of the SPC. The display selection and data register are located behind the display lamps on a separate chassis. The lamp power supply is located on a separate panel behind the display console.

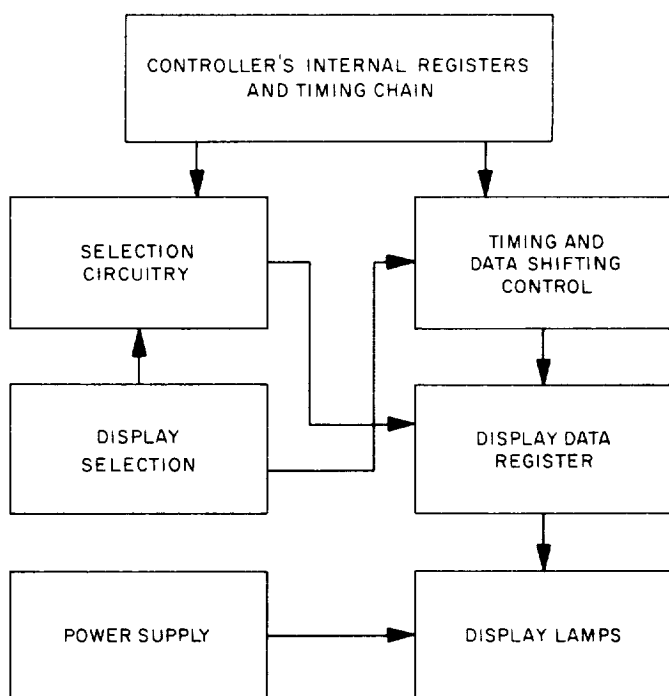


Fig. 40. Register display subsystem

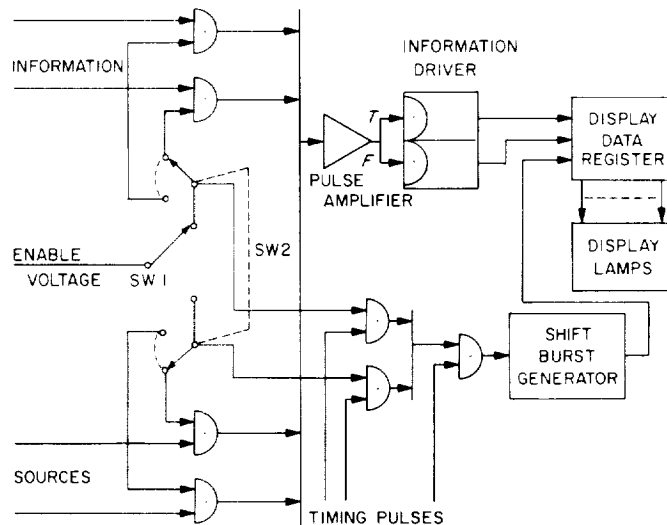


Fig. 41. Information flow in the register display subsystem

a. Data flow. Fig. 41 shows the data flow in the display subsystem. Information from the several internal registers of the SPC is selected by 24 two-input *and* gates whose outputs are combined in a 24-input *or* circuit, amplified and fed to a flip-flop which serves as an information driver. Normally, shift pulse bursts are generated once every 800 μsec . The group of internal registers selected by SW-2 determines the required timing of the shift burst, which is always 25 μsec long. When the display is externally triggered, the shift burst is initiated at the next suitable time following the trigger pulse. The trigger requires a positive-going pulse, 5 to 20 v amplitude, with a rise time of less than 0.2 $\mu\text{sec/v}$.

b. Selection circuitry. Fig. 42 presents the information selection circuits. The cards marked SG-12 and R-12 are special units built on T-pack blank modules. The outputs

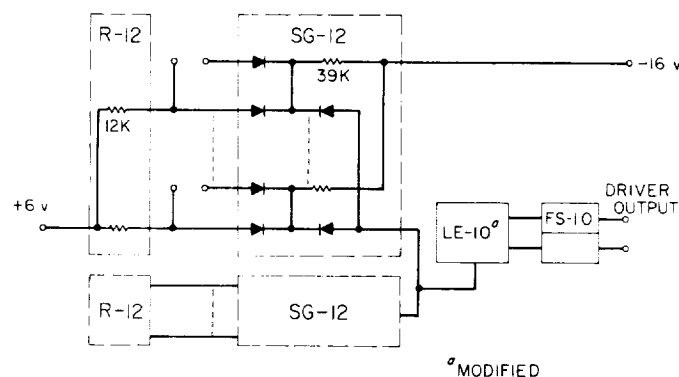


Fig. 42. Information selection circuitry

of the two SG-12's are tied together and fed into the inhibit input of an LE-10 which has been modified by shorting the inhibit input diode.

Fig. 43 gives the complete diagram of the shift burst generator. The major cycle pulse TF, occurring at T22, is stretched by TFS to encompass the timing pulses required for proper shifting of the data into the data shift register. The shift burst generator SGN gates the stretched major cycle pulse against the proper time pulse, setting an LE-10 flip-flop which regenerates until the occurrence of the corresponding time pulse 25 μ sec later. The time pulse is selected by the position of SW-1, a toggle switch that also selects the proper deck of the rotary selection switch SW-2. Because of the diode-capacitor gating used in the data shift register cards and the time at which the information driver flip-flop switches, it is necessary to delay the shift pulses $\frac{1}{2}$ clock period, i.e., $\frac{1}{2}$ μ sec. This is accomplished by bringing out a tap at the midpoint of a DP-10 unit delay. The input impedance of the shift register is high enough that it is not necessary to terminate the line at this point. The timing pulses are so selected that information in an internal register with the least significant bit appearing either at T3 or at T6 can be displayed properly.

The data shift register consists of three Digital Equipment Corporation (DEC) type 4223 cards connected end to end. Each card contains a ten-stage shift register. The register is driven directly from the control equipment described above.

c. Display lamps and power supplies. The indicator lamps are Amperex grid controlled glow indicators. The display register cards drive the indicator grids through 100,000-ohm resistors with no further amplification. The indicators are powered by a zener regulated 50-v dc supply.

The logic power requirements are supplied by the SPC. The DEC 4223 cards require nominal supplies of +10

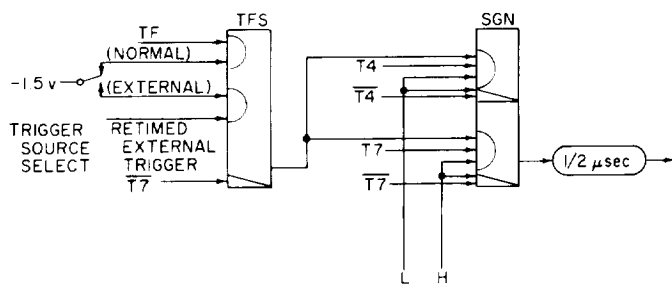


Fig. 43. Shift burst generator

and -15, but the +6 and -16 supplies available in the SPC are well within the operating tolerances of the cards.

d. Registers available for display. The following 14 registers have been connected to the display system, with provisions for adding 10 more as needed.

AC Hi: Accumulator, high-order half

AC Lo: Accumulator, low-order half

MQ Hi: Mult/Quot, high-order half

MQ Lo: Mult/Quot low-order half

CR: Command register

PC: Program counter

EF: Transfer address storage

IR-1: Index register 1

IR-2: Index register 2

IR-3: Index register 3

LL-1: Limit line 1

LL-2: Limit line 2

LL-3: Limit line 3

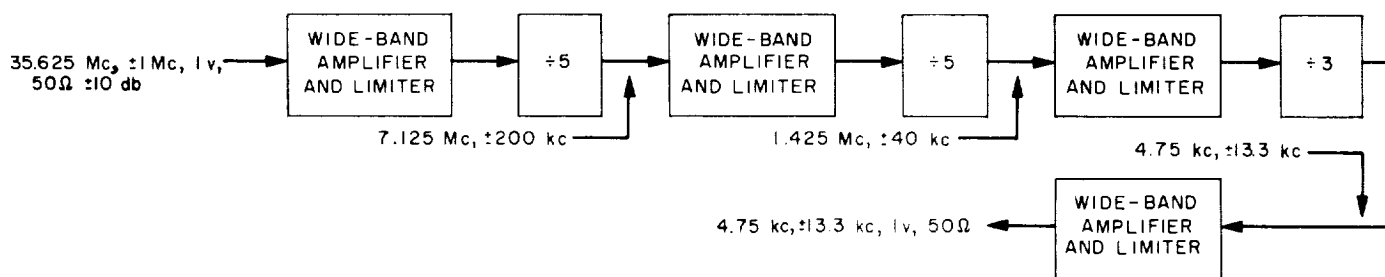
SR: Storage register

D. RF Signal Generation and Control

1. Parametric Frequency Dividers

a. Summary. Parametric frequency dividers are a promising development for simplifying frequency synthesizer systems and receiver/local oscillator systems. A $\div 75$ wide-band divider has been designed and built for use in the Mod IV local oscillator. Phase noise measurements indicate that the divider contributes less than 0.002 deg peak-to-peak.

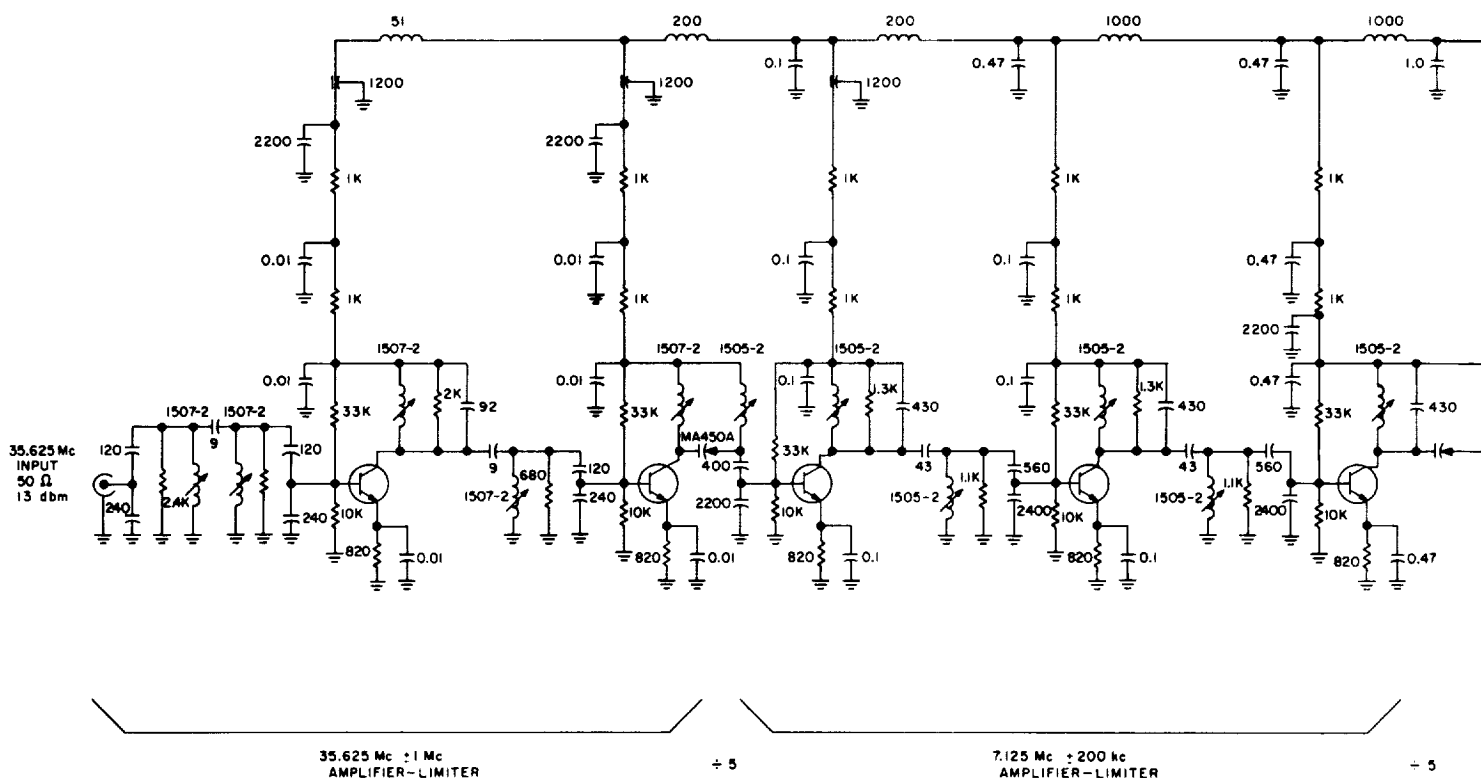
b. Description of divider and evaluation. A frequency divider was needed to divide by 75 from 35.625 Mc to 475 kc. The required bandwidth was ± 1 Mc at 35.625 Mc. A

Fig. 44. Parametric frequency divider ($\div 75$) block diagram

block diagram of the divider is shown in Fig. 44. The complete circuit diagram is shown in Fig. 45; a photograph showing the layout and decoupling is shown in Fig. 46. The individual divider circuits are similar to those described in Ref. 29. Because of the bandwidth desired, and the need for high isolation and low leakage of spurious signals generated in the divider circuitry, multiple stages of double-tuned amplifiers are used between all dividers and at the input and output. The bandwidth of the input is 2 Mc at 35.625 Mc or 5.6%. The maximum leakage at each of the internal frequencies is given below. No measurable leakage at other frequencies exists.

Frequency	Maximum leakage (plate-to-plate, input or output connector, or power line)
475 kc	0.8 μ v
1.425 Mc	1.0 μ v
7.125 Mc	0.35 μ v
35.625 Mc	3.5 μ v (noise level of NF 105 used to measure leakage)

Using the test setup of Fig. 47, phase noise measurements were made. Residual noise of the measurement system masked the noise due to the divider, but an upper



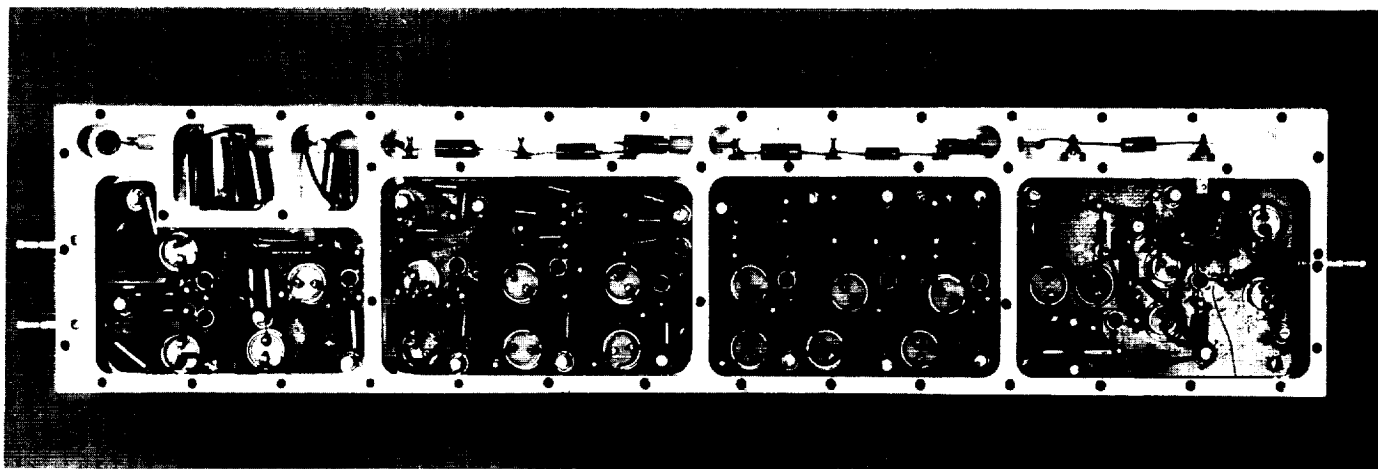


Fig. 46. Photograph of parametric frequency divider ($\div 75$)

cps. After multiplication to 6 Mc, these frequencies approximately open the -1.5 -db range of the PN generator.

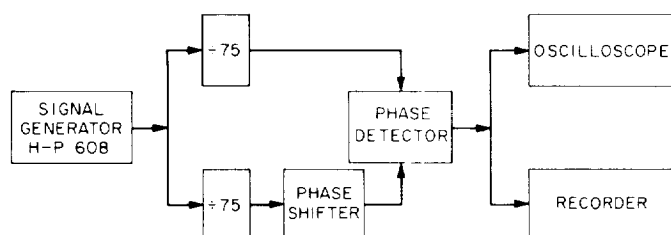


Fig. 47. Phase noise measurement test setup

A series of measurements was made of the phase noise of the system. First, the error input to the first VCO was grounded and the second VCO locked to it in a phase-locked loop of $2B_L = 5$ cps. The phase noise was measured to find how much noise was due to the two oscillators alone. The the first VCO was locked to the desired line in the PN spectrum and the second VCO locked to it. The noise was measured again for this condition. The difference in these two noise measurements should give an indication of the system noise contributed by the PN generator. These test results are presented in Table 14. Since the third set of crystals was faulty, meas-

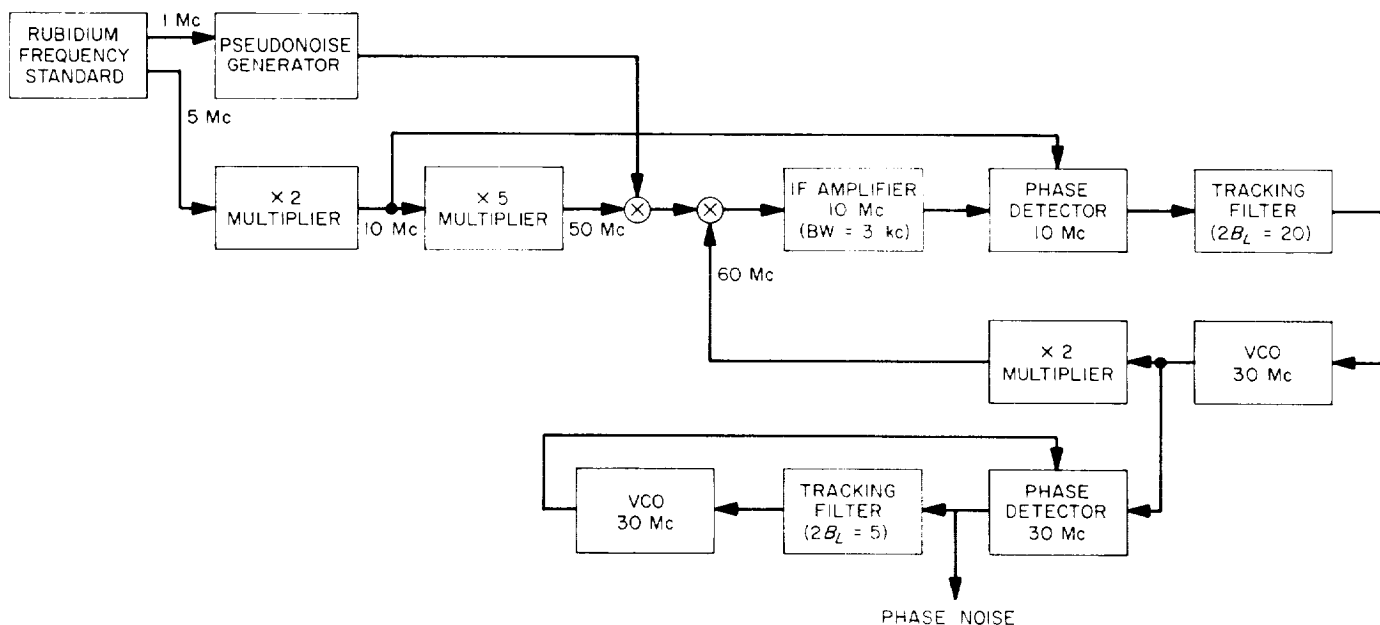


Fig. 48. Experimental PN frequency synthesizer

Table 14. Phase noise measurement of an experimental PN frequency synthesizer

VCO frequency	Peak-to-peak noise due to two oscillators	Peak-to-peak noise in system with PN generator
30,000,657. ...	0.16 deg \pm 20%	0.16 deg \pm 20%
30,000,000.	0.10 deg \pm 20%	0.15 deg \pm 20%
20,999,344. ...	0.10 deg \pm 20%	0.10 deg \pm 20%
29,975,724. ...	0.18 deg \pm 20%	0.18 deg \pm 20%
29,975,067. ...	0.20 deg \pm 20%	0.20 deg \pm 20%
29,974,410. ...	0.18 deg \pm 20%	0.18 deg \pm 20%

urements were made at only two sets of three frequencies each. One set of measurements was made around the center frequency and another at one extreme of the range. The estimates of error on the phase noise measurements are based on past experiments and on cross checks with a thermocouple type meter. In each case the notation "peak-to-peak" as a noise measurement is to be interpreted as an estimate of the 6- σ value. Because of the large uncertainty in the measured values of phase noise, little can be said about the noise due to the PN generator. However, an upper bound of 0.1 deg peak-to-peak is certainly reasonable from this data.

Several improvements in the system are planned to further refine and extend this data. Some of these improvements are:

- (1) Obtain better crystals for the VCO's to lower the system noise.
- (2) Narrow the bandwidth of the 10-Mc IF amplifier to obtain better rejection of the adjacent lines in the spectrum and reduce the data confusion due to these lines.
- (3) Modify the PN generator to obtain variable line spacing and finer frequency resolution.

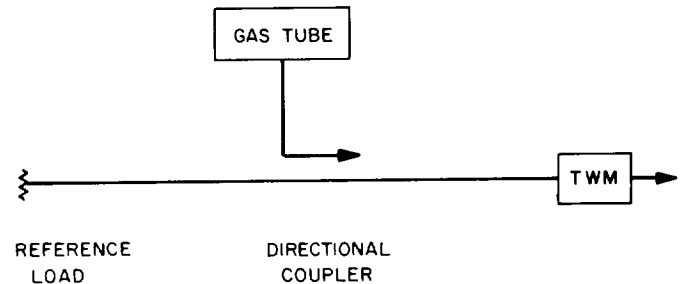
E. S-Band Implementation for DSIF

1. TWM for DSIF

a. Summary. The first traveling wave maser/closed cycle refrigerator (TWM/CCR) subassembly was shipped to Goldstone and installed in the Cassegranian cone. After

checkout at the antenna test range, the cone was installed on the Pioneer antenna. Satisfactory maser performance was obtained.

The prototype TWM/CCR at the Venus site was recently serviced and made ready for prolonged planetary radar experiments. This CCR has been used for a total of 7000 hr of which the last 2500 hr have been at the Venus site.

**Fig. 49. Schematic diagram for measurement of noise temperature**

b. Recent work. Prior to shipment of the TWM to Goldstone, an accurate measurement of the equivalent noise temperature of the system was made. The configuration used is shown schematically in Fig. 49. This is the standard technique used at JPL and consists of a calibrated gas tube and a low-temperature reference termination. Fig. 50 shows a photograph of the equipment used. An all-waveguide liquid helium cooled load was used as the reference termination. This load had a noise temperature of 5°K at its terminals and is believed to be the lowest reference temperature obtained to date. The contribution due to the waveguides (dark waveguide in photograph) was 2°K.

The followup receiver contributed another 3°K and the TWM had an equivalent noise temperature (including the waveguide directional coupler) of 7 to 8°K.

Both Airborne Instruments Laboratory and JPL back-up TWM's showed essentially the same noise performance.

Preliminary measurement results for the TWM are shown in Table 15. Work to improve the gain stability is continuing.

Table 15. Preliminary performance data for TWM

Characteristics	Measured	Specifications
Operating frequency	2295 Mc	2295 Mc
Tunable range	± 50 Mc	± 30 Mc
Bandwidth (1-db points)	10 Mc	10 Mc
Bandwidth (3-db points)	17 Mc	15 Mc
Gain	33 db	30 ± 1 db
Noise temperature at waveguide input	$9 \pm 1^\circ\text{K}$	$16 \pm 2^\circ\text{K}$
Gain stability (short term)	± 0.05 db	± 0.02 db in 10 sec
Gain stability (long term)	± 0.50 db (on moving antenna)	± 0.2 db in 12 hr
Operating temperature of TWM	4.5°K	$4.4 \pm 0.2^\circ\text{K}$

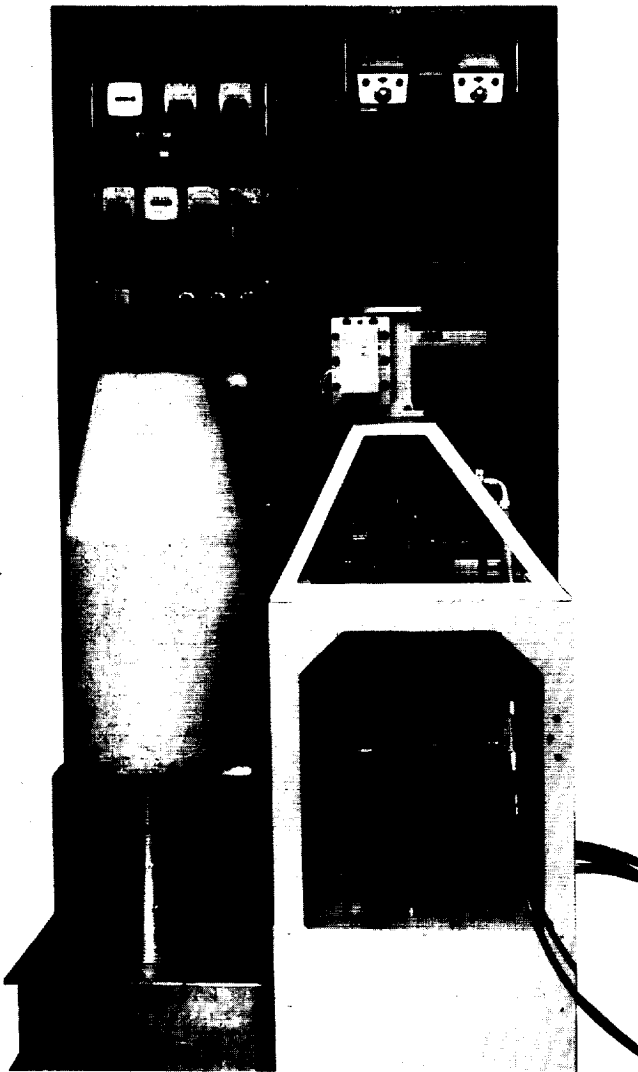


Fig. 50. Equipment used for determining TWM noise performance

2. Acquisition Aid for DSIF

a. Summary. The basic design of the S-band acquisition aid (SAA) for DSIF 85-ft antennas has been completed, and all components are on order for three stations.

b. Recent work. As described in Ref. 31, an S-band acquisition aid is being developed for the DSIF. This system is basically similar to the existing L-band system, but with angle error receiver channels added to improve the tracking presentation to the operator.

The SAA is identical to the SCM feed horn which is the feed for the S-band Cassegrainian system, and consists of a multimode, suppressed sidelobe, single horn monopulse unit. A contract presently exists with the Hughes Aircraft Company (HAC), Fullerton, California, for the design, development, and construction of three units, one each for the Woomera, Johannesburg, and the Canberra Stations. The latter is designated the prototype and has been delivered to the Goldstone Pioneer Station for temporary installation and for evaluation tests. All other components necessary for these tests are on order. Aircraft evaluation tests at the Pioneer Station are presently scheduled for March 1964.

F. Mesa Antenna Range

a. Summary. Construction of the $\frac{3}{4}$ -mi range for S-band spacecraft antenna pattern measurements is described.

b. Recent work. Work is continuing on the $\frac{3}{4}$ -mi range (Ref. 32). The facility of the remote transmitter site—the "East Mesa"—is now complete. The illuminator mounting tower has been constructed (Fig. 51). This tower has provisions for two paraboloidal antennas with a 10-ft maximum diameter. The antennas are bolted to polarization positioners which are fastened to adjustable mounting fixtures. This permits exact adjustment of the illuminator antennas toward the devices under test at the Mesa. The tower, with one 10-ft dish in position (Fig. 52), has withstood recent high winds without any damage.

A run of conduit, consisting of three 4-in. conduits plus two 2-in. conduits, was installed between the an-

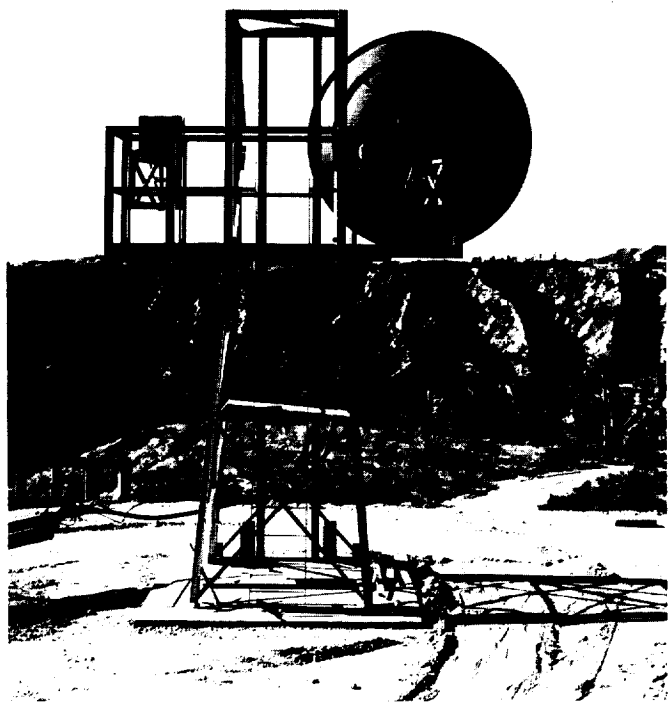


Fig. 51. Remote site illuminator tower

tenna tower and the instrument building. Its purpose is to protect the necessary power-, signal-, and control-cabling which runs from the instrument building to the antenna tower.

The azimuth rotator which is used on the Mesa side of the range is shown in Fig. 53. This rotator positions the spacecraft models illuminated from the East Mesa.

To complete the Mesa end of the range, two more facilities will be provided in the near future: (1) a control room, and (2) a pad with monitoring antennas. The control room will house the necessary recording equipment, the controls for the azimuth rotator, and the equipment to remotely control the "East Mesa" transmitter. The

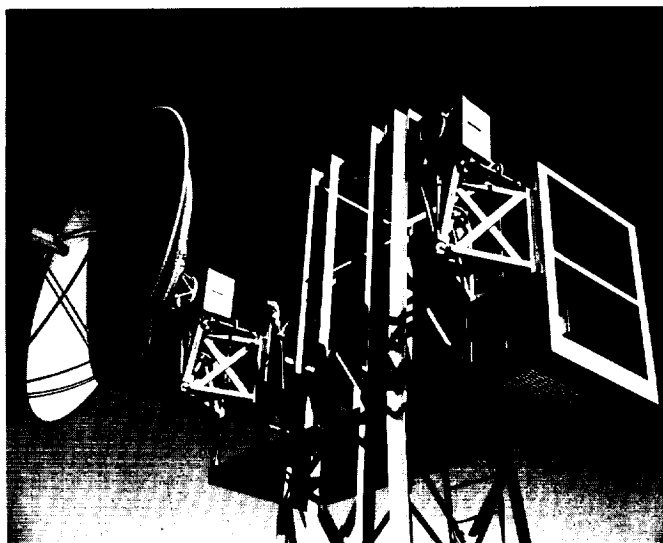


Fig. 52. Adjustable mounting of 10-ft dish

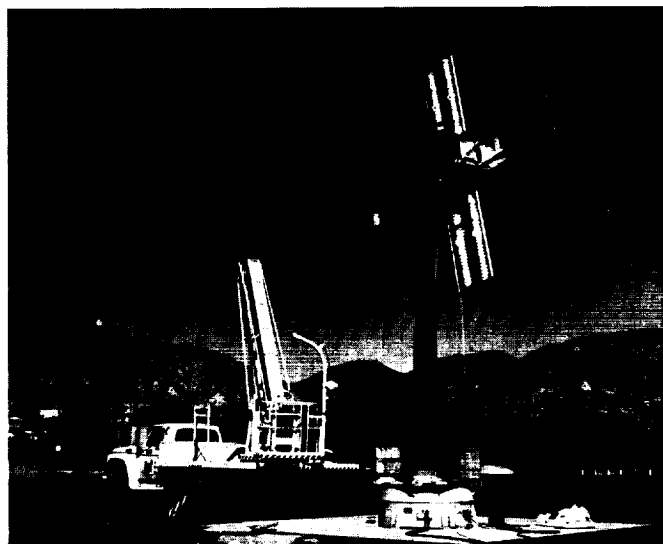


Fig. 53. Spacecraft model mounted on Mesa azimuth positioner of $\frac{3}{4}$ -mi range

monitoring antenna will be used for checking RF output, modulation, and frequency of the "East Mesa" transmitter.

References

1. "30-ft Diameter Azimuth-Elevation Antenna," *Space Programs Summary No. 37-20*, Vol. III, pp. 28-31, Jet Propulsion Laboratory, Pasadena, California, March 31, 1963.
2. "Antenna Instrumentation," *Space Programs Summary No. 37-20*, Vol. III, pp. 31-34, Jet Propulsion Laboratory, Pasadena, California, March 31, 1963.
3. "Antenna Instrumentation," *Space Programs Summary No. 37-24*, Vol. III, pp. 33, 39-43, Jet Propulsion Laboratory, Pasadena, California, November 30, 1963.
4. "Antenna Instrumentation," *Space Programs Summary No. 37-25*, Vol. III, pp. 24-25, Jet Propulsion Laboratory, Pasadena, California, January 31, 1964.
5. "Cassegrain System 960 Mc," *Space Programs Summary No. 37-14*, Vol. I, pp. 99-105, Jet Propulsion Laboratory, Pasadena, California, May 1, 1962.
6. "Feeds and Feed Systems," *Space Programs Summary No. 37-16*, Vol. III, pp. 47-52, Jet Propulsion Laboratory, Pasadena, California, July 31, 1962.
7. "Boresight Calibrations for the DSIF Antennas," *Space Programs Summary No. 37-24*, Vol. III, pp. 30-39, Jet Propulsion Laboratory, Pasadena, California, November 30, 1963.
8. "Boresight and Gain Calibrations for DSIF Antennas," *Space Programs Summary No. 37-23*, Vol. III, pp. 28-29, Jet Propulsion Laboratory, Pasadena, California, September 30, 1963.
9. "Boresight Calibrations for DSIF Antennas," *Space Programs Summary No. 37-25*, Vol. III, pp. 21-25, Jet Propulsion Laboratory, Pasadena, California, January 31, 1963.
10. "Feeds and Feed Systems," *Space Programs Summary No. 37-18*, Vol. III, pp. 24-27, Jet Propulsion Laboratory, Pasadena, California, November 30, 1962.
11. "Prototype S-Band Monopulse Cassegrain System," *Space Programs Summary No. 37-18*, Vol. III, pp. 65-68, Jet Propulsion Laboratory, Pasadena, California, November 30, 1962.
12. "Feeds and Feed Systems," *Space Programs Summary No. 37-20*, Vol. III, pp. 38-39, Jet Propulsion Laboratory, Pasadena, California, March 31, 1963.
13. "Microwave Configuration for Lunar System," *Space Programs Summary No. 37-24*, Vol. III, pp. 53-54, Jet Propulsion Laboratory, Pasadena, California, November 30, 1963.
14. "AC Ratio Transformer Techniques," *Space Programs Summary No. 37-22*, Vol. IV, pp. 189-196, Jet Propulsion Laboratory, Pasadena, California, August 31, 1963.
15. "Temperature Calibrations of Microwave Terminations," *Space Programs Summary No. 37-25*, Vol. IV, pp. 118-121, Jet Propulsion Laboratory, Pasadena, California, February 29, 1964.
16. "Antenna Damage by Hailstones," *Space Programs Summary No. 37-16*, Vol. III, pp. 29-31, Jet Propulsion Laboratory, Pasadena, California, July 31, 1962.

References (Cont'd)

17. Stoller, F. W., Preliminary Report, "Investigation of Hailstorm Damage to DSIF Antennas," Technical Memorandum No. 33-81, Jet Propulsion Laboratory, Pasadena, California, February 23, 1962.
18. "S-Band Antenna Gain and Pattern Calibrations," *Space Programs Summary No. 37-24*, Vol. III, pp. 24-25, Jet Propulsion Laboratory, Pasadena, California, November 30, 1963.
19. "Mod III Transmitter System, 2388 Mc, 100 kw," *Space Programs Summary No. 37-19*, Vol. III, pp. 23-27, Jet Propulsion Laboratory, Pasadena, California, December 31, 1962.
20. "Silicon Rectifier Reliability," *Space Programs Summary No. 37-24*, Vol. III, p. 46, Jet Propulsion Laboratory, Pasadena, California, November 30, 1963.
21. "Tiefort Mountain Antenna Range," *Space Programs Summary No. 37-21*, Vol. III, pp. 83-84, Jet Propulsion Laboratory, Pasadena, California, April 30, 1963.
22. "RF Switch Isolation," *Space Programs Summary No. 37-23*, Vol. III, pp. 43-44, Jet Propulsion Laboratory, Pasadena, California, August 31, 1963.
23. "Nine-Channel Autocorrelator," *Space Programs Summary No. 37-25*, Vol. III, pp. 33-38, Jet Propulsion Laboratory, Pasadena, California, January 31, 1964.
24. "Monostatic Radar," *Space Programs Summary No. 37-19*, Vol. III, pp. 29-32, Jet Propulsion Laboratory, Pasadena, California, January 31, 1963.
25. "Monostatic Satellite and Lunar Radar (MSSLR) Transmitter," *Space Programs Summary No. 37-25*, Vol. III, pp. 50-51, Jet Propulsion Laboratory, Pasadena, California, January 31, 1964.
26. Titsworth, R. C., "Optimal Ranging Codes," Technical Report No. 32-411, Jet Propulsion Laboratory, Pasadena, California, April 15, 1963.
27. Baugh, H. W., "Mod II Ranging Equipment," Technical Report No. 32-337, Jet Propulsion Laboratory, Pasadena, California, September 15, 1962.
28. "Monostatic Radar System Description," *Space Programs Summary No. 37-24*, Vol. III, pp. 61-69, Jet Propulsion Laboratory, Pasadena, California, November 30, 1963.
29. "5/221 Parametric Frequency Divider," *Space Programs Summary No. 37-22*, Vol. III, pp. 7-9, Jet Propulsion Laboratory, Pasadena, California, July 31, 1963.
30. "PN Generator Frequency Synthesizer," *Space Programs Summary No. 37-24*, Vol. III, pp. 95-97, Jet Propulsion Laboratory, Pasadena, California, November 30, 1963.
31. "Acquisition Aid for DSIF," *Space Programs Summary No. 37-25*, Vol. III, p. 53, Jet Propulsion Laboratory, Pasadena, California, January 31, 1964.
32. "Mesa Antenna Range," *Space Programs Summary No. 37-19*, Vol. III, p. 32, Jet Propulsion Laboratory, Pasadena, California, January 31, 1963.

V. Advanced Antenna System

A. Synopsis

A 210-ft-diameter Advanced Antenna System (AAS) is being designed and constructed for the Mars Station, Goldstone. It will operate in the Deep Space Instrumentation Facility (DSIF) at the S-band frequencies of 2.1 to 2.3 Gc. Completion of this antenna, as an operational receiving station, is scheduled for June 1966.

Completion of the Advanced Antenna System involves a number of areas of effort. These are the Contractor Furnished System (CFS) under contract to Rohr Corporation, Chula Vista, California; site development and utility installations; ancillary equipment, instrumentation and support system; and the DSIF equipment required to outfit the AAS for superior receiving capability.

The CFS has progressed through the preliminary design phase and is well into final design. On-site work at the Mars Station, Goldstone, began on October 14, 1963. Site clearance, initial grading, installation of underground water and sanitary facilities, and foundations for the pedestal and instrument tower have been completed. Reinforced concrete work for the instrument tower and the

pedestal walls is nearing completion. A 200-ton capacity, 315-ft-high guyed derrick has been erected and is in use for the construction. Figs. 1 through 6 depict the on-site construction progress.

In providing site development and utility installations, an extension of the present Goldstone road system has been completed to provide access to the Mars Station. Temporary communications and power for the initial construction phase have been installed. Procurement actions are underway to provide an integrated power system for the antenna of three 2400-v, 1200-rpm, 500-kw, diesel-powered electric generators with associated electrical switch gear, fuel oil tankage, concrete block building, and associated facility services. Planning and development of inter and intra site communications, ancillary equipment, instrumentation and support systems, and DSIF receiving and data handling equipment is in progress.

Preliminary design of the Contractor Furnished System has been completed by Rohr Corporation and formal JPL acceptance has been forwarded. In addition to design of individual components of the antenna, the preliminary design phase included system integration, wind load, and

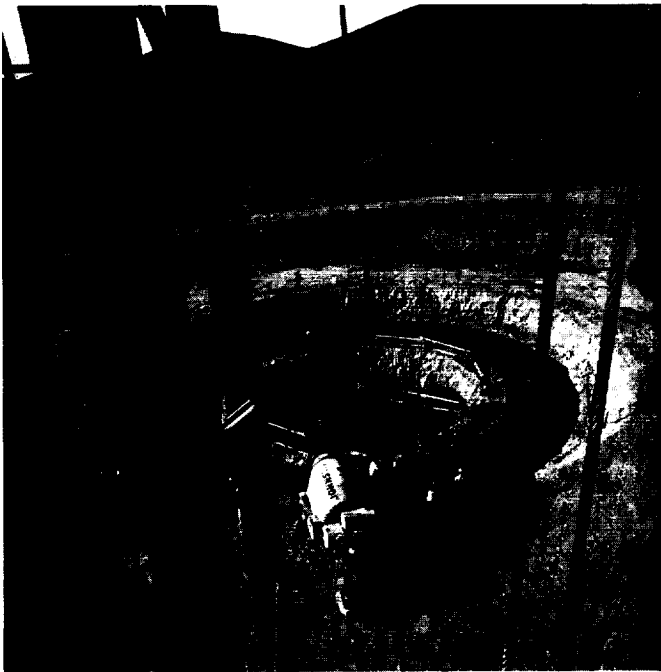


Fig. 1. Pedestal and instrument tower construction progress as of December 18, 1963



Fig. 2. Aerial view of on-site construction progress at the Mars Station as of January 3, 1964

reliability studies. System integration studies are comprised of reflector analysis, structural dynamics, control system analog studies, error analysis, and reliability analysis. These studies have served throughout the preliminary design phase as a principal means of evaluating, interpreting, and optimizing the developed design concept. System integration and reliability studies will continue

throughout the design, construction, and testing phases of the CFS to ensure that all requirements for the Advanced Antenna System are met.

The following are brief descriptions of major components of the antenna as determined during the preliminary design phase; Fig. 7 is a sketch of the antenna showing these components.

a. Pedestal (Component 1). The pedestal will be a reinforced concrete cylinder with a flat slab top which will have a concrete collar in the center (Ref. 1). It will provide support for the rotating parts of the antenna. Operational working space and facilities will be provided within the pedestal.

b. Instrument tower (Component 2). The instrument tower will consist of a silo type foundation which extends to 35 feet below finished grade. It will be comprised of a concrete cylinder to the top of the pedestal and a steel cylinder and truncated cone to the elevation axis. (Ref. 1). The purpose of the tower is to serve as the ground reference and mounting platform for the Master Equatorial unit (component 3) which is the primary pointing reference for the antenna system.

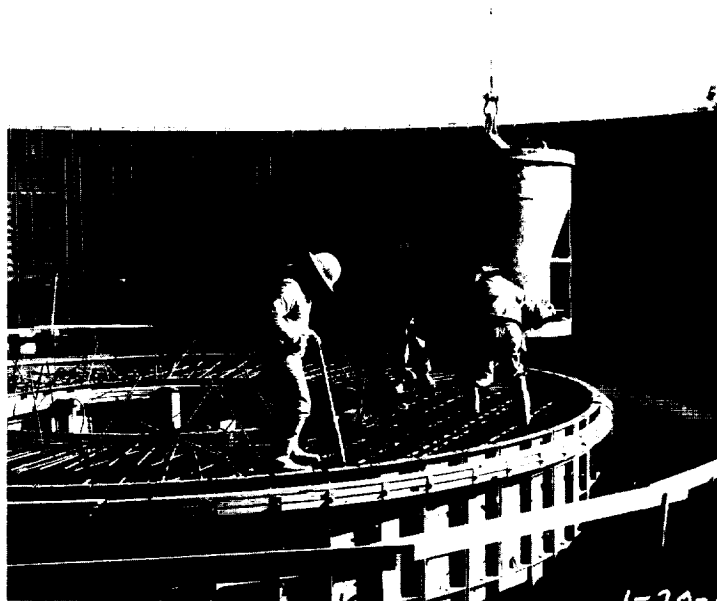
c. Alidade building and alidade (Components 7, 8). The alidade will be of steel construction and will be constructed of four heavy wide flange structural shapes, welded together to form a column section. Its function is to permit azimuth rotation and to support the tipping parts. The alidade building will be located on the bottom base triangle of the alidade. The floor will be of steel plate supported on structural framing which sets on the base triangle of the alidade. The walls will be metal panels supported by a steel girt and column framework. The roof will be a ribbed metal deck, topped with a built-up roof and supported on a structural frame. The alidade building will house the main antenna control room, the hydraulic equipment for the drives, and the pumps for the hydrostatic thrust bearing. The estimated weight of the alidade and building is 1,682,000 lb.

d. Azimuth hydrostatic thrust bearing (Component 4). The azimuth hydrostatic thrust bearing will support the moving parts of the antenna and permit rotation about the azimuth axis. The antenna and its alidade will be carried on a pressurized oil film approximately 0.008 in. thick. Attached to each of the three alidade legs will be a bearing pad and alignment mechanism. Each pad will have six pressure recesses individually supplied by a hydraulic pumping system. These pads will ride on a steel

PLACEMENT FOR INSTRUMENT TOWER WALLS
35 ft BELOW GROUND FLOOR LEVEL



PLACEMENT FOR INSTRUMENT TOWER
AT GROUND FLOOR LEVEL



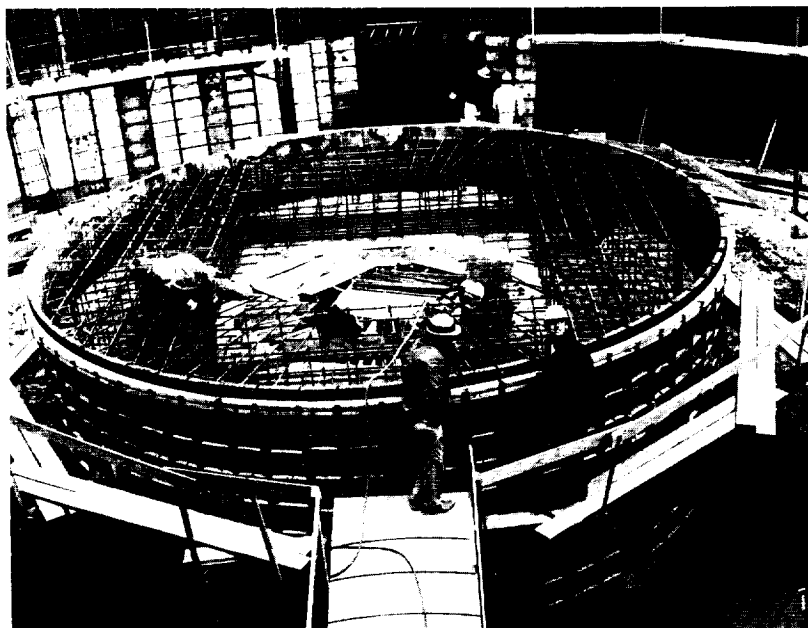
PLACEMENT FOR FIRST 8-ft LIFT
OF PEDESTAL WALL



PLACEMENT FOR ANTENNA PEDESTAL
FOOTING 11 ft BELOW GROUND FLOOR LEVEL

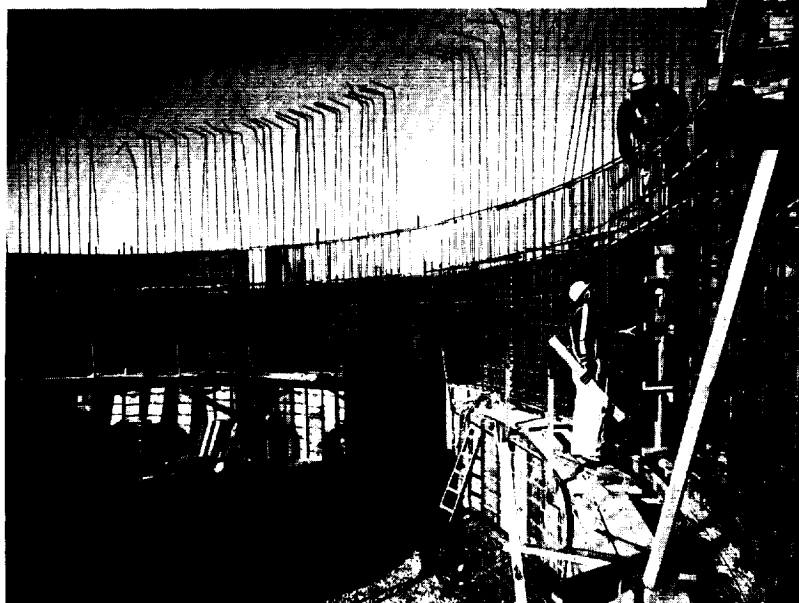
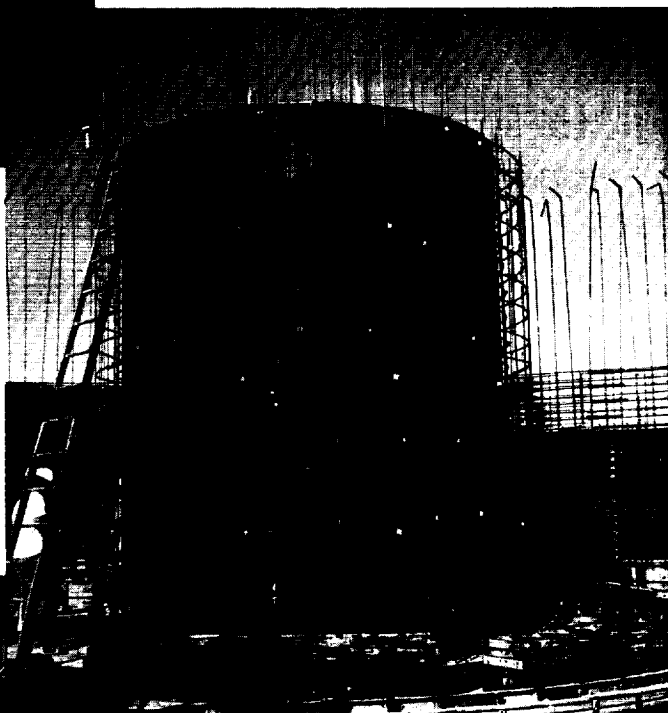


Fig. 3. Placement of reinforcing concrete for the pedestal and instrument tower



PLACEMENT FOR INSTRUMENT TOWER
AT GROUND FLOOR LEVEL

PLACEMENT FOR INSTRUMENT TOWER
ABOVE GROUND FLOOR LEVEL



PLACEMENT FOR PEDESTAL WALLS ABOVE
GROUND FLOOR LEVEL

Fig. 4. Placement of reinforcing steel for the pedestal and instrument tower

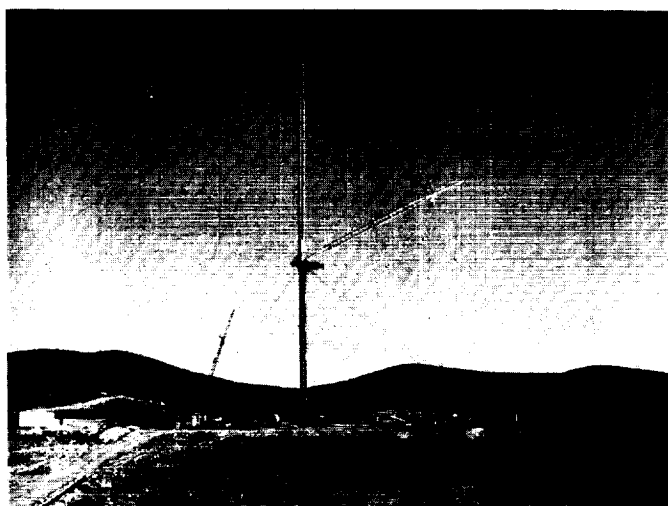


Fig. 5. Guyed derrick used in construction of the antenna



Fig. 6. Construction of the pedestal and instrument tower as of February 5, 1964

ring of approximately 76-ft diameter which rests (and is retained in position) on the pedestal. The estimated weight of the hydrostatic thrust bearing is 265,000 lb.

e. Azimuth radial shear bearing (Component 5). The azimuth axis will be defined by the azimuth radial bear-

ings which will restrain the alidade in a horizontal plane. The radial bearing will consist of a vertical steel plate runner that will be supported by the concrete collar of the pedestal, three pairs of flanged wheels, and a preload device that will connect the wheels to the alidade structure. These assemblies will be located at 120-deg intervals around the azimuth axis. The estimated weight of the azimuth radial shear bearing is 103,000 lb.

f. Azimuth and elevation drive assembly (Components 6, 9). The function of the drive system will be to convert electrical and hydraulic servo signals to reflector rotation. The assemblies will consist of bull gears and reducers. The reducers will be anchored to the alidade structure through tangential links. In the azimuth motion, four reducers will rotate the antenna around a stationary azimuth bull gear. Two of the reducers will be mounted on the back corner of the alidade base, and one each of the remaining reducers will be mounted on each of the two forward corners. Pairs of reducers will be counter-torqued against each other to eliminate backlash errors. The azimuth bull gear will be supported by a segmented sole plate which will be anchored securely to the pedestal concrete. Two bull gears and four reducers will be used for the elevation axis drive system. The elevation bull gears will be bolted to the face of the rims of the elevation wheels which will be part of the reflector backup structure. Each pair of reducers driving each bull gear will be counter-torqued against one another to eliminate errors due to gearing backlash. The estimated combined weight of the azimuth and elevation drive assemblies is 214,000 lb.

g. Servo system (Component unnumbered). The servo drive and control system will consist of three main parts: the hydraulic drive, the analog data system, and the servo electronics. The hydraulic servo drive will drive the antenna about both axes at rates up to 0.5 deg/sec with winds up to 30 mph and rates to 0.2 deg/sec in winds to 45 mph; it will be capable of stowing the antenna from any position in winds up to 50 mph and holding any position, with brakes applied, at winds to 70 mph. The hydraulic drive equipment will be installed in the alidade room and will rotate with the antenna in azimuth. The analog data system will provide a backup data system to the precision Master Equatorial system. The servo electronic equipment will provide the operating control console, the necessary servo system input-output equipment, feedback transducers, and the over-all servo system condition monitor. The control console will be located in the alidade control room to provide a view of the reflector motion from the console operator's position.

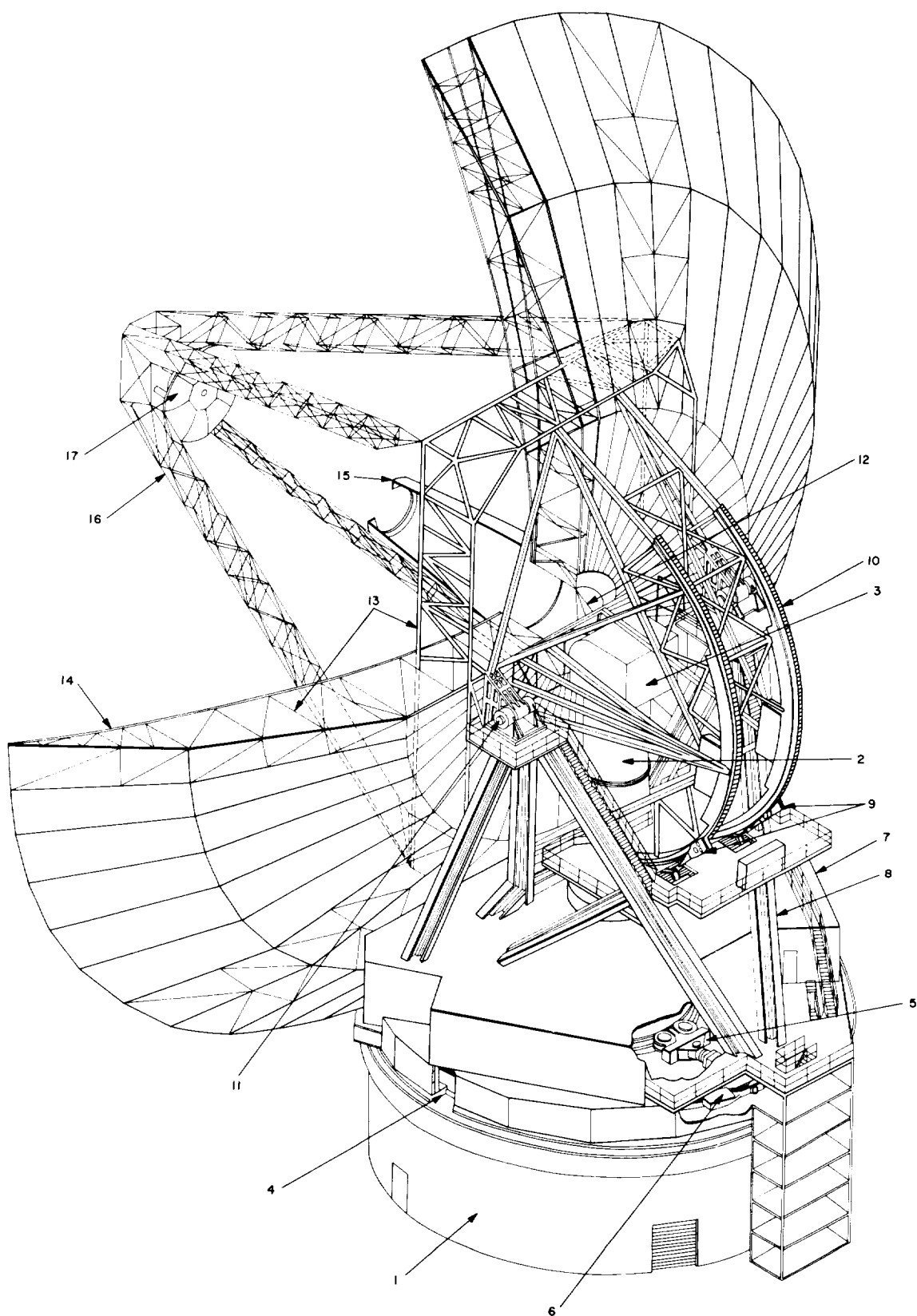


Fig. 7. Cross-sectional drawing of antenna structure

h. Elevation bearing assembly (Component 11). The elevation bearings will consist of two bearing assemblies and will support the dead loads of the antenna reflector and associated structure. The bearing assemblies will set directly on the top weldments of the alidade. Each assembly will consist of two split housings, two self-aligning spherical roller bearings, a stub shaft, alignment and adjustment blocks, wedges, and hydraulic cylinders. The estimated weight of the elevation bearing assemblies is 142,000 lb.

i. Primary reflector structure and surface (Components 10, 13, 14). The reflector will be a 210-ft-diameter paraboloid with a focal length of 88.941 ft. The structure will basically consist of 48 radial rib trusses connected by 12 circular hoop trusses. This assembly will be supported by an integral rectangular girder system. The RF reflector surface will be constructed of approximately 1200 individual 0.08-in.-thick aluminum sheeted panels. The surface will be solid out to 50% of the radius. The remaining 50% of the radius will be perforated panels with 1/4-in.-diameter holes spaced for 50% porosity. The backup structure will be a self-supporting, three-dimensional space frame consisting of two elevation wheel trusses connected to the elevation bearing weldment and to the main girder of the reflector. A tie truss connects the two elevation wheels. The backup structure will also support the reflector counterweight located within the elevation wheels. The estimated weight of the primary reflector structure, surface and backup is 1,748,000 lb.

j. Intermediate reference structure (Component 12). The function of the intermediate reference structure will be to furnish the reference boresight axis of the reflector assembly and to link this axis by autocollimators mounted on the intermediate reference structure plane to the Master Equatorial, the fixed reference plane. The intermediate reference structure will be affixed to the central core of the reflector. The estimated weight of the intermediate reference structure is 7000 lb.

k. Feed cone (Component 15). The feed cone will be located in the vertex of the primary reflector. The over-all feed cone will have a base diameter of approximately 15 ft, a top diameter of 10 ft, and a height of approximately 40 ft. It will be divided into four 10-ft modules that will be inter pin referenced for rapid removal and/or replacement. A stress skin design will be used for the upper three modules using steel angles and sheets. The bottom module will be of open framed truss construction. The lower two modules will be cylindrical, and the upper two modules will be conical. The RF feed horn will be located in the

top module. Receiving equipment will be located in the second module; the third module is for future transmitting equipment. The base module will contain the parabolic surface monitoring equipment. The estimated weight of the feed cone is 48,000 lb.

l. Quadripod (Component 16). The quadripod will support the subreflector. The quadripod will be a tubular space frame structure composed of four trapezoidal shaped legs. These legs will be connected to the four corners of the rectangular girder of the primary reflector structure. These will converge into a single apex structure above the primary reflector focal point. The apex of the quadripod combines the interconnection of the quadripod legs and the subreflector supporting structure. The quadripod will also be the supporting structure for the feed cone handling pulleys. The estimated weight of the quadripod is 24,000 lb.

m. Subreflector (Component 17). The subreflector will be attached to the quadripod and will reflect the primary reflector signal into the feed cone. It will be composed of a 20-ft-diameter, solid hyperboloidal reflector surface with a 12-in. conical perforated skirt. The reflector surface panels will be supported by a backup structure consisting of 12 radial ribs with hoops and braces. Three jack screws, controlled from a remote position, will connect the subreflector to the apex of the quadripod and permit adjustment of the axial positioning of the subreflector. A center support between the backup structure and quadripod apex will permit the adjustment motion and provide lateral support. The estimated weight of the subreflector and adjustment mechanism is 17,000 lb.

B. Supporting Studies

1. Scale Model Feed for AAS

a. Summary. RF tests on the 30-ft antenna, previously carried out at X-band and described in Ref. 2 are currently being extended to the K_u -band. The Tiefert Mountain antenna range will again be utilized for far-zone gain, boresight, and pattern determinations.

These K_u -band studies will provide direct AAS support in several areas. The RF study program, which includes correlation of measured data with certain machine computations such as aperture efficiency, radiation patterns,

and RF performance as a function of structural deformations, will be continued. Experience in pointing the narrow beam (9 min of arc) will be obtained for the listening and monopulse modes. The nonorthogonal quadripod structure will be studied, particularly for the effect on monopulse error channel patterns and null depth. Possible use of the monopulse mode for closed-loop servo operation will be considered.

b. Recent work. The full-scale AAS, 500-wavelength aperture at S-band causes excessive far-field collimation range requirements; however, the 30-ft antenna at K_u -band, in conjunction with the Tiefert facility, provides a convenient scale model for AAS feed design work. Consequently, some rather careful scaling work is in progress for the hyperboloidal subreflector and beamshaping flange, and the quadripod structure for the 30-ft antenna. The subreflector will be attached to a positioner capable of remote (control room) boresighting and focusing. The quadripod will be of open tube construction with scaled cross-section.

Initially, the Mesa antenna range will be used to develop scaled feeds and illuminator-gain standard antennas. Two feeds are being constructed:

- (1) A linear polarization monopulse tracking feed having performance similar to the Hughes SCM (a DSIF feed presently under development).
- (2) A low-noise (dual-mode) listening feed.

Two 48-in. reflectors have been selected for use as polarization diverse Cassegrain illuminator-gain standards.

The Mesa antenna range is currently being fitted with K_u -band equipment for amplitude and phase (serrodyne system) pattern measurements. Fig. 8 shows the block diagram; the system is similar to previous arrangements (Ref. 3).

Fig. 9 shows the amplitude and frequency stabilized transmitter to be installed on Tiefert Mountain. A 100-mw klystron is phase-locked to a reference crystal oscillator having a long-term (weekly) frequency stability of 1 part in 10^6 . The 5-w traveling wave tube amplifier drives either a 48-in. reflector or an auxiliary standard gain horn. Diode modulators are used to provide 1-kc AM modulation and amplitude leveling at the antenna ports, referenced to a stable, adjustable, dc source.

The receiving terminal equipment for the initial monopulse evaluation, to be located in the 30-ft antenna Cas-

segrain cone, electronics cage, and Goldstone Venus site control room is shown in Fig. 10. Three modes of operation will be used: (1) amplitude patterns for the three monopulse channels, (2) relative phase for the error channels referenced to the sum channel, and (3) simultaneous observation of the error channel amplitudes, to assist boresighting determinations. This arrangement will be replaced for absolute gain measurements.

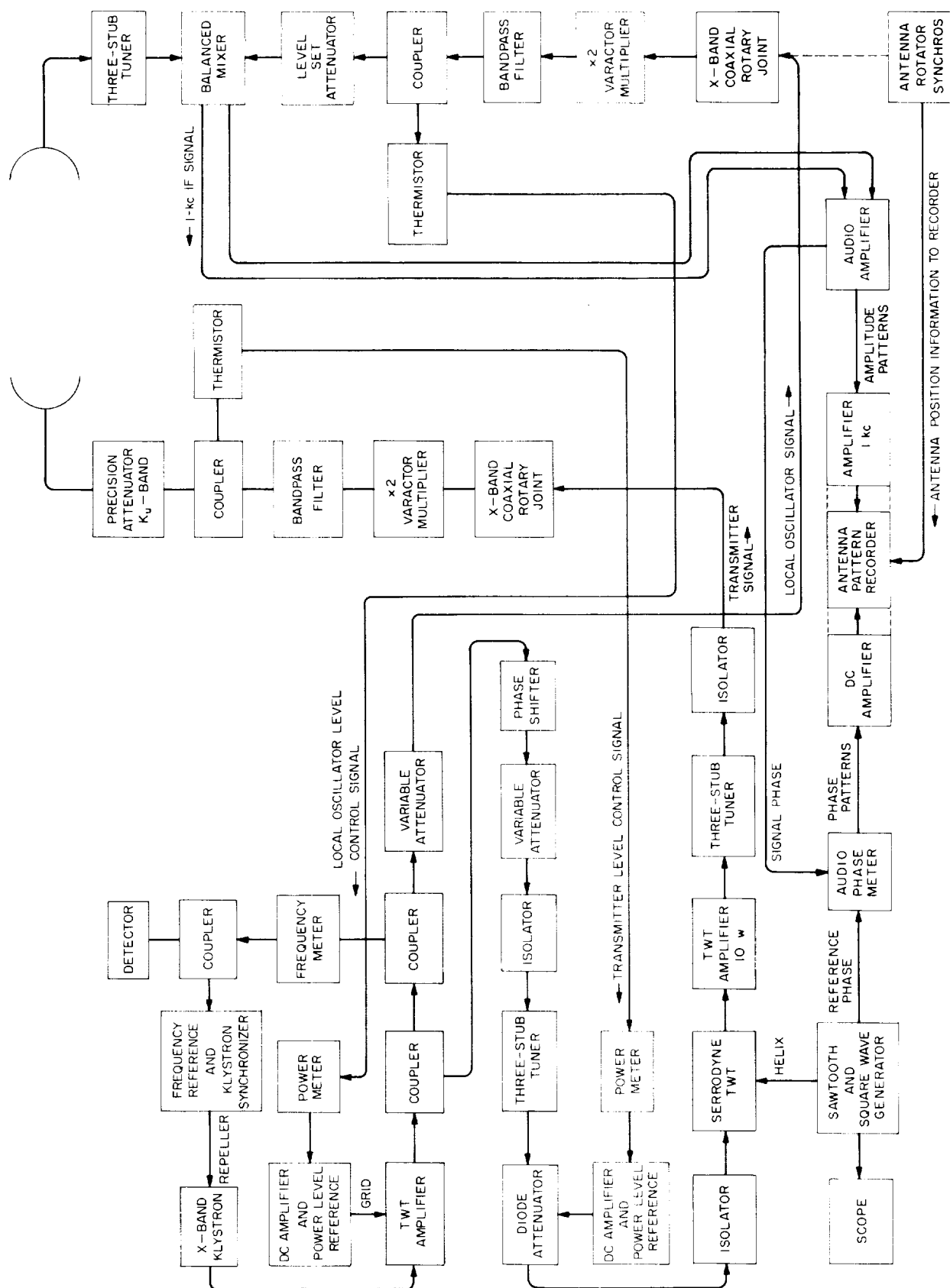
Convenient use of these K_u -band facilities for future developments in high aperture efficiency and/or low-noise feeds is being considered during initial construction.

2. Master Equatorial Preliminary Design Analysis

a. Summary. An optical instrument on a precision equatorial mount will be placed at the intersection of the axes of the 210-ft AAS antenna. It will be used to instrument the pointing of the AAS reflector. A preliminary error analysis of the conceptual design of such an instrument is given. The expected accuracy of the Master Equatorial device is 6 to 7 sec of arc.

b. Recent work. The pointing position of the 210-ft-diameter antenna (AAS) will be referenced to a Master Equatorial instrument placed on a special instrumentation tower. In the precision pointing mode, the instrument is commanded and the antenna is slaved to follow. In the auto track mode, the instrument is commanded and the antenna is slaved to follow. In the auto track mode, the antenna tracks an RF source and the Master Equatorial instrument is slaved to follow, and thus provide beam positions.

A portion of the total system pointing error will be caused by imperfections and anisotropic qualities of the Master Equatorial unit. The configuration studied is shown in Fig. 11. The pointing vector, normal to the plane mirror mounted at the center of the declination shaft, can be specified by an hour angle, ψ , and a declination angle, θ . On a perfectly aligned and rigid instrument, these two angles correspond, respectively, to the angular displacement of either end of the polar shaft and to the angular displacement of either end of the declination shaft. On an actual instrument, however, the mirror pointing vector does not correspond exactly to the displacement of the shaft ends, and it is this discrepancy or error angle that is to be considered. A preliminary study has been made to evaluate the contributions to this error angle caused by gravity loading, shaft bearing runout, orthogonality alignment of the two shafts, and temperature gradients in the structure.

Fig. 8. Mesa serrodyne system modified for K_u -band

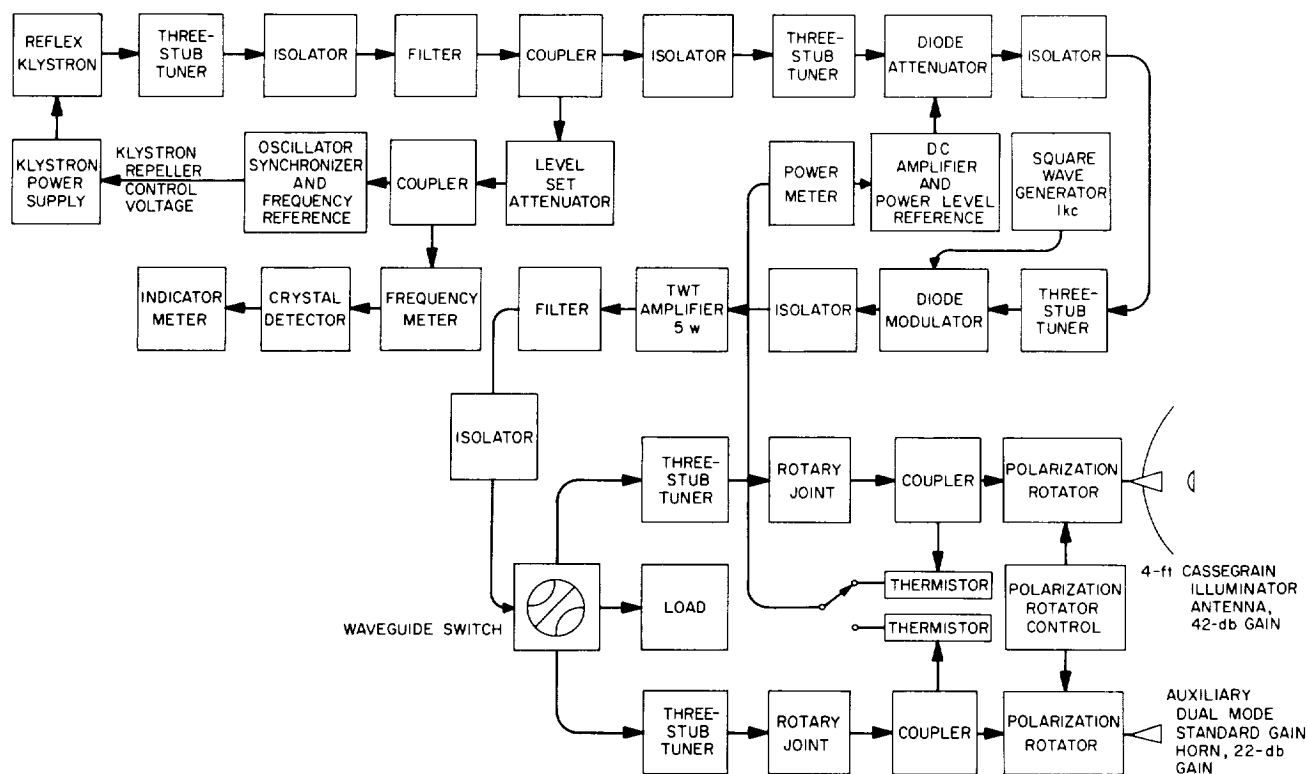


Fig. 9. Tiefort K_u-band transmitter

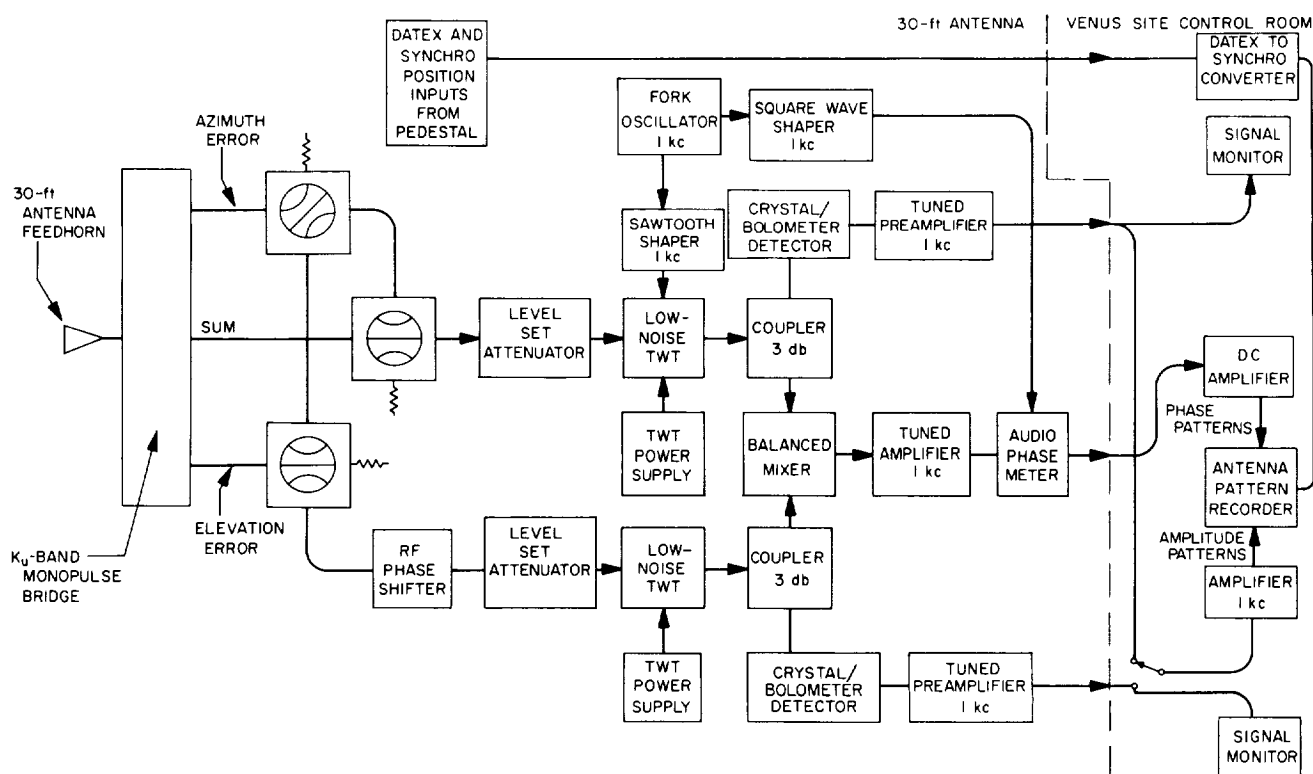


Fig. 10. K_u-band receiver

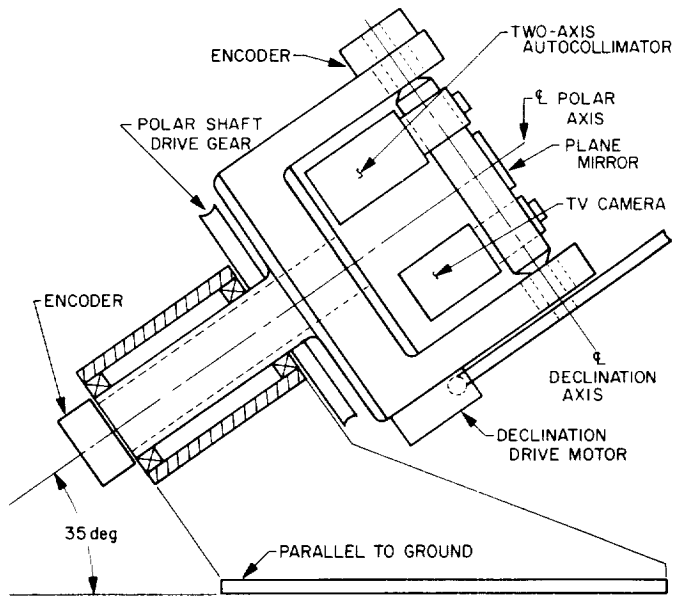


Fig. 11. Assembly view of Master Equatorial instrument

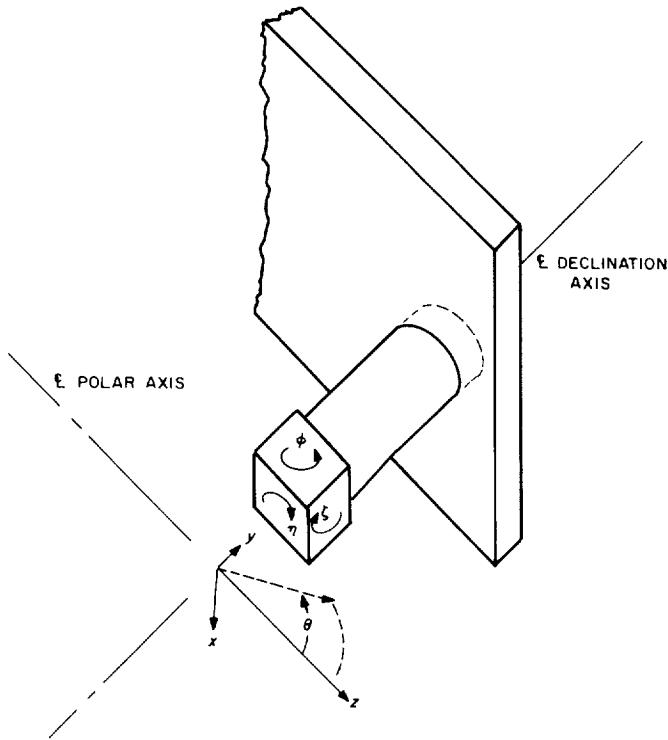


Fig. 12. Orientation of error components

From Fig. 12, it may be shown that the error angle is:

$$\epsilon = [(\phi \cos \theta + \zeta \sin \theta)^2 + \eta^2]^{1/2} \quad (1)$$

Gravity loading error. The dimensions of the movable part of the structure and the location of concentrated

masses attached to the declination axis are shown in Fig. 13. It is assumed that the structure is symmetrical about the polar axis and statically balanced about both axes; therefore, it is necessary to consider only asymmetrical gravity loads, since only these contribute to an angular deflection at the center line of the declination shaft. As the polar shaft is round, its contribution to the error angle is independent of the hour angle, ψ , and can be compensated. Therefore, for this analysis we consider the structure fixed at the juncture of the polar shaft and yoke.

Because the stiffness of the yoke in planes yz and xz are different, the error angle caused by gravity loading will vary with the hour angle, ψ . Under the additional assumptions that no moment can be transferred through the declination shaft bearings, and that each leg of the yoke is a prismatic beam, formulae have been developed for the angular deflection components ϕ , η , and ζ for two hour angle positions, namely for the case where the declination shaft is parallel to the ground ($\psi = 90$ deg), and for the case where the declination shaft lies in a vertical plane ($\psi = 0$). For intermediate values of ψ , there would obtain intermediate error angles.

For $\psi = 0$

$$E\phi = \frac{1}{I_3} \left[0.024 Wa (2L_3 + \frac{a^2}{L_3} - 3a) \right] + \frac{1}{I_{1x}} \left[\frac{WL_1^2}{L_3} (0.382 \frac{aL_1}{L_3} - 1.64L_2) - 0.41\gamma \frac{L_1^2 L_2}{L_3} (A_2 L_2 + A_3 L_3) \right] \quad (2)$$

$$E\eta = \frac{0.727 aRW}{K_3} \quad (3)$$

$$E\zeta = 0 \quad (4)$$

For $\psi = 90$ deg

$$E\phi = \frac{1}{I_3} \left[0.024 Wa \left(2L_3 + \frac{a^2}{L_3} - 3a \right) \right] + \frac{1}{I_{1x}} \left[0.382 \frac{WaL_1^3}{L_3^2} \right] \quad (5)$$

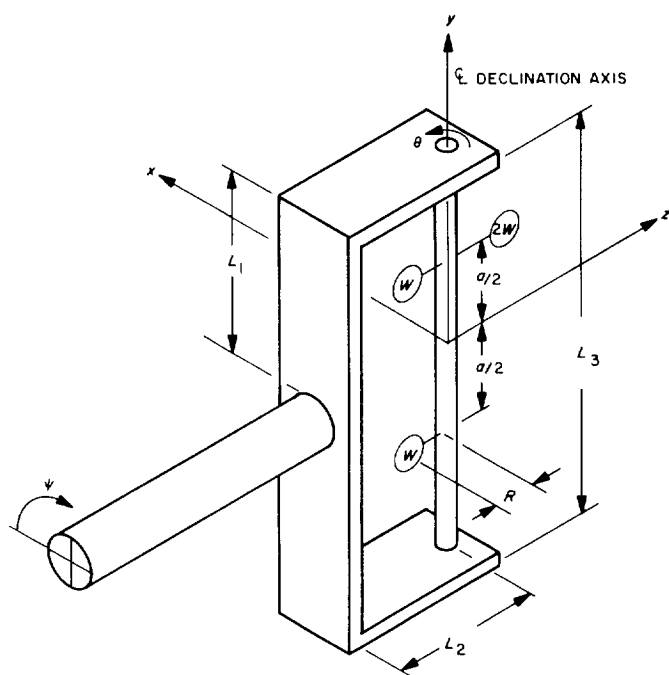


Fig. 13. Schematic of Master Equatorial yoke

$$E\eta = \frac{L_2^3}{I_{2y}} \left[0.82W + 0.144A_3\gamma L_3 + 0.136A_2\gamma L_2 \right] + \frac{L_1 L_2}{K_1} \left[4.1W + 0.727A_3\gamma L_3 + 1.025A_2\gamma L_2 \right] + \frac{1.25aRW}{K_3} \quad (6)$$

$$E\zeta = 0.819Wa \left[\frac{0.042}{I_{3y}} \left(2L_3 + \frac{a^2}{L_3} - 3a \right) + \frac{0.67}{I_{2y}} \frac{L_2^3}{L_3^2} + \frac{0.67}{I_{1z}} \frac{L_1^3}{L_3^2} + \frac{5}{K_1} \frac{L_1 L_2^2}{L_3^2} \right] \quad (7)$$

where

E = modulus of elasticity

γ = weight density

A = cross-sectional area

I = moment of inertia of area

K = torsional deflection factor

Number subscripts refer to beam number

Subscripts x, y, z indicate axis of moment of inertia of area

L, a, R are indicated in Fig. 13

ϕ, η, ζ , are indicated in Fig. 12

Bearing runout error. If the two shafts of the Master Equatorial instrument are supported by anti-friction bearings, there will be an error component caused by runout of the inner races and another caused by the epicyclic action of nonuniformly sized rolling elements.

The concept that there is a line, within a bearing supported shaft, which does not move in space during rotation of the shaft, is based on the assumption of a perfectly circular inner race. Unfortunately, this concept does not apply to real bearings because no inner race is perfectly circular. A more realistic concept assumes that the inner race is elliptical and that there is a finite variance among the diameters of the rolling elements. These latter assumptions yield the following angular error component for the runout of each shaft:

$$\epsilon = \frac{2\Delta d + (a + b)}{l} \quad (8)$$

where $2\Delta d$ is the difference between the diameters of the largest and smallest rolling elements, a and b are the semi-major and semi-minor axes, respectively, of the elliptically shaped inner race, and l is the spacing between the two bearings.

The inner race radial runout as listed in most bearing catalogs corresponds to the numerator of Eq. (8). For the best grade ball bearings of the size appropriate for this instrument, this value is approximately 200 μ in.; specially made bearings could be slightly better.

Thermal gradient error. If the two legs of the yoke have different average temperatures, an angular error will be produced. The electronic equipment mounted on the declination shaft and the drive motors mounted on the yoke constitute heat sources. By suitably insulating the mounting of these power units and providing a temperature controlled environment, it is believed that the effective temperature difference between the legs of the yoke will not be greater than 3°F. The resulting error angle is:

$$\phi = \frac{3\alpha L_2}{L_3} \quad (9)$$

where α is the coefficient of linear expansion in $1/^\circ\text{F}$.

Orthogonality error. It is necessary that the declination shaft be very nearly perpendicular to the polar shaft. In boring the yoke for the declination shaft bearings, a relative offset error will result. In order to limit this component of angular error to, say, 2 sec of arc, the relative offset error could not exceed 0.00035 in. for a 36-in.-wide yoke. It does not seem reasonable that this kind of offset tolerance could be obtained on a yoke of the size under consideration. Therefore, it is necessary to incorporate an adjustment of one bearing position. This can be achieved by making the outer diameter of one bearing eccentric with respect to its center. Such a feature can be accomplished in several ways, all of which offer certain difficulties. It is quite important that the radial deflections of the bearings at each end of the declination shaft be nearly the same, or an additional error component will exist. The design of the adjustable bearing must be very carefully done.

If the relative offset error of the declination shaft bore can be limited to 0.004 in., and this eccentricity built into the adjustable bearing, a very sensitive orthogonality adjustment is possible. If the smallest practical adjustment of the eccentric bearing is taken as 2 deg, the maximum orthogonality error is:

$$\phi = \frac{0.00012}{L_3} \quad (10)$$

Sample analysis. A preliminary investigation has established that a yoke of the width and depth shown in Fig. 14 is large enough to provide for the mounting of tentatively chosen autocollimator and television units. In order to obtain a numerical estimate of the angular error components, the foregoing analyses are applied to this particular design. The material chosen is steel, polar bearings are spaced 22 in. apart; concentrated mass weight, W , is 20 lb; dimension R of Fig. 13 is 12 in.; and other necessary parameters can be computed from the dimensions of Fig. 14.

By the application of Eqs. (2) through (7), the following error angle components caused by gravity loading are obtained:

$$\phi_{\psi=0} = -0.63 \text{ sec}, \quad \phi_{\psi=90} = 0.03 \text{ sec} \quad (11)$$

$$\eta_{\psi=0} = 0.18 \text{ sec}, \quad \eta_{\psi=90} = 1.28 \text{ sec} \quad (12)$$

$$\xi_{\psi=0} = 0, \quad \xi_{\psi=90} = 0.067 \text{ sec} \quad (13)$$

When the foregoing values are substituted into Eq. (1), the maximum error caused by gravity loading, for the two hour angles, is obtained; the results are:

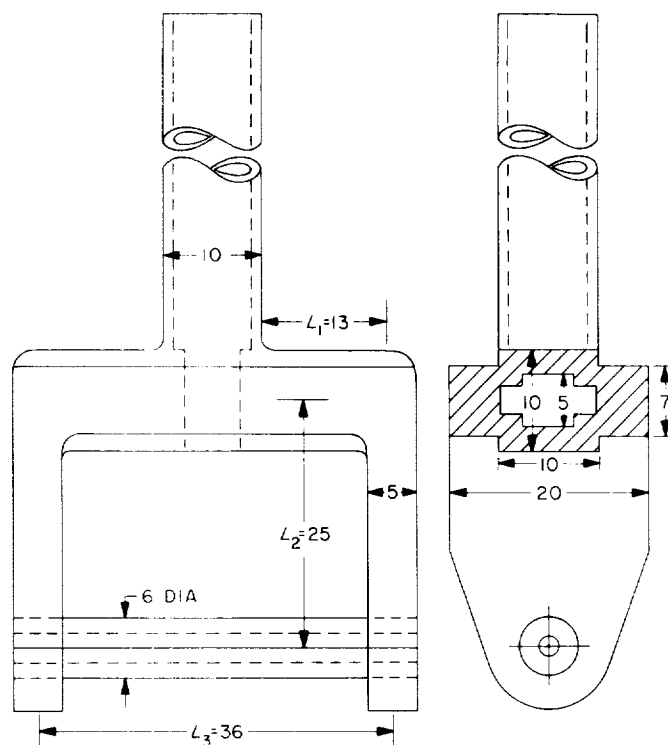


Fig. 14. Configuration yoke for Master Equatorial instrument

$$\epsilon_{G\psi=0} = 0.66 \text{ sec} \quad (14)$$

$$\epsilon_{G\psi=90} = 1.28 \text{ sec} \quad (15)$$

The predominate component of $\epsilon_{G\psi=90}$ is the angle η . It is instructive to consider the expression for η [(Eq. (6))] as a function of the beam lengths, L . For instance, if all of the lengths, L , and the dimension, "a," are reduced by 20%, the value of η is reduced by approximately 40%. More important, perhaps, for the same value of η , the weight of the yoke could be reduced by approximately 40%. As the weight of the yoke shown in Fig. 14 is in the neighborhood of 3100 lb, there may be other reasons for wanting it lessened. Therefore, for the purpose of reducing this particular error component, it would be appropriate to make the width and depth of the yoke as small as is practical.

The bearing runout errors are estimated from Eq. (8) by setting the numerator at 200 μ in. For the polar shaft, the error may be in the direction of ϕ or η and is:

$$\phi \text{ or } \eta = 1.87 \text{ sec} \quad (16)$$

For the declination shaft, the error may be in the direction of ϕ or ζ and is

$$\phi \text{ or } \zeta = 1.14 \text{ sec} \quad (17)$$

From Eq. (8), these runout errors are seen to vary inversely with the bearing spacing.

From Eq. (9), the temperature gradient error is, for the assumed temperature difference:

$$\phi = 2.17 \text{ sec} \quad (18)$$

From Eq. (10), the orthogonality error is:

$$\phi = 0.69 \text{ sec} \quad (19)$$

By properly combining Eqs. (11), (12), (13), (16), (17), (18), and (19) and substituting into Eq. (1), the following maximum total angular errors are found:

$$\epsilon_{\substack{\psi=0 \\ \theta=0}} = 6.50 \text{ sec} \quad (20)$$

$$\epsilon_{\substack{\psi=90 \\ \theta=0.65}} = 6.03 \text{ sec} \quad (21)$$

The error component from one part of the bearing runout error, namely, that from a variation of rolling element size, is a random error. The temperature gradient error is also random. The other errors are systematic in the sense that they could be repeated.

Although the numerical errors given above are based upon a somewhat nebulous design, they provide insight into what is expected of a final design.

3. Wind Study Program

Final checkout of the data recording instrumentation system was completed in January as part of the Advanced Antenna System wind study program. The instrumentation system has been recording wind data since December 20, 1963.

The drag spheres at the 40- and 80-m levels on the main tower (Fig. 15) near the Mars Station were lowered to the ground by the Pacific Crane and Rigging Company, calibrated through use of the analog portion of the data recording instrumentation system, and then replaced on the tower.

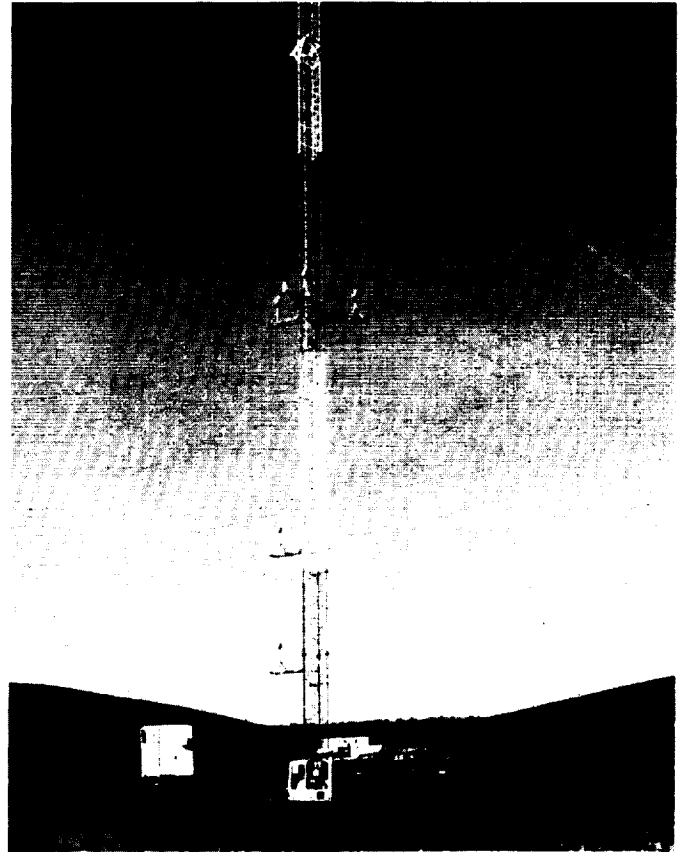


Fig. 15. Main wind tower near Mars Station

Since periodic calibration of the drag spheres is necessary, along with the cost of rigging, a calibration box was designed and constructed to facilitate the calibration of the drag spheres in a zero wind environment while in operating position on the tower.

Grounding of the van, guys, and towers, involving excavations for underground cables, became necessary because of noise problems, and has been completed (Fig. 16).

The present supporting structure for attaching the drag spheres to the tower is inadequate for support of both a sphere and maintenance personnel. A new structure, therefore, was designed with the incorporation of siderails and safety belt hangers. Two are under construction for the 40- and 80-m levels, heights which cannot be reached by existing equipment.

Wind tunnel tests (Fig. 17) have been conducted in investigation of force transfer characteristics of the drag spheres and quadripod pipe stand and tower effects. Test data is to be analyzed during the next reporting period.

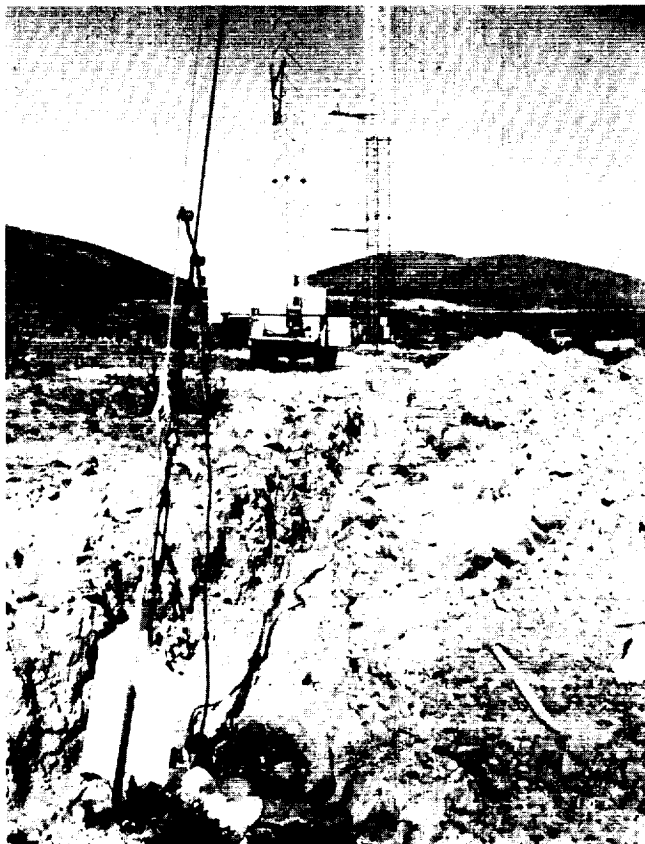


Fig. 16. Grounding of wind study system

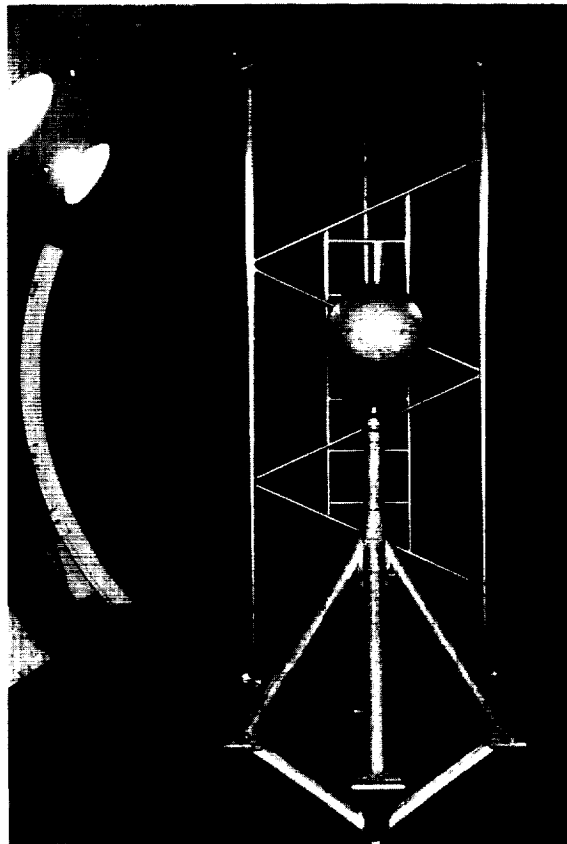


Fig. 17. Drag sphere and tower section
in wind tunnel

References

1. "Advanced Antenna System," *Space Programs Summary No. 37-25*, Vol. III, pp. 59-62, Jet Propulsion Laboratory, Pasadena, California, January 31, 1964.
2. "RF Tests on 30-ft Antenna," *Space Programs Summary No. 37-21*, Vol. III, pp. 27-33, Jet Propulsion Laboratory, Pasadena, California, May 31, 1963.
3. "JPL Mesa Antenna Range," *Research Summary No. 36-13*, p. 61, Jet Propulsion Laboratory, Pasadena, California, March 1, 1962.